2009

Computational modeling of multiphase fibrous flows for simulation based engineering design

Stephen Patrick Gent
Iowa State University

Computational modeling of multiphase fibrous flows for simulation based engineering design

by

Stephen Patrick Gent

A dissertation submitted to the graduate faculty

in partial fulfillment of the requirements for the degree of

DOCTOR OF PHILOSOPHY

Major: Mechanical Engineering

Program of Study Committee:
Kenneth M. Bryden, Major Professor
Michael B. Pate
Tom I-P. Shih
Shankar Subramaniam
Eliot H. Winer

Iowa State University

Ames, Iowa

2009

TABLE OF CONTENTS

LIST OF FIGURES

LIST OF TABLES

NOMENCLATURE

Symbols

α_k	-volume fraction of phase k [-]
γ	-distributed resistance coefficient [kg s/m^5]
β	-distributed resistance coefficient [kg/m^4]
ρ_k	-phase density [kg/m^3]
$\tau_k ; \tau_k^t$	-laminar and turbulent stresses, respectively [N/m^2]
μ_k^t	-turbulent eddy viscosity [N s/m^2]
υ_α	-turbulent kinematic viscosity [kg/m*s]
$\mathbf{F}_D$	-drag force, per unit volume [N/m^3]
$\mathbf{M}_k$	-interphase momentum transfer source [N/m^3]
$\mathbf{u}_k$	-mean phase velocity vector [m/s]
$\mathbf{u}_r = \mathbf{u}_c - \mathbf{u}_d$	-relative particle velocity [m/s]
A_c	-particle cross sectional area [m^2]
A_p	-projected area of the particle in the flow [m^2]
$A_{particle}$	-surface area of the particle in the flow [m^2]
C_D	-modeled particle drag coefficient [-]
d	-particle diameter [m], [cm]
K_i	-distributed resistance in the direction i

v_i	-velocity in the direction ζ_i
L	-length [m], [cm]
Δp	-pressure drop [N/m^2]
P	-perimeter [m]
Re_D	-relative particle Reynolds number [-]
V	-volume of the particle [m^3]
r	-radius [m], [cm]
t	-time [s]

Subscripts

d	-dispersed phase (bulk solids phase)
c	-continuous phase (air phase)
connectivity	-connectivity effects
k	-phase k
D	-drag
air	-air phase
solid	-bulk solids phase

ACKNOWLEDGEMENTS

I would like to take this opportunity to thank several important people in my life. First, I would like to thank my wife Melissa and my daughter Maya for their love, understanding, and patience, especially during the last few months of graduate school, and for reminding me to always look towards the future. I would like to thank my parents, Patrick and Mary, my brother Robert, and my late sister Bridget, for their love and support, and for teaching me the value of hard work, perseverance, and determination.

Additionally, I would like to thank Dr. Mark Bryden for his direction, insight, and wisdom as I prepare for my academic and professional career. I would also like to thank Dr. Michael Pate, Dr. Tom Shih, Dr. Shankar Subramaniam, and Dr. Eliot Winer for taking the time to participate on my committee. Also, I would like to thank Dr. Gregory Maxwell for his participation and involvement at my final examination. Finally, I would like to thank each member of the Virtual Engineering Research Group for their contributions, especially Doug McCorkle and David Muth for their assistance and guidance at the early stages of this research, Michael Dunlay for assisting me in conducting this research, and Chad Garber and Jared Abodeely for working with me to continue this research.

ABSTRACT

This dissertation develops a modeling framework for predicting the behavior of fibrous bulk solids in pneumatic conveyance systems that are currently not possible with conventional computational models. The developed framework allows designers to computationally predict flow characteristics of fibrous bulk solids, which impacts pneumatic conveyance system performance. These performance characteristics include air and fibrous bulk solids velocity profiles, fibrous bulk solids concentrations, pressure loss, and general system behavior. The motivation for this research is to expand the capabilities of computational models within in the engineering design process, rather than relying solely on generalized experimental correlations and previous design experience.

This framework incorporates the primary characteristics of fibrous biomass-based bulk solids including low density, large characteristic length, and non-spherical shape. The main features of the developed modeling framework are (1) the effects of the particle drag on the flowing air and (2) the resistive effects of the interconnected fibers between the particles. The models are implemented within a commercially available CFD solver package with user-defined functions. Velocity profiles, bulk solids concentration, and air pressure are modeled with the differential conservation equations for mass and momentum based on the Eulerian-Eulerian multiphase modeling approach. The inter-particle and the particle-air interactions result in momentum exchanges, and these exchanges are incorporated into the model through a series of externally defined user functions that account for the momentum exchange due to drag of the particles and the resistance of the connected fibers. These user-defined functions allow the user to set a series of parameters specific to the transported bulk solids and to the

loading conditions. The model is applied to two specific studies, which include (1) cotton-air flow through a positive pressure pneumatic conveyance system and (2) biomass-air flow through a negative pressure (vacuum) conveyance system. The model parameters are chosen to match existing experimental data obtained from their corresponding lab tests.

CHAPTER 1: INTRODUCTION

In a world confronted with limited fossil energy resources and climate concerns, biomass is a critical source of renewable, sustainable energy. Biomass sources include annual and perennial crops, crop residues, forest residues and municipal refuse. Biomass can be synthesized to create biofuels, bioproducts, and biopower (Office of the Biomass Program, USDOE EERE Biomass Program, 2007). Recognizing the importance of biomass energy, the U.S. Congress mandated in the 2007 energy bill a fivefold increase in biofuel use for transportation by 2022, and the U.S. Department of Energy has a goal of replacing up to 30 percent of our transportation fuel needs with biorenewables by 2030. These are challenging goals. Currently, biomass provides approximately three percent of our nation's transportation and electrical energy (Energy Information Administration, 2009).

To achieve this goal, new ways are needed to harvest, collect, sort, handle, and transport biomass feedstocks efficiently and economically. It is projected that collecting, storing and preprocessing biomass feedstocks can constitute as much as 20 percent of the current cost of cellulosic ethanol (Biomass Research and Development Board, 2008). These processes require high throughput, reliable delivery, and minimal damage of the biomass throughout the transport, processing, and segregation processes. However, many of the technologies required to make bioenergy successful on a large scale do not yet exist. For instance, single pass harvesters that have the ability to harvest and segregate cellulosic biomass and grain can lower the cost of biofuel production by using less time, labor, and energy. Single pass harvesting will require developing the capability to continuously harvest and sort stems, nodes, and grain. In addition, conveyance systems found in biorefineries will

need to be designed for reliable and efficient operation to transport the bulk solids from the delivery station through the biorefinery.

Current transport, processing and handling technologies for irregular biomass particles are not reliable. Biomass particles are often so extreme in their physical characteristics that it is difficult to predict their performance during transport and handling. Unusual characteristics of biomass commonly include a combination of mean particle size, wide size distributions, extreme shapes (flakes, chips, fibers, splinters, stalks, etc.), particle flexibility and pliability, compressibility, and general heterogeneity (Mckendry 2002). As a result, industrial biomass processes are limited, and the potential of biomass as a source of renewable energy is largely unrealized (Cui and Grace 2007a).

1.1. Pneumatic Conveyance Systems

A common approach to handling biomaterials is through the use of pneumatic transport conveyance systems. Pneumatics is derived from the Greek word *pneumaitkos*, which means ‘coming from the wind,’ and is defined as the use of pressurized air in science and technology (Ratanyake, 2005). A pneumatic system conveys bulk solids, which can range in size from microns to centimeters in diameter. Systems involving pneumatics have been in use for well over a century (Fokeer et al. 2003). The applications of pneumatic principles in systems are widespread in agricultural, industrial, domestic, chemical, pharmaceutical and commercial processes. Pneumatic systems are used to transport bulk solids within horizontal, vertical, and diagonal piping systems with the use of a vacuum or compressed air stream. Once the bulk solids have been transported to a destination, the bulk solids are segregated and deposited in a container. Pneumatic systems are used in processes

in which heterogeneous solid particles are segregated based upon the properties of the solid mixture components. An example of this is in the threshing and segregation operations in a combine in which mature plants are harvested in the field and the grain is separated from the stems, nodes, and leaves of the plant.

Pneumatic conveyance systems have several inherent advantages over mechanically based conveyance and segregation systems, such as conveyor belts, auguring screws, and moving buckets. These advantages include 1) pneumatic systems are generally easier to install and operate than the mechanically based counterparts due to their simple design, 2) installation of pneumatic conveyance systems are simpler to install and less costly than their mechanically based counterparts due to the flexibility of the piping and conduit of pneumatic systems, 3) pneumatic systems have the capability to reach containers that would be difficult to connect with mechanical conveyance systems, 4) the flexibility and simplicity of pneumatic systems reduces the capital, installation, and maintenance costs, and 5) pneumatic conveyance systems are completely enclosed, which prevents cross-contamination with other products and reduces dust emissions. In addition, depending on the system design and configuration, the conveyed product will undergo less damage and degradation compared to being conveyed in an auger screw. Although pneumatic conveyance systems have several distinct advantages, they have several major drawbacks, which may reduce their viability in industrial, commercial and agricultural applications. Pneumatic systems generally require higher energy consumption due to the inefficiencies of airflow in piping. Also, the energy in the flow is just dumped at the end of the pipe and cannot be recaptured. In dilute transport, product degradation and piping erosion can occur. In dense phase transport, substantial plugging can occur.

Another disadvantage of pneumatic conveyance systems is the difficulty of designing new systems. Pneumatic systems are difficult to design for two reasons. The first challenge is managing the airflow within the system. Every aspect of the system needs to be considered and properly matched. The blower has to be sized properly to the length, diameter and roughness of the piping. In addition, any special features in the pneumatic system, including bends, valves, and manifolds, will change the airflow characteristics. The second challenge is predicting the behavior of bulk solids within the system and how the presence of bulk solids will affect the airflow characteristics within the systems. The transport characteristics of bulk solids are inherently complicated due to bulk solids volumetric flow rate, air volumetric flow rate, air velocity, and bulk solids physical properties (particle size, shape, density, moisture content, etc). Because of this, the design of pneumatic conveyance systems is more of an art than a science and is the trickiest of all the bulk-handling arts (Stoess 1983). This idea is further reinforced in the introductory paragraph of the 1917 catalog of the Pneumatic Conveyor Company, Chicago:

> "… The simplicity and efficiency of these systems depends entirely on the accurate design based on a comprehensive knowledge of pneumatics in general and an intimacy with the characteristics of the materials in question, and more valuable than both, actual experience."

Today, almost 100 years later, this is still true. It is still difficult for a designer to obtain the experience to gain a good understanding of the fundamentals of pneumatics, in addition to the experience of physically studying the bulk solids flows in pneumatic systems. Because of the difficulties of designing pneumatic conveyance systems, it is important for a designer to have effective processes for determining proper designs of these systems.

Pneumatic conveyance systems are also constrained by high power consumption, limited transport distances, and challenges unique to conveyed bulk solids. Today, pneumatic systems that handle bulk solids are designed and built based on experimental studies, previous designs, and empirical correlations (Mills et al. 2004). Biomass transport and handling is challenging because of its heterogeneous properties, as these properties are influenced by crop variety, moisture content, and other field performance characteristics. Also, biomass transport and separation systems need to have the ability to accommodate the differences in the behavior of the bulk solids.

1.2. Simulation Based Engineering Design

One particular engineering tool that has become increasing popular is the use of computational models. Computational models have become popular in the past few decades due to the increased capabilities and widespread use of computers. In addition, computer simulations are often less expensive to develop and easier to obtain than experimental data. In many cases, technology has enabled engineers to utilize computer-generated and virtual prototypes to replace experimental models and physical prototypes in the engineering design process.

In 2006, the National Science Foundation published a report focused on Simulation Based Engineering Science (SBES) (Oden et al. 2006). *Simulation* is the application of computational models to the study and prediction of physical events of the behavior of engineered systems. *Simulation Based Engineering Design* is defined as the discipline that provides the scientific and mathematical basis for the simulation of engineered systems. SBES fuses the knowledge and techniques of traditional engineering fields—mechanical,

civil, chemical, aerospace, nuclear, biomedical, and materials science—with the knowledge and techniques of fields such as computer science, mathematics and the physical and social sciences.

One promising application of SBES is the utilization of computational fluid dynamics (CFD) in engineering design. CFD has been in use for the last forty years in the automotive and aerospace industries to study flow patterns, temperature profiles, etc., within their respective products. CFD models have been in use in the automotive and aerospace industries since the 1960s and 1970s (Tannehill et al. 1980) and have become invaluable in determining airflow patterns on objects such as airfoils and automotive bodies. The algorithms and mechanisms for solving the conservation of mass, momentum and energy are well established for solving single-phase fluid flows, and several commercially available CFD solver packages are available to support engineering design. The primary challenges today are turbulence quantification, reacting flows, multiscale, multiphysics and multiphase flows.

Traditionally, CFD has been applied to engineering design in two ways:

- The first application is to gain qualitative insight to an engineering problem. For instance, several key aspects of automotive development utilize CFD during early stages of design in order to identify, correct, and prevent re-design costs and also to reduce physical testing and prototyping (Srinivasan et al. 2004). Reduced product development cycles have made computer simulations essential to streamlining the design process. Potential performance problems due to design of flows can be determined and corrected using simulation. This can allow a reduction in the number of prototype based physical tests and associated costs. The simulations allow for

informed decisions to be made early in the design process, thus decreasing the product development time and cost.

- The second application of CFD in engineering is to create high fidelity quantitative models of design problems. This is similar to building a physical model to gather information. This classification of CFD models is for a specific purpose. These are used in situations where engineers are concerned with every characteristic of the model, and fidelity is necessary. In addition, this classification of model requires that the allowable error rate be clearly understood and minimized.

Often, CFD models are developed and utilized with one of these two applications in mind. Depending on the application, the model is created to either provide a solution quickly (lower fidelity) or with high accuracy (long convergence time). The tradeoff is related to the refinement of the model for accuracy of the CFD solution. In many, if not most cases, the engineer and analyst do not need to know the flow characteristics at each point in the analysis. Rather, they are concerned with specific performance metrics, which include power requirements, system bottlenecks, and flow patterns at locations of interest.

Recently, a third use of CFD is in the design process. CFD in design requires that the models be able to accurately answer specific engineering design questions in a timeframe appropriate for facilitating effective design. CFD models have been utilized more extensively in product or systems design for a variety of reasons. CFD has the capability of meshing high fidelity grids in a relatively short timeframe, and the increased availability of computational resources has made CFD more feasible in design. In addition, CFD can help guide the

designer in improving product designs by determining the flow behavior of a design before constructing a physical prototype, which saves time, labor, and money.

1.3. Motivation for this Research

Certain modeling capabilities are limited by traditional CFD solving methods. Modeling of multiphase flows (the simultaneous flows of a mixture composed of two or more phases) is not yet a mature field, and the modeling techniques (governing equations, formulation, etc.) are still debated. Specific types of flows involve relatively light mixtures of very small particles that can be adequately represented and modeled by currently available CFD tools. Other flows, such as soil or granular flows are primarily affected by particle-to-particle interactions and by the inertia of the particles. These types of flows may be modeled with commercially available discrete element modeling tools. Today, the types of flows found in pneumatic conveyance systems cannot be adequately represented with traditional multiphase modeling techniques. In many cases, the flowing air can be modeled with CFD, but once bulk solids are introduced, the flow characteristics change significantly.

Research has been conducted with experimental and numerical models to study the effects of bulk solids in pneumatic systems. Examples of bulk solids include coal dust and glass beads. The conveyed bulk solids of interest have primarily been dilute flows in which the particle size is on the order of microns and the density on the order of 500 to over 1000 times the density of the carrier phase. Bulk solids that have similar characteristics to coal dust and glass beads have been studied computationally and experimentally because of their small, near-spherical particles, high particle density, and near homogeneous consistency. However, fibrous biomass bulk solids have characteristics that are significantly different than

traditionally studied bulk solids. Biomass particles are typically larger than powder or glass beads in flow, the particles are not spherical in shape, and the particles have a high variability in size, shape, and consistency. The variability of these characteristics, in addition to the unique properties of biomass, makes it difficult to quantify, much less predict, their effects. Furthermore, the fibrous nature of biomass bulk solids incorporates additional effects in the flow regime, including rotation, agglomeration, and particle compressibility. Table 1.1 compares the densities and the characteristic sizes of biomass bulk solids to more traditionally studied particles—coal dust and glass beads. This is an important distinction because the low particle density, in conjunction with the large characteristic length of fibrous biomass bulk solids, significantly changes the flow characteristics and makes them especially challenging due to their unique and heterogeneous characteristics As a result, no traditional modeling techniques have yet to be developed to represent the effects of the flow regimes.

Table 1.1. Properties of several pneumatically conveyed bulk solids.

Bulk Solid	Solid Density (kg/m^3)	Characteristic Length
Coal Dust	650	<75 µm
Cotton Boll	80-300	0.5 to 4 cm
Glass Beads	2,400-2,800	0.1 mm
Wheat Chaff	75-200	0.2 to 6 cm
Wood Chips	200	0.25 - 1.0+ cm
Wood Pellets	650	0.3 to 0.5 cm

Figure 1.1 compares the particle diameter and the characteristic length of a variety of bulk solids. The ordinate axis shows the particle density of the bulk solids of interest, while

the abscissa shows the characteristic length of the bulk solids. Note that the abscissa is on a logarithmic scale. Examples of bulk solids that have been studied in the past are found on the left side of the graph. In comparison, the bulk solids of interest in this research are located toward the bottom right of the graph. All the bulk solids of interest have a lower particle density and are several orders of magnitude larger than their previously researched counterparts.

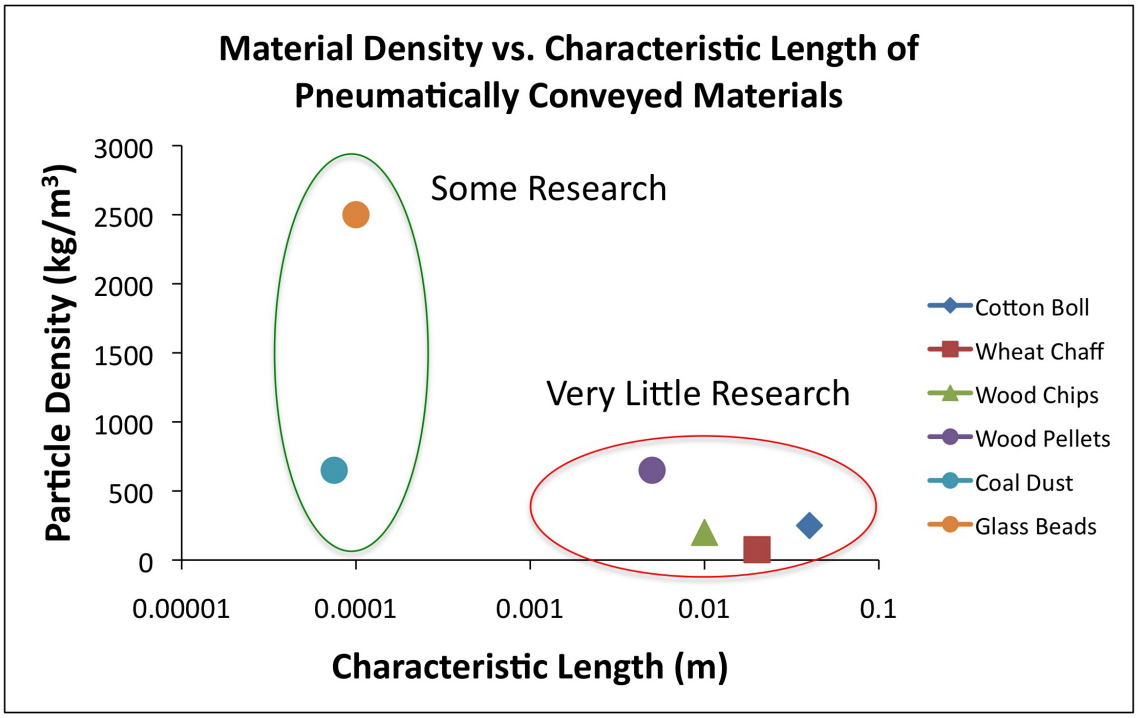

Figure 1.1. Comparison of pneumatically conveyed bulk solids.

1.4. Research Objectives

This research proposes to develop methodologies for implementing the multiphase effects of the flow cases previously described within a CFD solver package. The goal of this

research is to develop a methodology for representing these complicated biomass flow regimes within a computational model that is appropriate for engineering design. The primary flow effects are accounted for in the models and are compared with experimental data. The developed methods are then integrated into a commercially available CFD solver package.

The overall organization of this dissertation is as follows. Chapter Two provides a background of the fundamentals of gas-solid multiphase flows and a survey of previous research. Chapter Three reviews currently developed approaches for modeling multiphase flows. Chapter Four describes the development of the methodology of the computational model. Chapter Five outlines the process for obtaining experimental data to use in the computational model, while Chapter Six applies the developed methods for cotton-air flow. Chapter Seven demonstrates how the developed methods of this research may be extended to predicting biomass-air flow, while Chapter Eight offers the conclusions of this research and discusses opportunities for future research.

1.5. Summary of Research

This research presents an approach for representing the behavior of fibrous biomass bulk solids entrained in an airflow using a computational model. The model takes into account the unique properties of the biomass bulk solids, including its large size, non-spherical shape, and low bulk density. In addition, the model dynamically accounts for the loading concentration of the bulk solids within the system. Both these effects result in momentum exchanges between the phases and between the particles. The developed

modeling approach is then used to explore the flow behaviors of various fibrous bulk solids, which can be utilized in the design process.

CHAPTER 2: BACKGROUND

Pneumatic conveyance of bulk solids, although relatively simple in principle and appearance, is a complex process in which the air phase interacts with the bulk solids, and the bulk solids influence the behavior of the air phase. This chapter discusses the fundamentals of gas-solid flows in pneumatic conveyance systems and reviews previous research pertaining to gas-solid multiphase flows. Prior to surveying the research, this chapter will review the terminology in multiphase flows and pneumatic conveyance systems.

2.1. Description of Pneumatic Conveyance Systems

A typical pneumatic conveyance system is comprised of four major components. The first component is a conveying gas supply, which provides the necessary flow energy to the conveying gas. The conveying gas supply can consist of a compressor, fan, or blower for a positive pressure conveyance system, or a vacuum pump that provides air movement within a negative pressure conveyance system. The second component is the feeding mechanism that introduces the bulk solids into the conveying line. The feeding mechanism can be any type of rotary valve, screw feeder, or hopper. The bulk solids, in conjunction with the operating pressures and air velocities of the pneumatic system dictate the type of feeding mechanism. The third primary component is the conveying line, which consists of a series of pipes or channels that direct the flowing air and bulk solids from the feeding mechanism to the end of the conveying line. After the air and bulk solids travel through the conveying line, it enters the fourth component of the system, the separation equipment. At this final stage, the bulk solids are separated from the conveying airstream. Typical separation equipment includes

cyclone separators and bag filters. In addition, the separation system could be something as simple as a porous hopper which collects the bulk solid and allows the air to escape, or it could be the outside environment in which the bulk solid is scattered on the ground and the air is released to the atmosphere.

Pneumatic conveyance systems can be classified in a number of ways. The most common classification is if the system is a positive or negative pressure system. Figures 2.1 and 2.2 show the basic components and principles of positive- and negative-pressure conveyance systems, respectively. In a positive pressure system the absolute pressure of the conveying gas in the piping system is always greater than atmospheric pressure. The positive pressure system is the most common conveyance system, particularly in systems in which the bulk solids are conveyed from a single source to multiple receivers. The second most common type of conveyance systems is a negative pressure, or vacuum conveyance system. Much like a vacuum cleaner, the pressure in the conveying line is less than atmospheric pressure. The negative pressure induces an airflow, which subsequently moves the bulk solids. The negative pressure system is typically used in cases where there is a single receiving point from multiple sources, or in situations where dust control is required.

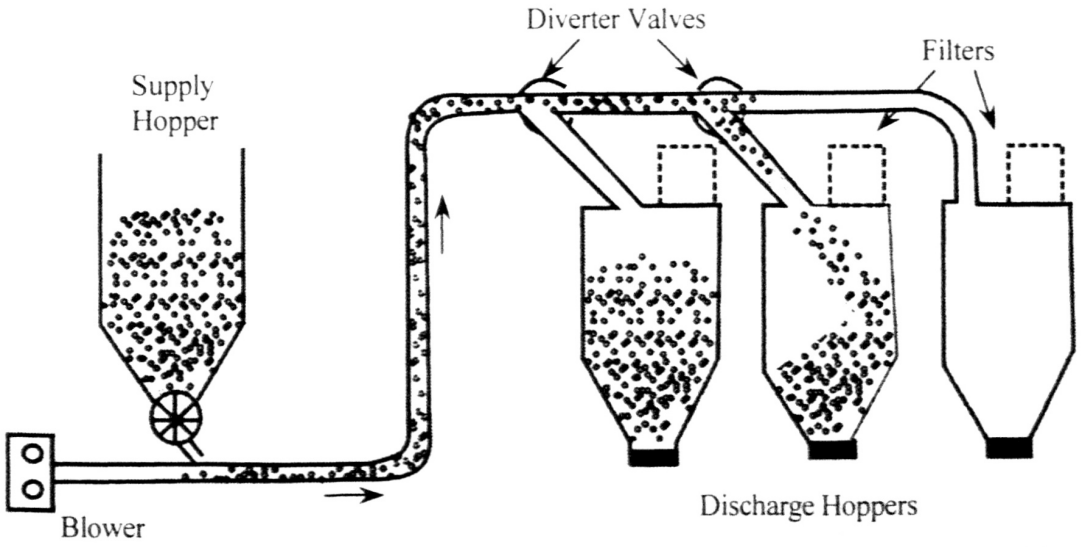

Figure 2.1. Positive pressure pneumatic conveying system (Mills et al. 2004).

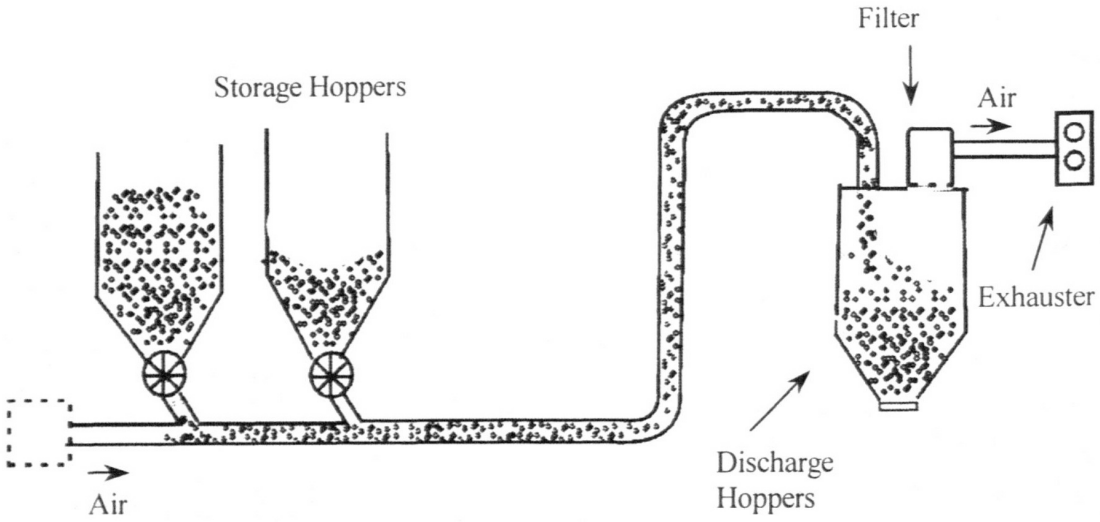

Figure 2.2. Negative pressure (vacuum) pneumatic conveying system (Mills et al. 2004).

The second classification of pneumatic conveyance systems is based on the interactions of the bulk solids contained in the pipeline, which are dilute phase and dense phase pneumatic conveyance systems. In dilute phase pneumatic conveying, a large volume of air moving at a high velocity transports the particulates in a suspended manner. The velocity of the air is sufficiently high enough to keep the bulk solids suspended. Conversely, a dense phase conveyance system transports the bulk solids, in which the bulk solids accumulate at the bottom of the conveyance pipe, in the form of a slug or strands. Often a pneumatic conveyance system will experience both dilute and dense flow regimes. Figure 2.3 shows the variability of the flow regimes experienced in a pneumatic conveyance system. Although the distinction between dilute and dense flow is not well defined, it is typically based upon the flow region in which the flow condition shifts from steady (dilute or lean) to unsteady (slug or plug) flow.

Previous experience in pneumatic conveyance system design indicates the presence of different flow regimes is due to variations in gas velocity, bulk solids mass flow rate, and conveyance line pressure drop. The following sections will discuss in greater detail how pneumatic conveyance systems are designed to account for these properties and variations. Figure 2.4 displays the Zenz diagram that compares the varying flow regimes between dilute flow, slug flow and plug flow (Fokeer 2006).

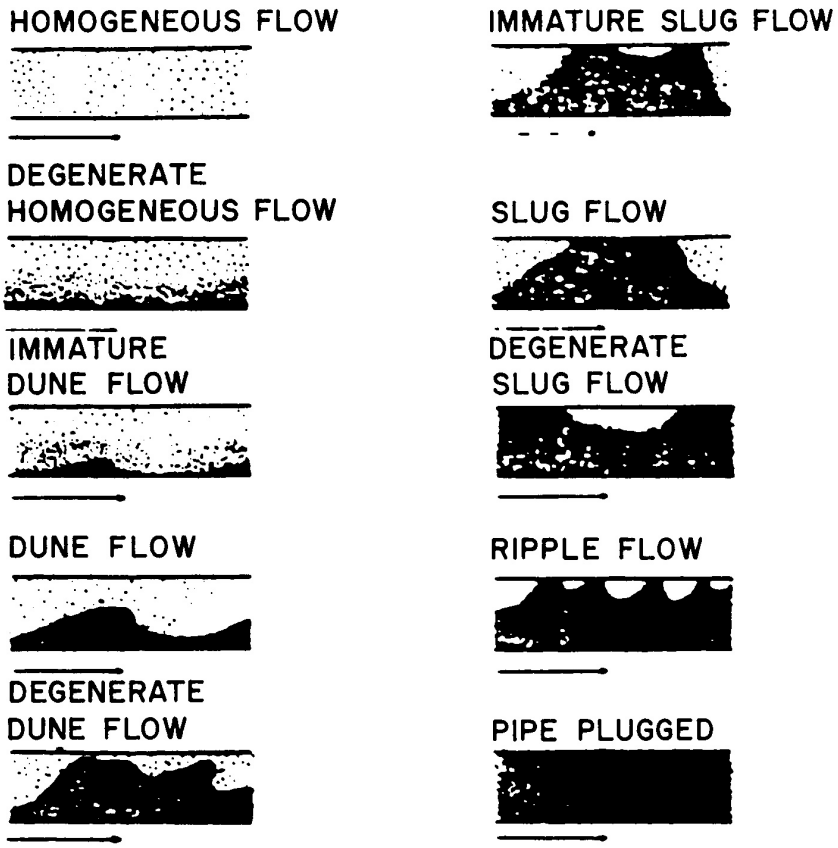

Figure 2.3. Flow patterns in a horizontal pipe (Klinzing 1997).

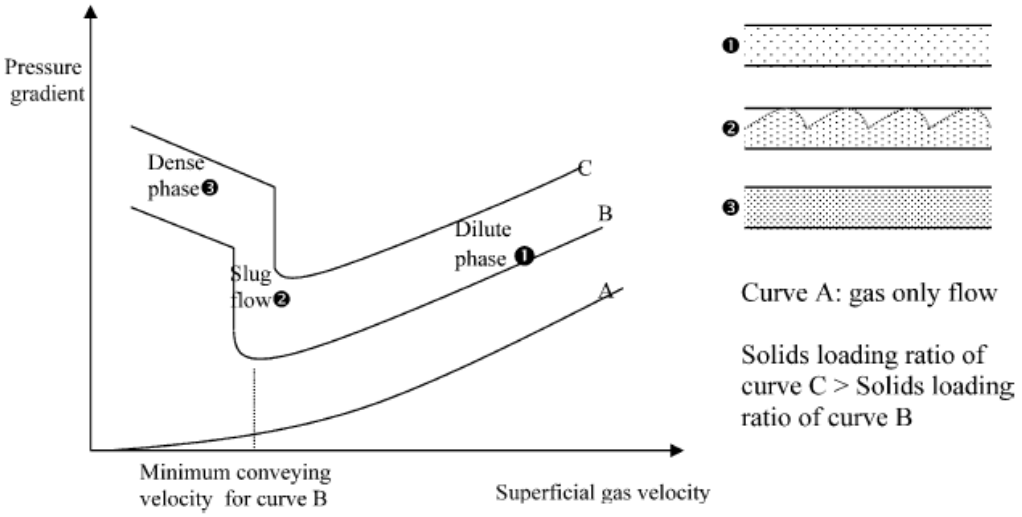

Figure 2.4. Generalized Zenz diagram for horizontal conveyance systems (Fokeer 2006).

From studying the Zenz diagram, we can draw several observations about the behavior of bulk solids in pneumatic conveyance systems. The most striking observation is the pressure gradient curves among the varying loading conditions, Curve A (air/gas only flow) has a significantly smaller pressure gradient curve than Curves B and C (C having a greater solids loading ratio than B). In addition, the Zenz diagram indicates that the minimum conveying velocity for a low solids loading ratio is slightly less than that of one with a higher solids loading ratio. Also, the differential velocity between slug flow and dense phase flow is significantly less than the differential velocity between the slug flow and the dilute phase flow.

This indicates that there is a small threshold between a developing slug flow and a dense phase flow, often indicating a plugging situation. Furthermore, the Zenz diagram shows that as a slug develops into a dense phase flow situation, the pressure gradient increases as the gas velocity decreases. This effect indicates that the flow of the bulk solids cannot be maintained if the superficial gas velocity is not sustained above a threshold velocity.

2.2. Survey of Gas-Solid Flows in Pneumatic Conveyance Systems

In pneumatic conveyance systems, an air mover induces airflow within a transport system in which bulk solids are entrained in the free air stream. Particle sizes transported pneumatically range from microns to centimeters in diameter. Although pneumatic conveying is simple in principle, there are several drawbacks in its use and implementation, which include high specific power consumption, particle breakage because of degradation, abrasion and wear on components, limited transport distances, and potential plugging. Often,

the transport system has features such as bends, and the product is required to flow through these bends. The inertial and drag forces then indicate where the particles will impact the wall at a bend and how the particles will react upon and after impact with the wall.

Pneumatic conveyance processes are influenced by several physical phenomena, including particle sedimentation, inter-particle collisions, lift and drag forces, and the presence of particles. These phenomena induce changes in the turbulence structure in the carrier fluid (Kartushinsky and Michaelides 2007). Large or heavy entrained particles in gas-solid flows have higher inertial effects, and these inertial effects play a dominant role in the particle trajectories. However, for smaller or lighter particles, the drag and the inertial forces are more equal (Fan and Zhu 2004).

2.2.1. Terminology of Pneumatic Conveyance Systems

Pneumatic conveyance has a well-defined set of descriptions that are specific to this field. These are described below and are used throughout the discussion. These definitions are adopted from the Pocket Glossary of Pneumatic Conveying Terms, Conveyor Equipment Manufacturers Association (CEMA) Standard 805 (Reinfried date unknown).

Flow Rate Definitions

The *bulk solids' mass flowrate* is the mass of the bulk solids conveyed over a specific time period, usually expressed in tons per hour or pounds per minute. This is also referred to as the *conveying rate* or the *system capacity*. The *volumetric gas flow rate* is expressed as free air delivered (FAD) through the conveyance system. Most air movers are specified as FAD, which is measured in standard cubic feet per minute (SCFM). The SCFM is the air

volumetric flow rate at standard atmospheric conditions (barometric pressure at sea level, temperature at 68ºF (20ºC) and 36% relative humidity), while the actual cubic feet per minute (ACFM) is the air volumetric flow rate at the operating conditions at the gas mover.

The *solids-to-air ratio* is the ratio of the mass of bulk solids conveyed to the mass of air conveyed. Other terms that are used interchangeably include *phase density*, *solids loading ratio*, and *mass flow ratio*.

Velocity Definitions

The *actual gas velocity* is the conveying gas's volumetric flow rate at pressure and temperature conditions per unit of a cross sectional area of the pipe. This is normally expressed in unit distance over unit time. The actual gas velocity can vary throughout the pipeline's entire length. This compares with the pneumatic system's *average gas velocity* (or *mean gas velocity*), which is defined as the mean of the beginning gas velocity and the terminal gas velocity, while the *bulk solids velocity* is the velocity of the bulk solids and is typically lower than the gas velocity. The bulk solids velocity is usually specified as a mean velocity or terminal velocity. It should be noted that the actual bulk solids velocity is typically estimated because no reliable way to measure it currently exists.

The bulk solids' *saltation velocity* is the gas velocity in a horizontal pipeline at which particles mixed homogeneously with the conveying gas will begin to fall out of the gas stream, while the bulk solids *choking velocity* is the gas velocity in a vertical pipeline at which the particles mixed homogeneously with the conveying gas will settle out of the gas stream. Related to the saltation velocity is the *minimum conveying velocity*, which is the lowest gas velocity that can be used to ensure stable pneumatic conveying conditions for the

bulk solids. Since the minimum conveying velocity occurs at the system's feed point, this velocity is also known as the *pickup velocity*. The *terminal gas velocity* is the velocity of the gas as it exits the system. This is also referred to as the *ending gas velocity* or the *conveying line exit velocity*. This contrasts with the *flotation velocity*, which is the velocity at which bulk solids will be suspended in a gas.

Pressure Drop Definitions

The *conveying pressure* for a pneumatic system is the pressure required to overcome resistance in the system caused by the interactions between the conveying gas, the conveyed bulk solids, the pipeline, and other system components. This resistance is also referred to as the *pressure drop*, or the difference in the pressure between the beginning and the end of the conveyance system. This pressure drop is directly correlated to the power required to convey the bulk solids.

Bulk Solids Properties

A bulk solids' *loose bulk density* (also known as the *poured bulk density*) is the initial weight per unit volume measured when a sample is in a loose, non-compacted condition. The loose bulk density is slightly less than the bulk solids *packed bulk density*, which is measured after the bulk solids have been packed or compacted in a silo, bin, or other container. Since the packed bulk density does not compare with the conditions found in a pneumatic conveyance system, the loose bulk density is used for the system design. The *fluidized bulk density* is the apparent bulk density of a material in its fluidized state and is generally lower

than either the loose or packed bulk density because air is entrained in the voids between the fluidized particles.

A bulk solids' *particle size distribution* is a tabulation of the percentage of particles by mass in each particle size range. The percentage is either that of passing or of being retained on a screen with a specified aperture size. The *maximum particle size* is the maximum lump dimension for lumpy bulk solids; for a bulk powder or granule, it is the maximum sieve size of the largest lump or particle. The *medium particle size* is the particle size distribution's median size or midpoint.

A bulk solids' *flowability* is the ease at which the bulk solids flows by gravity alone, while a bulk solids *cohesiveness* is the bulk solids tendency to adhere to itself. This cohesiveness can be caused by any number of phenomena, including electrostatic charging, surface tension effects, and interlocking of certain particle shapes, particularly fibrous shapes. This cohesion can cause erratic flow from bins, pipeline feeding problems, and adhesion to other surfaces. *Aeration* is the introduction of air to the bulk solids by any means. The aeration can cause the bulk solids to become agitated or fluidized. The bulk solids' *air retention* is its ability to retain air in the voids between particles after the air supply has been stopped. The time the bulk solids retains air can very from almost no time to several days, depending on the bulk solids other characteristics.

In general, it has been determined that the following characteristics affect the conveying of bulk solids:

1. particle size and distribution,
2. particle shape,
3. bulk density,
4. particle density,
5. flow permeability,

6. de-aeration rate and air-retention,
7. surface characteristics: sticky, wet, cohesive, and electrostatic charging, and
8. temperature sensitivity (hardness, modulus, and surface tackiness).

(Crowe 2006).

2.2.2. Current Design Process of Pneumatic Conveyance Systems

The design of pneumatic conveyance systems is a complicated, interrelated design in which every component in the system has an effect on the behavior on the remaining system. In designing pneumatic systems, several handbooks and empirically determined correlations are utilized to help guide the designer in predicting the performance characteristics of the system.

The flow charts in Figures 2.5 and 2.6 demonstrate the current procedures for designing pneumatic conveyance systems. If a designer were to design a new pneumatic conveyance system, they would follow the flow chart shown in Figure 2.5. When developing a new pneumatic conveyance system, the designer considers the desired mass flow rate of bulk solids, as well as the conveyance length and the geometry required in the system (bends, etc.). With this information, the designer can then determine if the desired mass flow rate can be conveyed with the specified pipeline bore and length. The feasibility check is the power requirement for the system, which is based on the pressure drop through the system. The most difficult part of this design process is to have a fundamental understanding of the conveying characteristics of the bulk solids. These characteristics include flowability, aeration rate and air retention, cohesiveness, etc. Often, these characteristics are difficult to quantify, and the bulk solids properties can have a significant impact on the pressure drop, air velocity, and other flow conditions.

Although much research has been done to quantify several bulk solids conveying characteristics, this stage presents a significant challenge in designing systems that are required to accommodate a variety of bulk solids. To further complicate the design process of new conveyance systems, the variability of bulk solids can also have a significant impact on the flow conditions of the system. The differences in the conveying characteristics of the bulk solids could mean the difference between having a conveyance system that operates in a reliable manner and one that cannot convey to the expected capacity. Therefore, designing new conveyance systems is an iterative process in which each component is sized and system performance is evaluated until a functional design is found.

Conversely, if a designer would like to determine the capability of an existing pneumatic conveyance system, they would follow the flow chart outlined in Figure 2.6. Rather than specifying a desired bulk solids mass flow rate, this procedure estimates the predicted bulk solids mass flow rate that can be achieved by the pneumatic conveyance system. In this scenario, the designer has the advantage of having prior knowledge of the conveyance system, particularly for the conditions at the boundaries and of the length and diameter of the conveyance pipe.

Although the flow charts given above appear to be relatively straightforward, they can still lead to an inefficient or improper design. In addition, the procedures considered in the flow charts may offer limited or incorrect insight to the designed system. The current procedures take the entire system into account, but are unable to provide performance information at certain locations of the system. For example, there could be a significant bottleneck in the conveying line that can be resolved by redesigning or

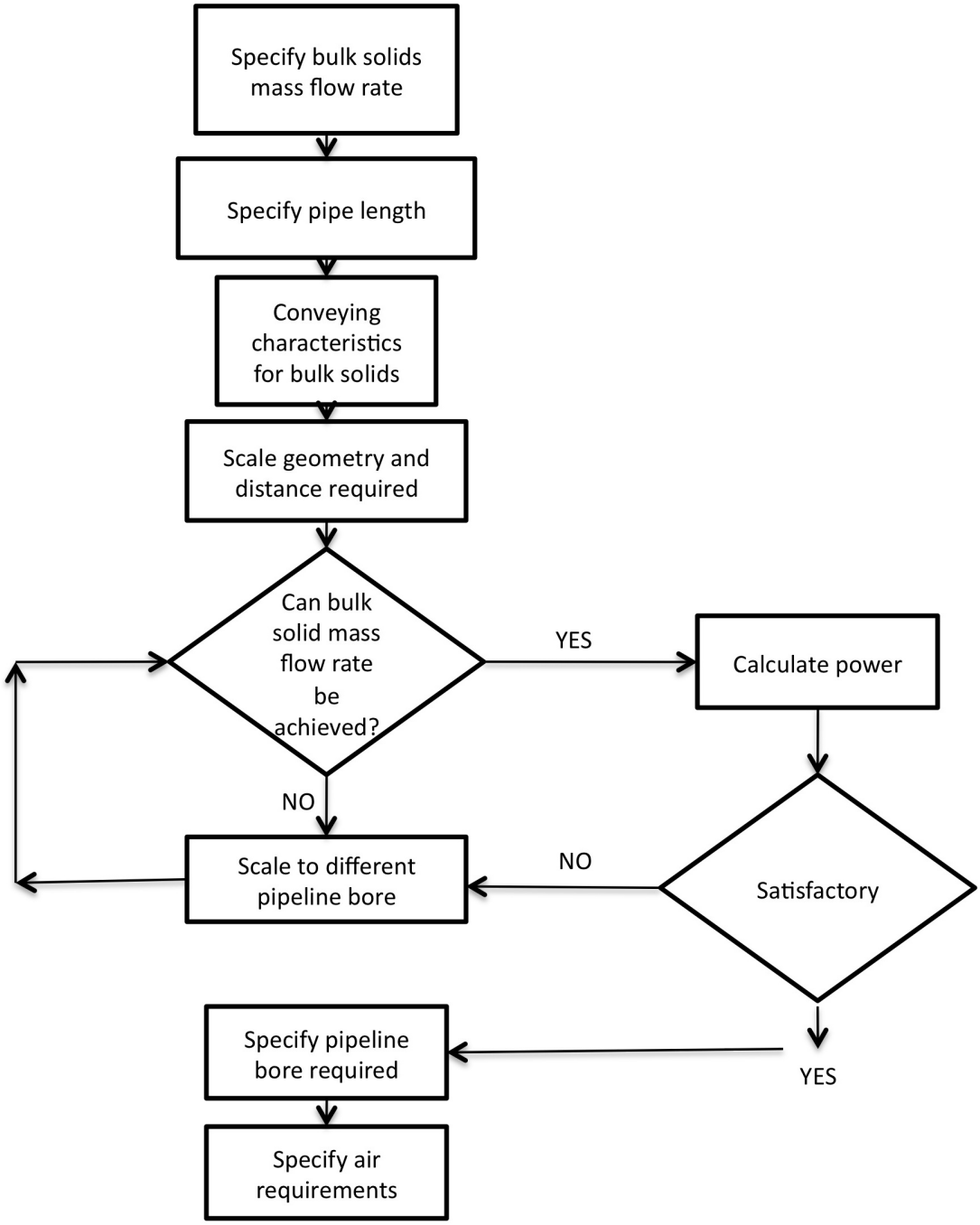

Figure 2.5. Flow chart for designing new pneumatic conveying systems (Mills 2004).

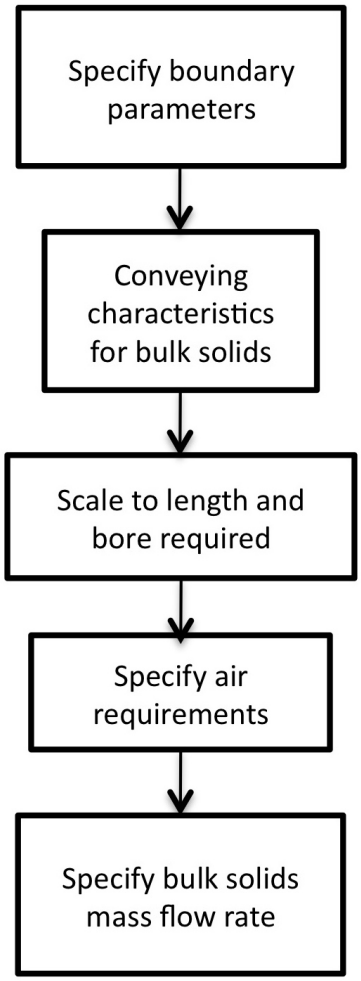

Figure 2.6. Flow chart for predicting the capability of existing system (Mills 2004).

rescaling the location of interest. Furthermore, the designs based on these processes would design a nominal conveyance system and would not be able to offer insight about any instability that may occur in the system. For instance, a conveyance system may have the ability to convey bulk solids without any issues, but once an anomaly is presented, the system may fail.

Studying Pressure Losses of Pneumatic Systems

Another technique used to predict the performance of pneumatic conveyance systems is to experimentally measure pressure drops through the pneumatic ducting based on airflow rates and bulk solids loading conditions. The data provides guidelines for the performance limits of the system and can be used to generalize trends for the transportability of various bulk solids. Figure 2.7 shows an example of an experimental apparatus in which a variety of bulk solids are conveyed through a test loop at various air volumetric flow rates. The pressure drop through the system is recorded based on various bulk solids, as well as the bulk solids mass flow rates, and air volumetric flow rates.

Figures 2.8 and 2.9 show the pressure drop trends of powdered cement and sandy alumina, respectively. For each bulk solids tested, the pressure drop curves are compared with the pressure drop curve of only air flowing through the system. Intuitively, the air-only flow cases would have the lowest pressure drop, while the increased loading of bulk solids would increase the pressure drop. What may not be intuitive is how differently the pressure drop curves are based on the type of bulk solids. For instance, a conveyance system configuration that is able to convey 17,500 kg/hr of powdered cement with a pressure drop of less than 200 kPa may only be able to convey half the mass flow

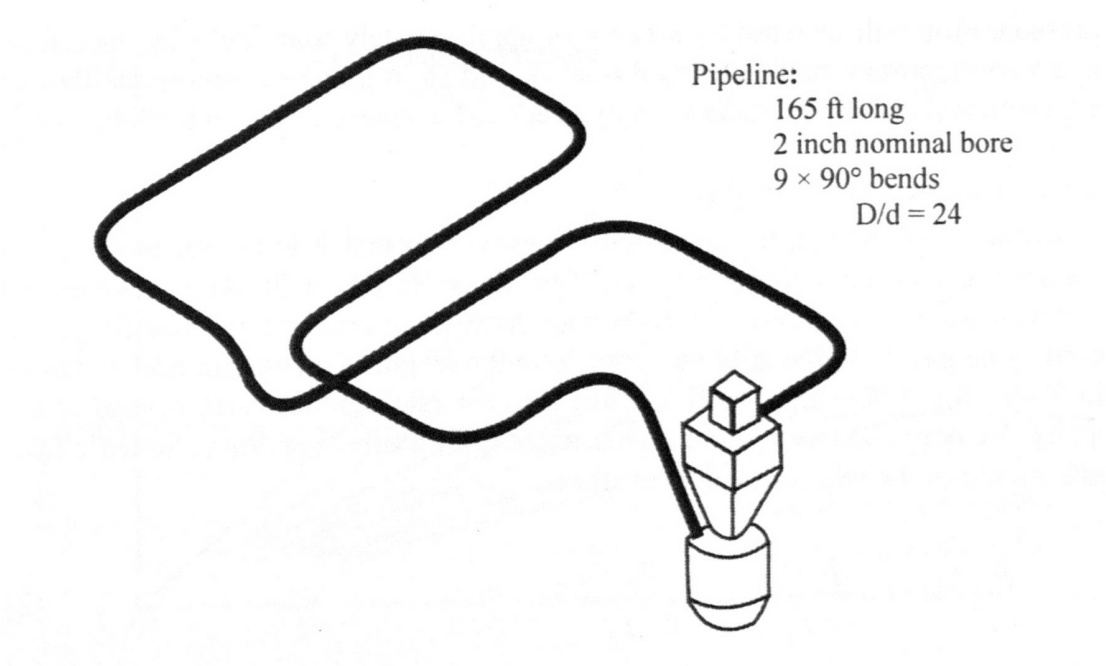

Figure 2.7. Details of pipeline used for conveying trials (Mills et al. 2004).

rate of alumina silica due to the differences in the properties (particle density, characteristic size, and air retention properties) of the bulk solids.

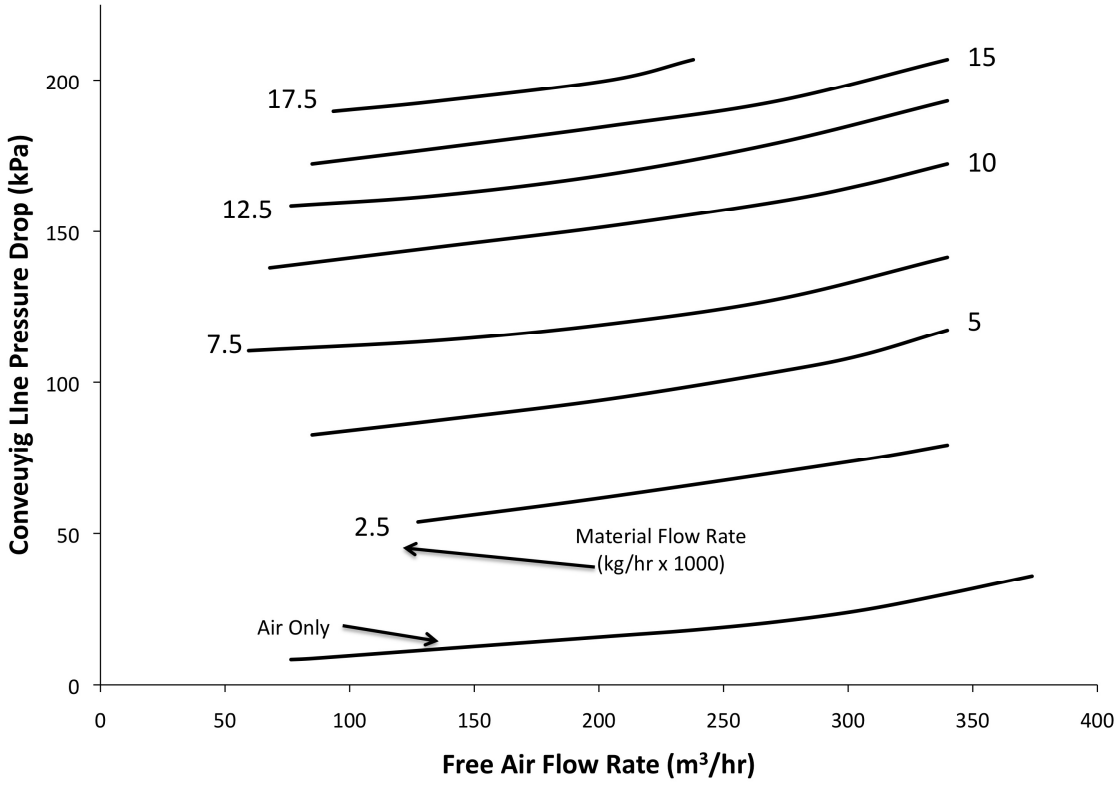

Figure 2.8. Pressure drop data vs. airflow rate data for cement (Mills et al. 2004).

In particular, powdered cement has good air retention properties and is capable of being conveyed at slower velocities in sliding dune flow. Coarse bulk solids, such as alumina silica, have a granular particle structure and have low air retention and permeability. Due to the low air retention and permeability, coarse bulk solids are generally only capable of being conveyed in dilute phase suspension in pneumatic conveyance systems. Therefore the air volumetric flow rate must be significantly greater for alumina silica than cement powder.

Without having a priori knowledge of the pressure drop trends for specific bulk solids, one would find it difficult to design conveyance systems for different bulk solids.

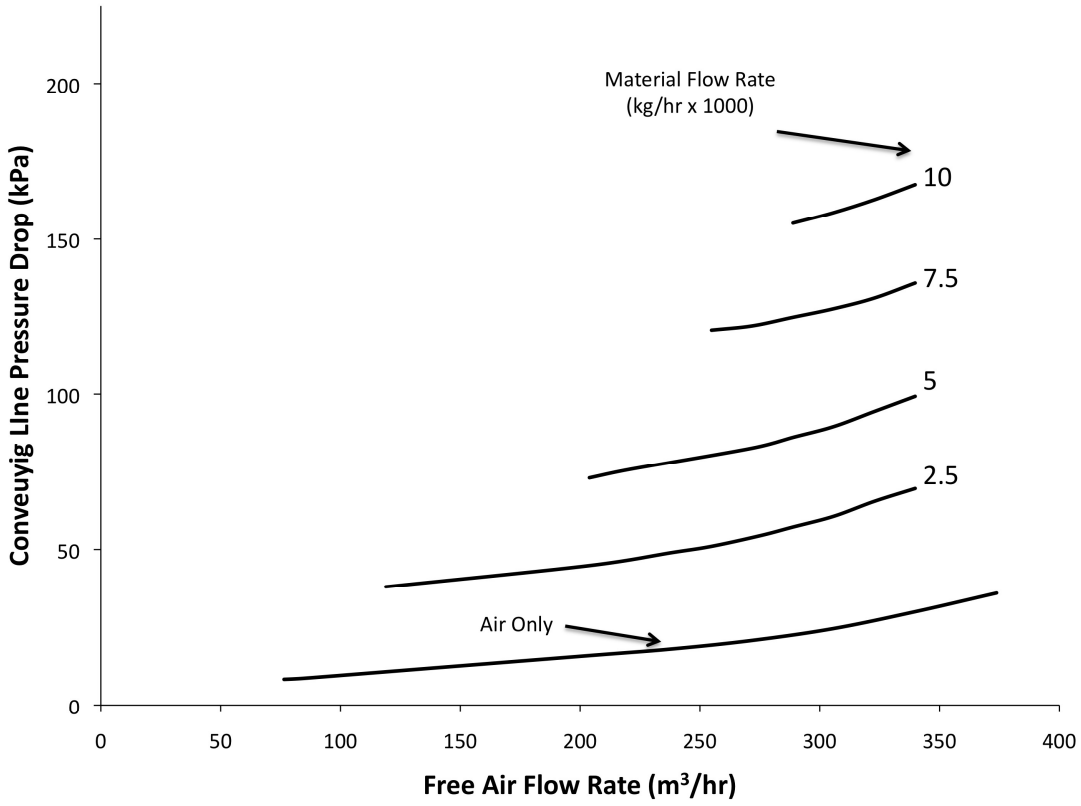

Figure 2.9. Pressure drop vs. airflow rate for sandy alumina (Mills et al. 2004).

Another method that is commonly used to predict conveyance performance is to compare the solids loading ratio of the bulk solids to determine the conveying limits of bulk solids. Representing the information in this manner can provide a designer with additional information about the minimum conveying airflow rate for a specific solids loading condition. Figure 2.10 compares the conveying line pressure drop of powdered cement based on solid loading ratio rather than a mass flow rate of bulk solids. However, rather than

specifying the curves as a mass flow rate, they are specified as the bulk solids loading ratio. Another interesting feature in Figures 2.10 and 2.11 are the respective convening limit curve for the bulk solids in the system. To the left of the bold curve is referred to as the “no go area” in which the conveying line velocity would become low enough that the bulk solids would drop out of the free airstream and would accumulate at the bottom of the pipe, creating slugs and plugs. Another interesting feature of this graph is that the bold line for the “no go area” boundary is not straight. Rather it meanders, indicating that as the solids loading ratio increases (which is proportional to the mass flow rate of bulk solids) the free airflow rate can decrease while still providing adequate conveying characteristics. This shift is due to two effects. The first is due to the reduction of the volume occupied by the air due to the increased presence of the bulk solids. The second is related to the first. As the pneumatic pipeline becomes more heavily loaded with bulk solids, the likelihood of dune and slug flow increases, and these moving masses will push any non-moving bulk solids along. This phenomenon has been observed when comparing the pickup velocities of bulk solids in dilute flows versus dense flows.

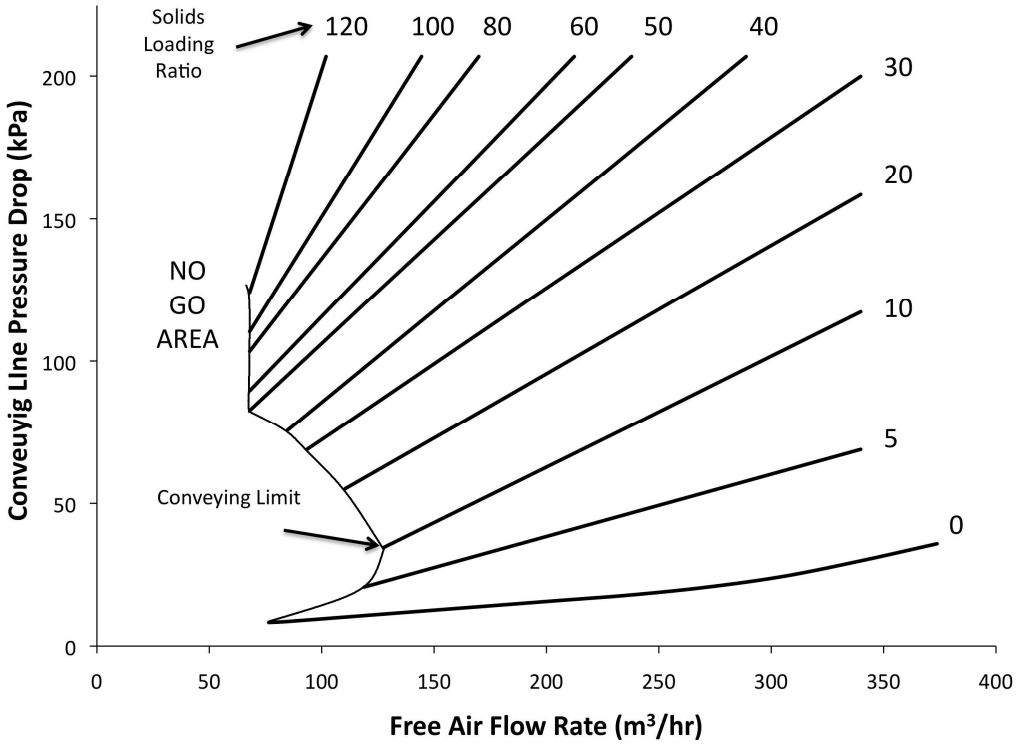

Figure 2.10. Solids loading ratio pressure drop data for cement (Mills et al. 2004).

A third way to examine this information is to have the bulk solid mass flow rate on the ordinate axis and the air flow rate on the abscissa while plotting the solids loading ratio trend lines as well as the conveying line pressure drop trend lines as shown in Figure 2.11. A graph such as this may be useful since it presents the “no go area” boundary as a straight line rather than a curve. This representation of information is better suited to determining trends than the previous representations since all the lines are straight rather than curved.

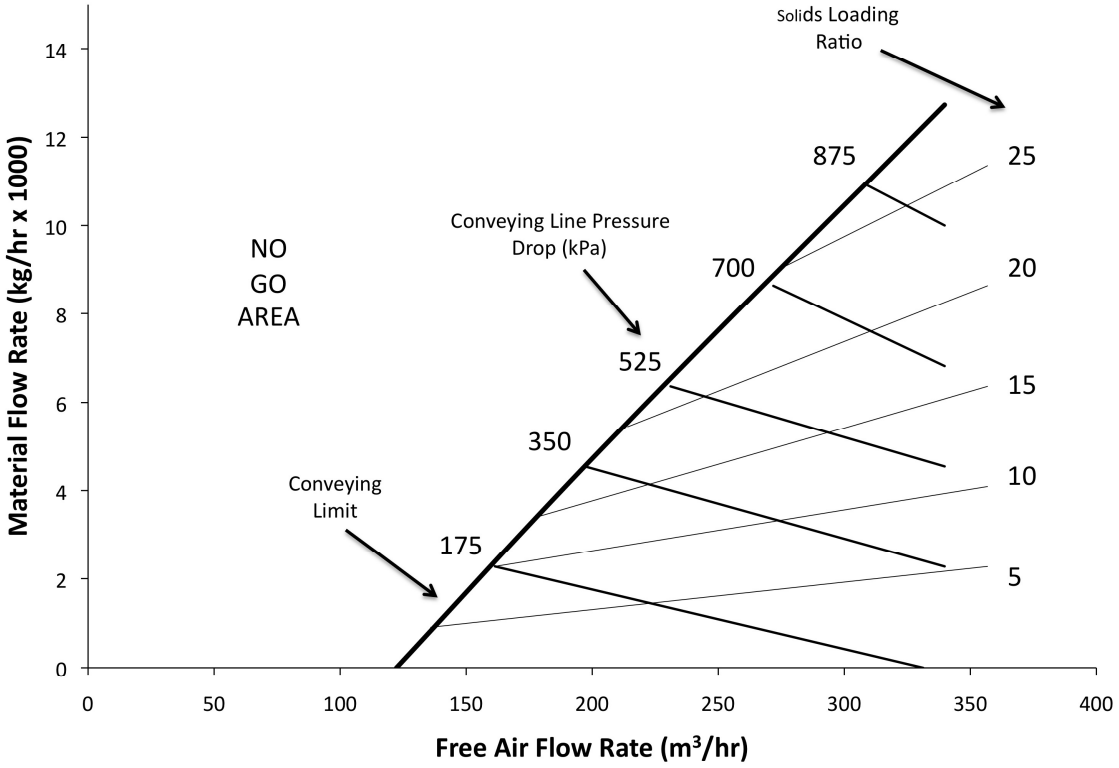

Figure 2.11. Solids loading ratio pressure drop data for sandy alumina (Mills et al. 2004).

Although these types of approaches may be useful in gaining a better understanding of the performance characteristics of pneumatic systems, they are limited in their applications to systems design. Also, these approaches do not allow a designer to predict pipeline wear or predict the behavior of non-standard piping configurations, particularly in bends, expansions, etc. The pressure drop curves are based upon a specific experimental pipeline configuration and on previously tested bulk solids within that pipeline. However, if one wanted to develop pressure drop curves for a new conveyance pipeline and/or for new bulk solids, they would

need to run a series of experiments and measure the pressure drop. This proves to be a time-consuming and tedious process. Later in this study, it is proposed that the pressure drop curves may be recreated computationally rather than experimentally for fibrous-based flows, and the computational models may be extended to new and interesting design problems.

2.3. Pneumatic Systems: Review of Experimental-Based Research

Pneumatic conveying design has relied upon empirical correlations, physical prototypes, and laboratory experiments to gain a better understanding of flow phenomena. Often, the goal of these experiments was to derive generalized relationships and correlations to describe the flow characteristic, pressure losses, and velocity profiles, which can then be applied to specific bulk solids and pneumatic conveyance systems configurations. This section offers a brief review of the experimental research and design of pneumatic conveyance systems.

Much of the early research done on pneumatic systems involved agricultural commodities. Segler (1952) compiled empirically derived data to classify systems that convey agricultural grains within positive and negative pressure systems. This work built upon the resistive effects of fluids flowing through pipes, λ, and he developed correlations and relationships that accounted for the additional resistive effects of the bulk solids being conveyed in the pipe, λG. An example of describing the extra resistance from the bulk solids and how it relates to a given pipe diameter is given in Figure 2.12. Notice that the resistive effects of the friction between the grain and the air are significant, particularly when the pipe diameter is small. These findings are useful in developing generalized rules of thumb for

designing grain conveyance systems, and make the pneumatic systems designers and operators more aware of the effects of pneumatic system configurations.

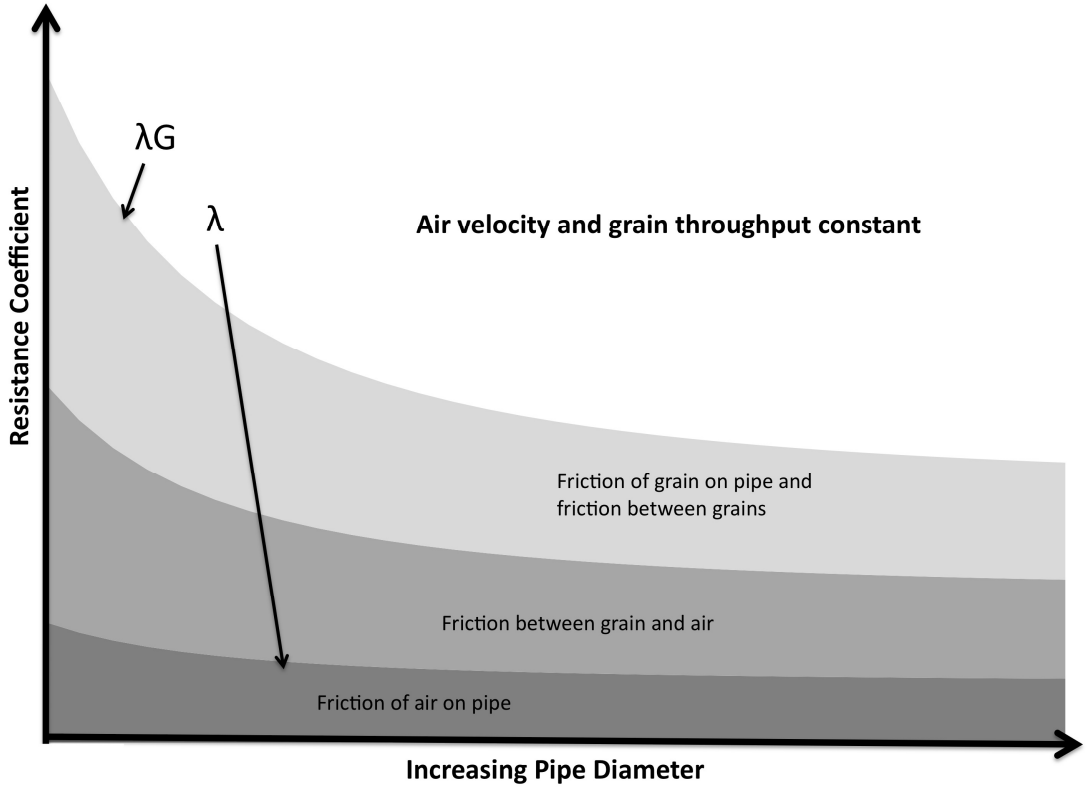

Figure 2.12. Distribution of friction when conveying bulk solids (Segler 1952).

Later on, pneumatic systems design became more widespread in the industrial applications, and design guides or handbooks were compiled to help designers configure and scale pneumatic systems for conveying industrial products such as powdered cement, glass beads, sand, etc, as well as agricultural commodities. In 1980, Kraus wrote a book investigating the design theory and procedures for pneumatic conveyance design, with a significant portion of the literature related to the flow characteristics of grains and agricultural bulk solids. An example of the work Kraus performed involves the pressure drop

increases of wheat and other grains for various bulk solids loading conditions. This was a significant advancement to Segler (1952) because it quantified specific bulk solids to a pressure drop increase for particular pneumatic system configurations. An example of the graphical relationships developed is shown in Figure 2.13, which correlates the specific pressure drop for wheat at various solid-to-air ratios and air velocities. This, and much of the correlation information compiled in these design guides are based upon data collected from the authors and from other commercial vendors of pneumatic systems. Up to this point, most of the quantitative information collected on pneumatic systems was based on pressure readings obtained for various air volumetric flow rates, air velocities and solids loading ratios. While this information can be used for generalized design of systems, there is insufficient information to predict plugging, wear, and other critical flow issues. This leads to overdesign and limits the application of pneumatic conveyance to new bulk solids.

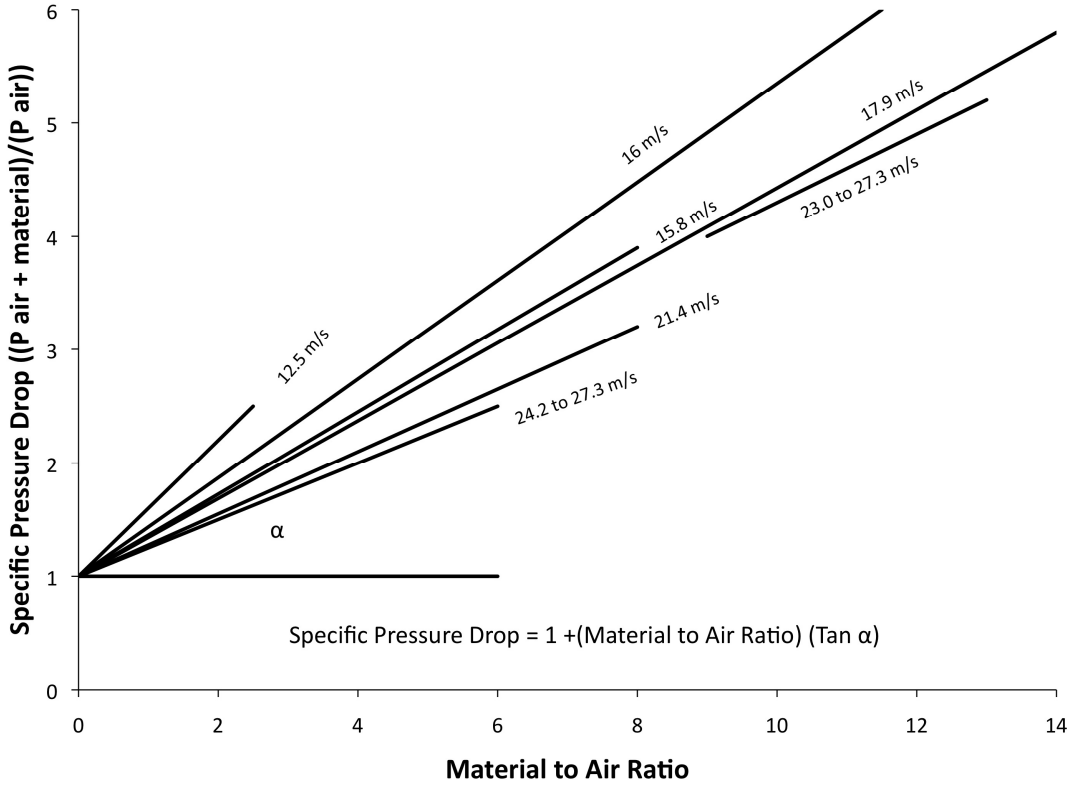

Figure 2.13. Test results for conveying wheat (Kraus 1980).

Beginning in the early 1980s, researchers had begun to visually study the velocity profiles of bulk solids flowing through pneumatic systems. This was due to the availability of non-intrusive measuring equipment. For example, Thorn et al. (1982) studied non-intrusive methods for determining velocities within pneumatic conveying systems using Doppler techniques, laser, microwaves and ultrasound. Others have followed suit by utilizing high-speed videos and particle image velocimetry (PIV) data to investigate the flow behavior of bulk solids. Deloughry et al. (2001) utilized compiled tomography imaging to study the flow regimes in pneumatic conveyance systems. They concluded that the flow regime present in a

conveyance system is dependant upon the size and shape of the particles, the geometry and orientation of the pipe, the relative densities of the solid particle and air, the conveyance velocity and the mass flow rate of the bulk solids. However, visualization of multiphase flow becomes increasingly difficult when the flow velocity is high or when it is difficult to distinguish the particle trajectories because of the large number of particles.

In the 1990s pneumatic transport of bulk solids became of increasing interest in research. These efforts attempted to segregate and classify the flow characterizes of bulk solids based on experimental observations. For his Ph.D. research in 1993, Ocone (2006) investigated the effects of flow rate, pipe inclination angles, and pipe diameter on the flow behaviors in horizontal and inclined pipes, while Bradley et al. (1995) studied the pressure drop in bends of various radii using pressure transducers. They concluded that the change in pressure due to a bend occurred in the straight section after a bend rather than the bend itself. This is due to the reacceleration of solid particles within the airstream. Littman et al. (1995) studied the flow of glass spheres and rapeseeds (a type of canola seed) within a vertical pneumatic channel and had developed drag correlations for these bulk solids that accounted for the particle diameter, particle density, and loading ratio. Laouar and Molodtsof (1998) examined sand particles within a horizontal transport duct to characterize the pressure drop of dense phase pneumatic transport at a low velocity and developed general pressure drop correlations for a carrier gas superficial velocity of less than 2 m/s, particle diameter of 0.2 mm, and a particle density of 2,700 kg/m^3. These efforts resulted in significant increases in the understanding of pneumatic conveyance of particles, but were limited to simple bend, inclines and straight-line pipe configurations with slow-moving air conveyance velocities and very small (near powder-size) particles.

Another aspect that had gained attention in pneumatic conveyance is the effect of the transported bulk solids on the piping. Burnet et al. (1998) studied the erosive wear on bends in pneumatic systems due to the interactions with the bulk solids. Ferreira et al. (2000) proposed new approaches to experimentally determine the interaction forces in hydraulic and pneumatic systems, with the goal to be able to predict the pressure gradients in conveyance systems. Schallert and Levy (2000) had experimentally and numerically studied the effects of coal roping. They had determined that as air and particles flow through an elbow, the particles stratify into a relatively small portion of the cross-section of the pipe, forming a dense rope-like structure. Once formed, the rope gradually disperses and mixes throughout the cross section of the pipe due to flow turbulence and secondary flows. In situations in which two or more closely spaced elbows are present, the dynamics of the coal rope leaving the last elbow is much more complicated.

At the beginning of this decade, the focus of experimental pneumatic conveyance research transitioned to the investigation of slightly larger particles with higher particle loading, as well as electrostatic effects. Hyder et al. (2000) investigated the effects of pressure drop in horizontal pneumatic pipes due to particle sizes in suspension flow. They found that the pressure drop increases with increasing particle size. The degree of the increase tends to be the largest towards the smaller particle size, and diminishes with particle size increase and with increased transport velocities.

Yilmaz and Levy (2001) studied lean phase upward flow in a vertical pneumatic conveying line following a horizontal to vertical elbow. They studied pulverized coal particles (less than 75 μm in diameter) in an experimental apparatus that measured particle velocities, concentration and mass fluxes with a fiber optic probe within the pipe. The

experimental results were compared with CFD simulations of gas-solid turbulent flow based on a Lagrangian-Eulerian model particle source-in-cell method.

Jaworski and Dyakowski (2002) studied flow instabilities, which include slugs and plugs, in dense-phase pneumatic conveyance systems with high-speed video cameras and twin-plane electrical capacitance photography. The data collected by these devices was processed to determine the shape and internal structure of the flow instability, the propagation velocity and frequency characteristics.

Das and Meloy (2002) studied the effects of close coupled bends in the pneumatic conveying process of fly ash and concluded that the pressure loss across two close-coupled 90 degree elbows cannot be considered as the cumulative effect of two isolated single bends. Hayden et al. (2003) experimentally investigated the effects of particle characteristics on the pickup velocity required to entrain in airflow. They concluded that pickup velocity is highly correlated to particle diameters between 5 and 200 μm.

One of the first detailed studies of fibrous-based bulk solids was performed relatively recently. Melander and Rasmuson (2004) developed a method to simultaneously measure the concentration and the velocity of wood fibers in pneumatic transport. The velocity was determined with the use of particle image velocimetry and the wood fiber concentration was measured from the raw PIV images. This method gave favorable qualitative and quantitative results for low fiber volume fractions, but the results were less favorable for high volume fractions due to the laser sheet not being able to penetrate the fiber suspension. In this study, they determined that the gas velocity profile was strongly affected by the volume fraction of the bulk solids. However, they determined that an improved method was needed to simultaneously measure the velocities of both the gas and fiber phases.

Hirota et al. (2002) concluded through experimental and modeling approaches that the pressure drop for conveying fine polypropylene powders through inclined pipes depends on the dynamic coefficient of friction of the powder as well as the inclination of the pipe. Zhu et al. (2006) have observed the dispersed, plug, eroding dunes and other various flow regimes in pneumatic conveying through vertical and inclined pipes.

Xiang and McGlinchey (2004) researched various effects of dense phase pneumatic conveying through horizontal pipes such as plug formation, collapse and movement with numerical simulations. Li et al. (2005) studied solids behavior in slug flow through a horizontal pipe and observed exchange of particles between the layer of deposited particles and the moving slug. However, this research determined that additional flow patterns might be due to electrostatic charge generation within a pneumatic conveyance system.

Kalman et al. (2005) experimentally investigated the pickup velocity (critical velocity) measurements of 24 various bulk solids, including glass, zirconium, alumina, iron, salt, and rice, while Kiliçkan and Guner (2005) investigated the pneumatic conveyance characteristics of delinted and fuzzy cottonseeds. Datta and Ratnayaka (2005) performed experimental studies to predict a pressure drop coefficient for horizontal and vertical channels using alumina and silica as the bulk solids, while Du et al. (2006) had used Phase Doppler Particle Analyzer (PBPA) to measure the size and velocity of particles flowing through a gas-solid separator.

Henthorn et al. (2005) performed a study to validate the pressure drop correlations commonly applied to CFD and compared them to experimental data for vertical channels. They concluded that the most notable deficiency in pressure drop correlations was the inability to accurately predict the pressure drop of gas-solid flows with highly aspherical

particles. This indicates that non-spherical particles are difficult to predict computationally compared to spherical particles, which highlights one of the significant challenges in fibrous flows. To help alleviate these discrepancies, Carruthers and Filippone (2005) investigated the aerodynamic drag on non-spherical objects, which include streamers and flags while Chen et al. (2006) investigated the flow around spheres due to dissipative particle dynamics.

In the last two years, research has been done to further investigate slug and plug flows within pneumatic conveyance systems, and how they may be represented. Tan et al. (2008) had performed an experimental study in which they measured the permeability of slugs traveling through a horizontal pipe. The authors state that a slug is viewed as a packed bed, and the pressure drop over the slug is represented by the Ergun equation or other empirical correlations. In this study, they measured the pressure gradient of slugs consisting of plastic pellets, dried peas, whole corn, hard wheat, and grain seed mixtures. With this information, they calculated the constants for the Ergun equations for these bulk solids. The premise of this is to use these coefficients with CFD solvers to predict pressure drops due to the presence of these bulk solids. This was a significant advancement in predicting non-standard flow regimes and has many parallels with the research discussed in this dissertation.

Also in the last two years, there has been a greater emphasis in studying the transient effects of dense multiphase flows. Williams et al. (2008) studied dense phase pneumatic conveying under the hypothesis that transient effects rather than steady state effects dominate the flow mechanism. Their study characterized the gas phase pulse velocity, pulse amplitude, and velocity and their effect on powder flows. Although the findings of this research seem reasonable, they are in many respects trivial. For example, they indicate how much we do not understand about the various phenomena occurring in multiphase flows, much less how to

analytically or computationally describe the effects for design of multiphase transport systems.

2.4. Pneumatic Systems: Review of Computational-Based Research

Computer modeling in engineering design has become increasingly popular in the last two decades. One modeling tool that has become more widespread is the use of CFD due to its ability to accurately predict the behavior of single-phase flows. However, for the multiphase flow applications found in pneumatic conveyance systems, it is still difficult to accurately predict flow patterns, pressure drops, velocity profiles, etc. Until recently, researchers have not been extensively developing CFD tools that solve the effects of bulk solids flows found in pneumatic conveyance systems. Because of this, CFD is not currently used to design pneumatic conveyance systems. Since computationally based solutions are generally becoming less expensive and more reliable than experimental results for engineering design, it would be advantageous to have viable modeling techniques to analyze the designs of pneumatic conveyance systems. This section offers a brief review of the research performed for computationally modeling of multiphase flows in the context of pneumatic conveyance systems.

Although CFD modeling has been in existence for more than four decades, computational studies of multiphase flows have been present for less than thirty years. The complexities of simulating the effects of each phase and the interactions between each phase make multiphase flows computationally challenging and still demanding of significant computing resources. In addition, many of the multiphase flow modeling codes were only available as research code and were not commercially available. Therefore, researchers had

to develop their own codes to describe their flows of interest. Klinzing (1987) created a continuum model that incorporated electrostatic effects but not frictional forces to analyze the ability to form clusters of particles during pneumatic transport. This model shows that the electrostatic effects of the clusters are influenced by particle size. Sommerfeld and Zivkovic (1992) and Oesterle and Petijean (1993) developed independently a similar stochastic particle-particle collision model that was based on the calculation of a particle collision probability along a particle trajectory in analogy with the kinetic theory of gases. Hong and Tomita (1995) introduced a continuum model to predict the transitions between suspension flow, stable stratified flow, and unstable plug flow in pneumatic conveying types of operation.

Huber and Sommerfeld (1999) summarized the developments of an Eulerian-Lagrangian approach for the calculation of dispersed gas-solid flows in pipe systems. Their calculations included important effects such as turbulence, two-way coupling, particle traverse lift forces, particle-wall collisions, including wall roughness, and interparticle collisions. They had presented results for pipe elements such as horizontal pipes, pipe bends, and vertical pipes for different flow conditions including conveying velocity and particle loading. The predicted modeled values were compared with experimental measurements obtained by phase Doppler anemometry. Nadaoka, Nihei, Yagi (1999) developed a grid-average Lagrangian (GAL) model for dispersed particle motion in multiphase turbulent flow to provide a large eddy simulation (LES) model for multiphase turbulent flow in which a large number of particles are involved. The GAL model is based on an averaging operation for Lagrangian type equations of the motion of a particle over a computational grid volume.

It was not until the late 1990s that commercially available code began to be used to model multiphase flow conditions, For instance, Bilirgen et al. (1998) had modeled turbulent two-phase flow using a commercial CFD computer code (FLOW3D®) to determine how well it was able to predict the flow conditions compared to experimental data. In addition, they argued that because of the complexity of the flows that occur in pneumatic conveying systems, the use of first-principle based modeling techniques has been restricted to the very simplest of cases.

Triesch and Bohnet (2001) developed computational models for predicting particle velocity and bulk solids concentration because an accurate calculation of these quantities is assumed to be important for a reliable prediction of the development of pressure. They used Fluent® to simulate upstream gas-solids flows in pipes and diffusers using the Lagrangian-Eulerian approach for calculating the dispersed phase. These models have been included via subroutines programmed by the user and concerns particle-wall interaction, particle-particle collisions, and particle angular velocity. These additional models included wall roughness, and Magnus and Saffman lift forces.

Sommerfeld (2001) created a stochastic inter-particle collision model for particle-laden flows and applies this model in the framework of the Lagrangian-Eulerian model. The computational particle is a representative of the local particle and exhibits the proper phase properties. In sampling the velocity of the computational particle, correlation with the velocity of the real particle as a consequence of turbulence is accounted for. Sommerfeld (2001) determined that in such particle-laden flows, the particle behavior can be considerably affected by inter-particle collisions in addition to the aerodynamic transport and turbulence

effects. If the mass loading is high, then regions of high concentration develop as a result of the inertial effects (bends, bottom of pipes).

Shrivastava (2002) applied a mathematical model that he developed, along with experimentally obtained correlations to estimate the pressure drops resulting from conveying grains through a horizontal pipe and compared the results with experimental data from his previous research. This model was used to estimate the pressure drop of conveying mustard seeds through horizontal, vertical and inclined pipes. The authors claim the pressure drops were off by less than a factor of 2.

Kilfoil (2003) developed a Matlab™ program for modeling two-phase flow and concluded that CFD software is not essential for modeling complex two-phase flow with heat and mass transfer. Provided that the geometry is relatively simple, any general purpose software that has programming capabilities can be used, and the model is sufficiently reliable for use in both research and system design. The Matlab™ program accounts for heat and mass transfer as well as particle transport with a series of algebraic equations solved sequentially to solve for the three described effects. The algebraic equations are based on the partial differential equations of heat transfer and fluid flow. The authors went so far as to state that CFD is not required to model complex two-phase flow with heat and mass transfer and that Matlab™ is capable of solving engineering design problems.

Also during the early 2000s, Wypych et al. (2003) developed a theoretical model to predict the various transport boundaries between low-velocity flow over a stationary or moving layer in horizontal pneumatic conveying. For his doctoral studies, Rahnayake (2005) formulated a comprehensive scaling up technique for designing pneumatic conveying systems by addressing the whole pipeline together with all accessories. Rahnayake used five

different bulk bulk solids (barytes, bentonite, cement, ilmenite, and alumina). These bulk solids, together with five qualities of one of these bulk solids have been used for the tests. Rahnayake conducted a large number of pneumatic conveying tests for five different pipeline configurations and successfully predicted the pressure drops for these bulk solids using Fluent®.

Landry et al. (2006) modeled the sludge flow in which the air and sludge are stratified and separated by a clear interface. Each computational cell in the model is either filled entirely one or the other phase, except for cells at the interface. Lim, Zhang, and Wang et al. (2007) claimed that they were the first to report the successful reproduction of dune flow in numerical simulations through the use of DEM models coupled with CFD models for granular bulk solids flowing in vertical pipes. The developed models had the capability of predicting the dune flow patterns and the pressure gradient in the pipe with results comparable to experimental results.

Kartushinsky and Michaelides (2007) have developed models that examine the turbulent flow of heavy particles in horizontal channels and pipes that were derived from principles using interparticle collisions. They consider the fluid in an Eulerian frame of reference while the particles are in a continuous polydispersed media of finite particles. The particle collisions are accounted for in the difference in the average and fluctuating velocities of the particles. These particles are characterized by size (diameter) and mass fraction. They modeled the momentum conservation equations of the particle phases in terms of the fluctuation correlations.

Mortensen et al. (2008) developed a direct numerical simulation of ellipsoidal particles suspended in turbulent channel flow and have one-way coupling of the fluid and

particle motion. This was done to study the orientation of the ellipsoidal particles. They predicted that near the wall, the particles orient in the mean flow direction and the flow in the core region of the channel becomes more isotropic.

2.5. CFD Software Packages with Multiphase Capabilities

There are several commercially available CFD solver packages on the market today that have the ability to model basic multiphase flows. Commercially available CFD packages have become increasingly common in the engineering design process due to their robust grid generation, built-in numerical differencing schemes, turbulence modeling and post-processing capabilities. Practically all commercially available CFD packages can solve single-phase fluid flows; however, most CFD packages have limited capabilities in solving multiphase flows. This section offers a brief overview of the more popular multiphase CFD solver packages, while describing their capabilities and limitations.

Three of the most popular solver packages are Fluent®, CFX®, and STAR-CD™. Fluent® has the capability to solve multiphase flow problems with either a mixture model or by an Eulerian-Eulerian model. In addition, Fluent® has the capability to incorporate user-defined functions (UDFs), and is known particularly for droplet modeling and cyclone separators. CFX® has capabilities similar to Fluent®. STAR-CD™ and STAR-CCM+™ have the capability to solve multiphase flows with either a Lagrangian-Eulerian or an Eulerian-Eulerian model. Similar to Fluent®, STAR-CD™ has the capability to model droplet flows and small solid particles.

In addition to commercially available multiphase solver packages, codes have been developed at national government laboratories. For example, Multiphase Flow with Interface

eXchanges (MFIX™) is a general purpose code developed at the National Energy Technology Laboratory for describing hydrodynamics, heat transfer and chemical reactions in fluid-solid systems, particularly with circulating fluidized beds. KIVA™, a package developed at Los Alamos National Laboratory, uses the arbitrary Lagrangian-Eulerian method for computing chemical reacting flows.

Other CFD solvers that advertise capacities in solving multiphase flows include Flow3D® (www.flow3d.com), which specializes in free surface flow modeling and multiphase mixtures, openFOAM™ (www.opencfd.co.uk) an open-sourced CFD solver package, Phoenics™ by Cham™ (www.cham.co.uk), and PORFLOW™ (www.acricfd.com/software/porflow/default.htm). However, most of these codes are focused on liquid or porous media flows rather than pneumatically conveyed solid flows.

Figure 2.14 shows a comparison matrix of several available CFD solver packages that have multiphase flow modeling capabilities. One will notice the similarities and differences among the available solver packages. In many instances, one CFD package provides the same features as its competitor. For example, Fluent® and STAR-CD™ both offer robust meshing utilities and post-processing capabilities. In other instances, a CFD solver will be developed for a specific application. Examples of these instances include the MFIX™ and KIVA™ CFD codes, in which the code was developed specifically for heat transfer and interface exchanges for chemical reacting flows.

	Lagrangian-Eulerian	Eulerian-Eulerian	User-Def. Functions	Open-Source	Collision Modeling	Features
Fluent	X	X	X		X	Meshing, post-processing, fluidized beds, nozzles
Star-CD	X	X	X		X	Meshing, post-processing, fluidized beds, free surface
CFX	X	X	X		X	Bubbles in liquid, particulates in gas
Flow3D	X	X	X		X	Fluid-Solid interaction, free surface flows
MFIX		X	X	X	x	Hydrodynamics, heat transfer, chemical reactions
KIVA/CFDlib	X		X		X	Chemical reacting flows
openFOAM	X	X	X	X	X	Bubbles, cavitation, mixing

Figure 2.14. Comparison of CFD packages with multiphase flow modeling capabilities.

2.6. Discrete Element Modeling of Bulk Solids

Although this research is focused on pneumatic conveyance of biomaterials research, concepts within Discrete Element Modeling (DEM) may be applicable and should to be considered. DEM is a well-established computational numerical method that has been in use for the last three decades to study the dynamic behavior of particulate systems in a wide range of disciplines (Raji and Favier, 2004. DEM considers a system to be a collection of discrete entities with bulk solids properties. DEM calculates the inter-particle contact forces, stresses and particle displacements over discrete time steps. DEM uses kinematics and Newton's laws of motion to determine the parameters of each particle. A DEM simulation

begins by giving the particles a velocity and a position. The forces on each particle are computed from the initial conditions and the physical laws. Macroscopic forces that need to be considered include friction, collision, damping, and gravity, while microscopic forces that may be considered include electrostatic and van der Waals forces (Yu 2003).

Most research with DEM only tracks a few hundred to a few thousand particles since the governing equations for the analysis become computationally intensive as the number of particles increases. Computational simplicity often results from the selection of larger particles, which assumes that the bulk solids behaves as a fluid and uses computational fluid dynamics.

DEM modeling has become popular because it has the ability to accurately model the dynamics of bulk flow within a system. The studies that report satisfactory results with DEM have ranged from tumbler mills in mixing processes (Gyenis et al. 1999), (Hlungwani et al. 2003), (Elperin and Vikhansky 2002), compressive loading (Raji and Favier 2004), hopper flows (Zhu and Yu 2005), and fluidized beds (Limtrakul et al. 2004). Another study that is more directly related to the proposed research includes transporting bulk solids via conveyor or auger within a manure applicator (Landry et al. 2006). Although this research involves the computational modeling and representation of biomass bulk solids, it was not used for pneumatic-based transport.

2.7. Discrete Element Modeling with CFD

CFD models analyze fluid flow characteristics, whether the fluid is a liquid, such as water, or a gas, such as air. CFD does have the capability of solving multiphase flows, but traditional CFD techniques do not have the ability to model dense particulate phases or

multiple phases where the particle sizes are over one mm in size. DEM models, conversely, are primarily applied to bulk solids flow simulations in which the particles are transported mechanically rather than being entrained in another fluid.

Several commercially available DEM solver packages are available. These packages include EDEM™ (www.dem-solutions.com), Particle Flow Code (PFC®) (www.itascacg.com/pfc3d), and MillSoft™ (www.processeng.com). EDEM® has been used to simulate and improve particulate handling, processing and manufacturing operations in agricultural, construction, pharmaceutical, chemical, mineral and materials processing as well as oil and gas production, and mining. Applications of EDEM include the simulation and optimization of processes such as particle attrition and grinding, particle and pill coating, conveyor transport, drum mixing and drying, shot peening, grain handling and soil-tool interactions.

EDEM™ has been used with the commercial CFD solver package Fluent® to perform multiphase simulation of particulates and fluids, including solid-fluid transport devices, fluidized beds, filtration and pipe erosion (www.dem-solutions.com/news.html).

2.8. Survey of Conveying Fibrous Bulk Solids

Most of the research on biomass pneumatic conveyance has been experimental, with little modeling work being reported. Papatheofanous et al. (1995) conducted studies of the biorefining processes of agricultural biomass residues, particularly with winter wheat straw and oilseed rape straw. Joppich et al. (1999) performed a study of the challenges and opportunities of using wood powder in a pneumatic conveyance system as a feedstock.

Raheman (2002) experimentally investigated the drag coefficients of agricultural grains in vertical pipes of pneumatic conveyance systems.

Badger (2002) at the Oak Ridge National Laboratory performed a cost analysis for receiving, handling, storing, and processing woody biomass feedstock of a biopower system from the point that the feedstock reaches the plant gate to the feedstock entry point of the conversion device. His study also included specific operational issues associated with specific feedstocks along with quality issues and or requirements. Crummer and Brown (2002) authored a journal paper discussing the auxiliary equipment in greater detail for biomass gasification, including fuel preparation and feeding of the feedstock (prior to gasification) and the gas cleaning systems (subsequent to gasification). Particularly, they stated that pneumatic transport is effective for long distance transport of properly sized fuel and that capital costs are fairly low, although they require high power consumption to generate the high-pressure air necessary for its operation.

Numerous researchers have performed economic and feasibility studies on the viability of biomass. Wyman (2003) has compiled a paper that offers his insight on what is required to make cellulosic ethanol successful. Logistics studies for transporting biomass from the field to the biorefinery have been done by Atchison and Hettenhaus (2003), Sokhansanj et al. (2002, 2003, 2006), Wu et al. (2006), Hoskinson et al. (2007), and Searcy et al. (2007). Others have focused on the chemical reaction processes of biomass, including Vessia (2005), Taylor (2008), and Larsen et al. (2008).

Cui and Grace (2006) have compiled a review of pneumatic conveying specifically of biomass particles. In it, they focus on investigating agricultural particles and pulp fibers. Handling and conveying biomass particles are challenging due to the unusual physical

properties of biomass particles. They note that experimental work has been performed to mainly determine pressure drop, particle velocity flow regime, and electrostatic charging effects in horizontal and pneumatic conveying.

Cui and Grace (2007) have stated that modeling efforts have been reported to be relevant to multiphase conveying of biomass bulk solids. However, mechanistic models including CFD have not been able to provide accurate simulations for concentrated biomass flow due to the complex nature of the particle interactions and particle fluid-interactions.

In short, most of the research for fibrous-based flows in pneumatic conveyance and segregation has been experimental, with minimal computational research being reported. Most of the modeling research has not investigated inclined conveying of biomass. This is most likely due to the segregation effects of the heterogeneous properties of biomass and fibrous bulk solids and to the complexity of the bulk solids behavior. In addition, the computing resources are not present to account for the complexity of every effect of every biomass bulk solids particle.

2.9. Summary of Background

Multiphase flows of biomass and other fibrous type products are present in many applications, including agricultural, industrial and power generation processes. Many of these involve relatively light mixtures of very small particle sizes that can be modeled by commercially available CFD codes. Other types of flows, i.e. seeds flowing through a hopper, are primarily affected by particle-particle interaction and the inertia of the particle. These types of flows may be modeled with discrete element modeling tools. However, there exist many types of flows that may not be adequately or accurately modeled by either of

these standardized techniques. These types of flows involve particles that are comparable in size to the CFD grid and in which the interaction of the solid particles with the air are a significant portion of the transport or separation process. This regime typically involves airflow containing a large numbers of relatively large, light particles with a high surface to mass ratio (flat or non-spherical).

However, most pneumatically conveyed commodities (relatively large in size and/or non-spherical) do not behave in a similar fashion as powder entrained flows or flows in which the particles are dense spheres. Many biomass bulk solids that are conveyed pneumatically have densities that are only 50 to 200 times the density of, air, depending on the moisture content. Furthermore, the sizes of biomass and fibrous particles are significantly larger than what traditional modeling techniques employ. Modeling high volume-fraction, particle laden flows that have an irregular particle shape, both in the sense of being non-spherical and in a sense of the particles being stringy, has not been extensively researched, and many of the conventional relationships for modeling multiphase flow do not apply.

CHAPTER 3: MODELING MULTIPHASE FLOWS

As seen in Chapter 2, the study of multiphase flows in pneumatic conveyance systems has to consider several effects. The first effect to consider is the behavior of the air. Single-phase airflow can be solved with a high degree of accuracy with currently available CFD solver packages. However, the presence of the bulk solids phase complicates the flow regime, hence the second effect to consider is the motion of the solid particles. These solid particles exhibit significantly different transport characteristics than the gas phase. The third effect to consider is the interaction of the entrained solid particles with the flowing air. Additional considerations include the solid particle effects on other solid particles and the bulk solids properties of the solid particles.

This chapter discusses the traditional approaches for modeling multiphase flows, compares the modeling techniques and provides descriptions of which approaches are used for which applications.

3.1. Multiphase Flow Definitions

A *phase* refers to the solid, liquid or vapor state of matter, which is characterized by the differences in intermolecular forces and spacing (Crowe et al 1998). In contrast, a *component* refers to a chemical species such as nitrogen, oxygen or water. Air would be an example of a single phase, multi-component substance. A *multiphase flow* is the flow of a mixture of phases such as gases (bubbles) in a liquid, liquid (droplets) in a gas, solid

(particles) in a gas, and so forth. An example of a multiphase, single component flow would be steam and water flowing through a tube.

Gas-solid flows are a classification of multiphase flows in which a moving gaseous phase entrains a flow upon bulk solids suspended particles. Gas-solid flows include pneumatic transport systems as well as fluidized beds. Generally, the continuous, or carrier phase is the dominating phase of the flow. The dispersed solid phase is the phase carried by the continuous phase and is influenced by the behavior of the air phase. For gas-solid flows, the carrier phase is the air while the dispersed phase is the suspended collection of particles.

In describing multiphase gas-solid flows, additional terminology is required to further define the properties or characteristics of multiphase mixture. For convenience the term *dispersed phase* will refer to the bulk solids, while the *carrier phase* will refer to the gaseous air phase.

The volume fraction is defined as the ratio of volume displaced by each phase. The volume fraction of the dispersed phase is

$$\alpha_d = \lim_{\delta V \to v^o} \frac{\delta V_d}{\delta V} \qquad [3.1]$$

where α_d is the volume fraction of the dispersed phase, V_d is the volume occupied by the dispersed phase, and V is the total volume, while the volume fraction of the continuous phase is

$$\alpha_c = \lim_{\delta V \to v^o} \frac{\delta V_c}{\delta V} \qquad [3.2]$$

where α_c is the volume fraction of the carrier phase, V_c is the volume occupied by the carrier phase, and V is the total volume. The sum of these two volume fractions must equal unity. The volume fraction is one of the metrics of indicating the concentrations of each phase.

The bulk density of the dispersed phase is the mass of the dispersed phase per unit volume of the mixture, or in terms of a limit is defined as

$$\bar{\rho}_d = \lim_{\delta V \to v^o} \frac{\delta M_d}{\delta V} \qquad [3.3]$$

where ρ_d is the volume fraction of the dispersed phase, M_d is the mass occupied by the dispersed phase, and V is the total volume. The bulk density is related to the bulk solids density by

$$\bar{\rho}_d = \alpha_d \rho_d . \qquad [3.4]$$

The sum of the bulk densities for the two phases is the mixture density

$$\bar{\rho}_d + \bar{\rho}_c = \rho_m \qquad [3.5]$$

where the subscript *m* refers to the mixture.

For multiphase flow through a pipe or channel, the superficial velocity for each phase is the mass flow rate of the particular phase divided by the product of the cross sectional area of the pipe and the bulk solids density, and is expressed as

$$U_d = \frac{\dot{M}_d}{\rho_d A} \qquad [3.6]$$

where U_d is the velocity of the dispersed phase, $\dot{M}_d$ is the mass flow rate by the dispersed phase, and A is the cross sectional area of the pipe.

The response time for a particle to changes in flow velocity is important in establishing non-dimensional parameters in characterizing the flow. The equation of motion for a spherical particle in a gas is given by

$$m\frac{dv}{dt} = \frac{1}{2}C_D\frac{\pi d_p{}^2}{4}\rho_c(u-v)|u-v| \qquad [3.7]$$

where u is the particle velocity, v is the gas velocity, and C_D is the drag coefficient. Using the information of the momentum response time for the carrier and the dispersed phases, the Stokes number can be determined.

The Stokes number is defined as the ratio of the aerodynamic response times of the particles, t_r, to a characteristic time of the fluid motion, t_f. For a given flow regime, the small Stokes number implies the inertial effects of the particles are small. This may be also addressed as a nominal length divided by a characteristic gas phase velocity

$$St = \frac{t_r}{t_f} = \frac{\rho_p {d_p}^2 U}{18 \mu_g L} \quad [3.8]$$

where ρ_p is the density of the solid particles, d_p is the diameter of the gas particles, μ_g is the dynamic viscosity of the gas, *U* is the characteristic flow velocity, and *L* is the characteristic length of the pipe.

3.2. Multiphase Flow Modeling Approaches

In multiphase flow modeling, there are three commonly accepted modeling approaches. The first is an Eulerian mixture model, which assumes the two phases act as a mixed fluid with a single set of fluid properties based on the composition of the multiphase mixture. The second modeling approach is the Eulerian-Eulerian two-fluid model, which treats both the carrier air phase and the dispersed solid phase in an Eulerian fluid. The third approach is the Lagrangian-Eulerian model, which models the carrier air phase in an Eulerian frame, but models the dispersed phase in a Lagrangian (particle trajectory) frame. Although the Eulerian-Eulerian and Lagrangian-Eulerian approaches treat the dispersed phase differently, if each approach is implemented properly, both should be able to solve the flow conditions.

The following sections offer an overview of the governing equation sets for incompressible, unsteady Navier-Stokes momentum equations for multiphase flow. This

derivation is as follows (Crowe 2006), but may be found in various forms in most multiphase flow textbooks.

The motion of the dispersed phase is influenced by the continuous phase and vice versa through momentum transfers between the two phases. If the flow regime is laminar, then the motion of the carrier phase and the dispersed particles can be deterministic since there is no variation on how the particles or the continuous phases may interact. However, it is more common to have the flow be turbulent, and the path in which the particle travels becomes more random. Therefore, it is more useful to have a stochastic approach for particle interactions.

3.3. Eulerian Mixture Method with Mixed Fluid Treatment

In the Eulerian Mixture method, the Navier-Stokes momentum equation treats the flow as a single-phase mixture. In this single-phase mixture, the two phases act as a single phase with fluid properties averaged based upon the volume fraction percentage of the carrier air phase and the dispersed bulk solids phase.

$$\frac{\partial(\rho_m u_{mi})}{\partial t} + \frac{\partial(\rho_m u_{mi} u_{mj})}{\partial x_j} = \rho_m g_i - \frac{\partial p}{\partial x_i} + \mu_m \frac{\partial^2 u_{mi}}{\partial x_j \partial x_j} \qquad [3.9]$$

where the subscript *m* denotes the mixture, and $\rho_m = \alpha_p \rho_p + \alpha_f \rho_f$ is applied throughout the domain. In a similar manner, the continuity equation for the mixture is given as follows,

$$\frac{\partial}{\partial t}(\rho_m) + \frac{\partial}{\partial x_j}(\rho_m u_{j,m}) = 0 \qquad [3.10]$$

The advantage of this equation set is that it reduces the multiphase flow into a single acting flow, with the same solving methods as a single-phase fluid. Using this method requires the use of assigned “fluid” properties to bulk solids.

The mixture modeling approach may be acceptable if the flow characteristics remain uniform in the flow, e.g., there is negligible separation of the phases in the flow, or the flow is solid-liquid (Manninen and Taivassalo, 1996). If a high volume fraction of bulk solids is being conveyed, this method can be useful because the separation and re-entrainment effects do not exist. However, if particle separation and re-entrainment are important, then the mixed fluid treatment will not suffice. Examples of flows in these conditions include ratholing and bulk solids separation from the flow regime, including coal roping.

3.4. Eulerian-Eulerian (Two-Fluid) Method

In the Eulerian-Eulerian method, each phase is governed by is own set of continuity and momentum equations. Each phase acts as a fluid, with momentum coupling occurring between the phases for closure. In this equation set, internal forces may also be assigned if desired.

The following Navier-Stokes momentum equations treat both the carrier and the dispersed phase in an Eulerian frame. The dispersed bulk solids phase momentum equation is applied throughout the fluid domain, given as follows,

$$\rho_p \frac{\partial(\alpha_p v_i)}{\partial t} + \rho_p \frac{\partial(\alpha_p v_i v_j)}{\partial x_j} = \alpha_p \rho_p g_i - \alpha_p \frac{\partial(p + p_{coll})}{\partial x_i} + \alpha_p \mu_f \frac{\partial v_i^{\,2}}{\partial x_j \partial x_j} + \alpha_p F_{\text{int},i} / V_p \; + M_{source,i} \qquad [3.11]$$

where F_{int} are the internal forces of the particle, and M_{source} is the momentum source term. The carrier air phase momentum equation is applied throughout the fluid domain

$$\rho_f \frac{\partial(\alpha_f u_i)}{\partial t} + \rho_f \frac{\partial(\alpha_f u_i u_j)}{\partial x_j} = \alpha_f \rho_f g_i - \alpha_f \frac{\partial p}{\partial x_i} + \alpha_f \mu_f \frac{\partial u_i^{\,2}}{\partial x_j^{\,2}} - \alpha_p F_{\text{int},i} / V_p \; - M_{source,i} \qquad [3.12]$$

In a similar manner, the continuity equation for the dispersed solid phase is applied throughout the domain, and is given as follows,

$$\frac{\partial}{\partial t}(\alpha_p \rho_m) + \frac{\partial}{\partial x_j}(\alpha_p \rho_p u_{j,p}) = 0 \qquad [3.13]$$

and the carrier air continuity equation is applied throughout the fluid domain

$$\frac{\partial}{\partial t}(\alpha_f \rho_f) + \frac{\partial}{\partial x_j}(\alpha_f \rho_f u_{j,f}) = 0 \qquad [3.14]$$

The advantage of the Eulerian-Eulerian methodology is that it allows coupling between each of the phases in both the continuity and momentum equation sets. The continuity and momentum equation sets are coupled by the condition that the summation of the volume fraction equal to unity at each computational cell. In addition, the momentum equations are coupled by the momentum exchanges occurring between each phase, as shown by the $M_{source,i}$ term. This coupling generally results in more accurate predictions of flow conditions in which particle separation and re-entrainment occur when compared to the mixture model. The primary disadvantage is that individual collision effects are not directly captured. Also, the dispersed phase is assigned "fluid" properties, although not technically a fluid. However, the effects of the collisions may be accounted for by having good estimates of the dispersed phase effects, generally from experiments.

3.5. Lagrangian-Eulerian Method

The following Navier-Stokes momentum equations deal with the dispersed phase in a Lagrangian (trajectory) frame while the carrier phase uses the Eulerian frame. The dispersed bulk solids phase uses Newton's law of motion momentum equation, which accounts for any body forces, surface forces, and collision forces. Any additional forces such as particle rotation or electrostatic forces may be included here as well. The dispersed and carrier phase momentum equations are coupled in a similar fashion as the Eulerian-Eulerian approach.

The advantage of the Lagrangian-Eulerian approach is that this approach accounts for the particle movement and that the collisions may also be taken into account. However, incorporating these effects begins to reach into the realm of DEM by accounting for the kinematic relationships of the particles (collision, reaction, coefficient of restitution, etc.) and increasing the computational requirements. The incorporation of these effects results in models that are much more difficult to solve, especially with large, three-dimensional models with unstructured grids.

The dispersed bulk solids phase momentum equation applied to the particle trajectories is given as

$$m_p \frac{\partial v_i}{\partial t} = F_{body,i} + F_{surf,i} + F_{coll,i} \qquad [3.15]$$

where m_p is the mass of the particle. $F_{body,i}$ are the total body forces acting on the particle, $F_{coll,i}$ are the surface forces acting on the particle, and $F_{surf,i}$ are the collision forces acting on the particle. This contrasts with the carrier air phase momentum equation, which is applied outside the particle volume to the continuous phase, and is given as follows:

$$\rho_f \frac{\partial(\alpha_i u_i)}{\partial t} + \rho_f \frac{\partial(\alpha_f u_i u_j)}{\partial x_j} = \alpha_f \rho_f g_i - \alpha_f \frac{\partial p}{\partial x_i} + \alpha_f \mu_f \frac{\partial u_i^2}{\partial x_j^2} - n_p F_{\text{int},i} \qquad [3.16]$$

where n_p is the number density of particles per unit volume of mixed fluid. $F_{int,i}$ is the inter-phase hydrodynamic force acting on the particles, and p_{coll} is the particle collision pressure. In a similar manner, the continuity equation for the carrier air phase is applied throughout the domain, and is given as follows,

$$\frac{\partial}{\partial t}(\alpha_p \rho_m) + \frac{\partial}{\partial x_j}(\alpha_p \rho_p u_{j,p}) = 0 \qquad [3.17]$$

3.6. Comparison of Modeling Approaches

A multiphase system behaves significantly different than the carrier phase, due to the different characteristics between the two phases. In addition, the dispersed solid phase has a profound effect on the behavior of the carrier phase. In multiphase systems, the primary challenge is accurately representing the interactions of the interfaces of each phase in the system.

The three modeling approaches discussed in this chapter are the most widely accepted methods in capturing the effects of multiphase flows. Each approach was primarily developed based on a particular application. Table 3.1 offers a brief summary of the similarities and differences in the multiphase modeling approaches discussed in this chapter.

The mixture model is most applicable to flow conditions in which the concentrations of two distinct phases in the mixture are assumed to remain constant throughout the flow, and that the inertial effects of one phase are similar to the other phase. However, the mixture model is not able to capture the effects of any flow cases in which there is a separation of the two phases, e.g. ratholing. In addition, the mixture model does not have the capability to capture any collision effects. Therefore, the mixture model can be applicable to flows including slurries and other liquid-solid flows, but the mixture model would be ill suited for gas-solid flows.

Table 3.1. Comparison of multiphase modeling approaches.

	Mixture	Eulerian-Eulerian	Lagrangian-Eulerian
Examples of Applications	Slurries Liquid-Solid Flows	Fluidized Beds Bubble Columns Gas-Liquid Flows Gas-Solid Flows	Droplets Combustors Nozzles Dust Separators
Particle Size	Small (<mm)	Small (<mm)	Very Small (μm)
Particle/Air Density Ratio	Low (<500:1)	Variable	High (~1000:1)
Volume Fraction	Low-Medium	0.0 to 1.0	Very Low (<0.01)
Bulk Loading	Variable	Variable, but higher than LE	Very Dispersed
Collision Modeling	Not Available	Not Available (typically)	Available

The Lagrangian-Eulerian model has been applied to several gas-liquid and gas-solid multiphase flows, which include nozzle flows, dust separators, combustors, and droplets. In most cases, the particle sizes in Lagrangian-Eulerian flows are on the order of microns in diameter, and the particle/air density ratio is typically very high, meaning that the properties of the dispersed phase are significantly different than the carrier phase. Since the Lagrangian-

Eulerian model treats each particle as a trajectory, information is available to calculate the motion of each particle, including velocity and momentum. Therefore, collision modeling is possible in Lagrangian-Eulerian models. However, collision modeling significantly increases the computational requirements of the model, especially when the number of particles increases. Often, Lagrangian-Eulerian equation sets are one-way coupled. One-way coupling of the equation sets means that the dispersed particles are influenced by the moving flow of the carrier phase. However, the effects of the dispersed particles are not coupled back to the carrier phase equation sets. Therefore, if the behavior of the dispersed particles significantly impacts the behavior of the fluid, the Lagrangian-Eulerian model would not be able to solve for these effects.

The Eulerian-Eulerian model has been implemented in a variety of flow applications, including bubble columns, fluidized beds, and other gas-solid and gas-liquid conditions. The dispersed phase size in traditional Eulerian-Eulerian models is rather small, on the order of millimeters or smaller in diameter, but is less stringent than in Lagrangian-Eulerian models. The Eulerian-Eulerian model is also less restricted since the dispersed phase volume fraction can be significantly higher than in Lagrangian-Eulerian models. In addition, most Eulerian-Eulerian models can accommodate a variety of loading conditions. However, the Eulerian-Eulerian model approach has limited collision detection abilities.

One significant advantage to the Eulerian-Eulerian modeling approach is the ability to couple the conservation equation sets of each phase. Eulerian-Eulerian models offer two-way coupling of mass and momentum transfers between the phases rather than one-way equation coupling typically found in Lagrangian-Eulerian models. Two-way coupling is when the effects of the dispersed phase have an influence of the behavior of the carrier phase in

addition to the dispersed phase influencing the behavior of the dispersed particles. Therefore, the effects accounted for by two-way coupling of the equation sets solve the velocity, pressure, and volume fraction calculations. Figure 4.1 diagrams two way coupling of the conservation of mass and momentum equations.

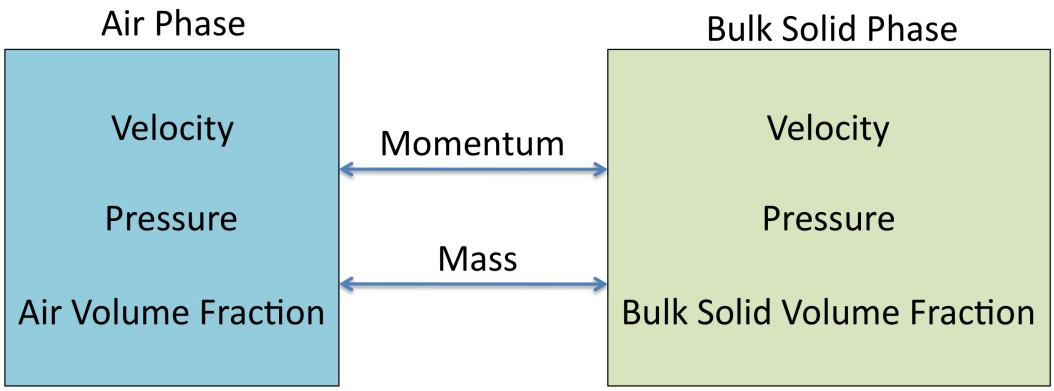

Figure 3.1. Two-way coupling of conservation equations.

The commercially available and open source CFD solver packages described in Section 2.5 are well suited for multiphase flows including droplet sprays from nozzles, fluidized beds and reacting flows. However, most of these software packages are ill suited for the types of flows for this study. The flow regimes for biomass require new and innovative

approaches for modeling. The multiphase biomass flow exhibits characteristics that may have the ability to be represented with Lagrangian-Eulerian, Eulerian-Eulerian and DEM approaches. However, creating a single model that utilizes a combination of these modeling techniques would be complicated, cumbersome, and computationally expensive. In many situations, models like what was described would become almost impossible to solve with these traditional methods.

3.7. Modeling Approach Selected for this Research

In this research, the Eulerian-Eulerian method will be used because it has the potential to capture the momentum exchanges between the gaseous dispersed and the dispersed bulk solids while the two other approaches have a less robust, if not any, way to account for the inter-phase momentum exchange. In addition, the Eulerian-Eulerian approach also has the capability to have two-way coupling between the phases and can be used to predict concentrations, or volume fractions, of each phase at each volume. Although the Eulerian-Eulerian approach is more computationally intensive than a mixture or single phase fluid flow approach, it is less computationally intensive than the Lagrangian-Eulerian approach. The number of tracked particles computationally limits the Lagrangian-Eulerian modeling approach, while the Eulerian-Eulerian approach does not require the computation of particle trajectories. This study will focus on the implementation of the Eulerian-Eulerian approach for modeling gas-solid multiphase flows, with the emphasis of representing and quantifying the momentum exchanges between the phases. Chapter 4 will describe the methods developed for simulating and representing the momentum exchanges between fibrous bulk solids and the continuous phase.

3.8. Multiphase Flow Modeling Summary

There are several conclusions that can be deduced from the survey of methods for modeling multiphase gas-solid flows. First, there are two relatively accepted techniques for multiphase flow modeling of gas solid flows: the Eulerian-Eulerian approach and the Lagrangian-Eulerian approach. The mixture modeling technique is ill suited due to the flow regimes encountered in gas-solid flows. Second, the dispersed phase flows that are typically modeled for pneumatic conveyance systems are powder-type flows, such as coal dust, or are small spherical particles. In either case, the dispersed particle density is over 1000 times the density of the carrier phase. Third, the coupling between the two phases is nonexistent, particularly with the Lagrangian-Eulerian models. In the dilute flows that are modeled with the Lagrangian-Eulerian approach, the effects of the carrier phase are coupled to the dispersed phase, but the dispersed phase effects are assumed to not affect the carrier phase. This assumption may be appropriate for very dilute flows; however, would not be appropriate when there is a higher concentration of the dispersed phase, e.g., impact regions. Fourth, multiphase flow models are significantly more computationally expensive than the comparable single-phase models. For the Eulerian-Eulerian two-fluid model, two sets of governing equations needs to be calculated for each time step, while the Lagrangian-Eulerian model requires a position and velocity calculation for each particle during each time step. Therefore, either approach is limited by the size and complexity of the computational model.

Current multiphase flow modeling approaches have several limitations and currently cannot be used extensively for modeling fibrous-based flows. Traditional flow modeling currently requires that the bulk solids particle size be much smaller than the computational

grid volume, or be the order of powder size. In addition, multiphase gas-solid flow modeling cannot readily handle dense flows, or flows in which the presence of the bulk solids significantly affects the flowing air. In a similar manner, CFD models of multiphase flows cannot predict the differences in flow behavior as flow instability, e.g., plugging occurs. Furthermore, the currently available CFD solver packages are not capable of modeling the behavior of irregularly shaped objects or an agglomeration of particles that extend beyond the computational grid. Each of these limitations greatly restricts the utility of CFD models for designing systems involving multiphase flows.

CHAPTER 4: THE COMPUTATIONAL MODEL

The mathematical description of the Eulerian-Eulerian approach chosen for modeling pneumatic multiphase flows presented in Chapter 3 consist of the differential conservation equations of mass and momentum for the carrier air phase and the dispersed bulk solids phase as well as the interactions between the two phases. The two flow domains are coupled by the momentum transfers occurring between the two phases and by the summations of the concentrations (volume fractions) of each phase at each differential element in the computational domain, while the continuity equations are coupled by the summations of the volume fractions at each differential volume. In this research, determining an appropriate representation of the inter-phase momentum transfer is of particular interest. The momentum exchange between the two phases is determined through the use of algebraic expressions and empirically based correlations, which are based on the physical properties and characteristics of the bulk solids. The remainder of this chapter defines the process of developing a computational model for predicting the flow behavior of fibrous bulk solids within a pneumatically based conveyance system.

4.1. Research Goals

The goal of this research is to develop a methodology for representing the complex effects of biomass flow regimes within a computational model that is appropriate for engineering design of pneumatic transport and segregation systems. These models are needed to answer engineering questions in regards to the performance of particular designs and configurations. The design questions include the power requirements, influence of the

presence of biomass bulk solids, and predicting biomass accumulations. In addition, the goal is to create a modeling framework that will allow engineers to use the developed multiphase flow models in a manner that supports engineering design. That is, the methods and models ought to be lightweight enough to be readily incorporated into the engineering design and analysis process. However, these models also need to incorporate sufficient fidelity of the physical effects happening within the system, e.g., trajectory of each particle, boundary layer profiles around the fibrous particles, rotation of fibers, etc. to be able to accurately support the design process. In this thesis, the impacts of these effects are estimated through a series of experimentally derived functions and correlations, which will incorporate these effects.

4.2. Hypotheses of Fibrous Bulk solids Flows

Fundamentally speaking, the fibrous bulk solids studied in this research are unique compared to previously studied flows due to the low bulk density (less than 500 kg/m^3), non-spherical shape (ellipsoids or cylinders vs. spheres), large characteristic length (mm or cm vs. µm scale), connected strings, and heterogeneous composition. The result of these observations is that the interphase momentum exchanges are at a larger scale than traditionally studied multiphase flows. In biomass flows, one of the primary effects of the bulk solids flow is a wider spatial momentum exchange with in a flow that would normally be experienced due to turbulent diffusion with the flow field. This wider distance of momentum exchange influences the flow by taking regions of low momentum and exchanging them with regions of high momentum, and conversely regions of high momentum get exchanged with regions of low momentum. Instead of momentum exchanges occurring at the particle level (the sub-millimeter level), the momentum exchanges are

present at the macro level. In a computational sense is, the momentum exchanges are occurring with particles that are on the same order of magnitude as a computational grid. Therefore, the interphase momentum exchanges could occur for a single particle extending across several computational grid points.

Several assumptions are implemented in the development of the computational models in this research. These assumptions are:

1. The physical properties of the bulk solids phase are homogeneous, in which the bulk solids particle size, shape, and density remains constant and does not deform. In this research, the size and shape of a single fibrous bulk solids particle occupy at least one computational grid point, yet are at least an order of magnitude smaller than the conveyance line in which they travel. The bulk solids of a particular size and shape cause the primary effects of concern. Therefore, the homogeneous properties are adequate for this study.

2. The size and shape of the bulk solids particles can be represented as three-dimensional ellipsoids based on representative characteristic lengths of the modeled bulk solids. In the two flow cases studied in this research, cotton-air flow and biomass-air flow. The cotton bolls studied are generally ellipsoidal in shape, with a major axis dimension of 4 cm and minor axes of 2 cm. Similarly, a particle of ground biomass studied in this research may also be represented as an ellipsoid with a major axis dimension of 6 mm and minor axes of 3 mm.

3. As the particles are entrained in the flow field, the orientation of the particles is based on the long axis of the ellipsoid being oriented perpendicular to the flow. This assumption is reasonable since this effect is observed in many instances of objects entrained in flows. For example, if one were to drop a feather from a moderate height, the feather would typically orient itself to have its greatest surface area be perpendicular to its direction of travel. In the same manner, non-spherical objects orient with the greatest surface area being perpendicular to the flow. These trends were also observed by the research conducted by Mortensen et al. (2008) for the orientation of ellipsoidal particles in turbulent flow.

4. The interphase momentum exchange is partially based on the drag effects of individual bulk solids particles entrained in the airflow. The calculated drag values can be represented by experimentally obtained drag correlations based on physical properties of a single particle, including particle size, shape, as well as the flow characteristics of the particle in relation to the air, i.e., particle Reynolds number.

5. The interphase momentum exchange is also dependent on resistive effects outside the realm of the single particle drag. These effects are a number of other particle behaviors, including rough particle surfaces, particles connected by a series of fibers or strings, and air flowing through large, porous particles. Predicting and correlating the influence of each of these additional effects would be challenging. In addition, even if one could model each of the additional effects, the model analysis and execution costs would become too expensive. However, all these additional effects

have an influence on the behavior of the airflow. Therefore, these additional effects are lumped together as additional resistances to the flow and are correlated to specific biomass bulk solids. The additional resistive correlations may be obtained through a series of laboratory experiments, with the data collected from test rigs of the fibrous bulk solids of interest flowing through devices that are representative of the conveyance systems of interest, including size of ducting and the curvature of the bends, etc.

6. The effects of particle rotation are neglected. In fluid mechanics, studies have been performed on spherical and cylindrical shapes rotating in airflow. Although the rotation of the object will cause an asymmetrical velocity distribution around the object, it has been shown in fundamental fluid mechanics text (Munson et al. 2006) and in research conducted by (Holzer and Sommerfeld 2009), (Takayama and Aoki 2004) and that the rotation of the object will his will have an insignificant effect on the drag coefficient.

4.3. Model Description

This research implements the Eulerian-Eulerian multiphase flow models within a commercially available software package. The chosen CFD package for this research is STAR-CD™ V4. STAR-CD™ has extensive capabilities with creating meshes for the complicated geometry that industry demands, has a robust solver with several turbulence models, and has a well-developed post-processing package. Of similar importance, STAR-

CD™ has Eulerian-Eulerian multiphase solving capabilities that allow a user to incorporate external user defined function or subroutines.

The Eulerian-Eulerian multiphase model in STAR-CD™ considers the solid and gas phases an interpenetrating continuum that shares the space in each finite volume. A control volume based approach to solving the governing differential equations of the flow system is represented as a series of algebraic equations, which may then be solved numerically. The volume averaged discretization method integrates the governing equations at every control volume, and these equations conserve mass and momentum. The discretized equations, in conjunction with the initial and boundary conditions are solved simultaneously to obtain a converged solution. The conservation equations of mass and momentum are solved simultaneously by solving the continuous air phase and dispersed bulk solids phases separately. The momentum equations for each phase are coupled by the interphase momentum exchanges and by the volume fraction condition requiring the summation of the volume fractions of each phase be equal to unity.

The Eulerian-Eulerian conservation of mass and conservation of momentum equations are relisted for the convenience of the reader. The conservation of mass equations is given as follows for the air phase

$$\frac{\partial}{\partial t}\left(\alpha_{air}\rho_{air}\right)+\frac{\partial}{\partial x_j}\left(\alpha_{air}\rho_{air}u_{j,air}\right)=0 \qquad [4.1]$$

with a similar representation for the dispersed bulk solids phase

$$\frac{\partial}{\partial t}(\alpha_{solid}\rho_{solid})+\frac{\partial}{\partial x_j}(\alpha_{solid}\rho_{solid}u_{j,solid})=0 \quad [4.2]$$

.

The continuity equations for the two phases are coupled at each control volume in which

$$\alpha_{air}+\alpha_{solid}=1.0. \quad [4.3]$$

In the same manner, the conservation of momentum equations are given as follows, for the carrier air phase,

$$\rho_{air}\frac{\partial(\alpha_{air}u_i)}{\partial t}+\rho_{air}\frac{\partial(\alpha_{air}u_iu_j)}{\partial x_j}=\alpha_{air}\rho_{air}g_i-\alpha_{air}\frac{\partial p}{\partial x_i} + \alpha_{air}\mu_{air}\frac{\partial u_i^{\,2}}{\partial x_j^{\,2}}-\alpha_{air}F_{\mathrm{int},i}/V_{air}\ -M_{transfer,i} \quad [4.4]$$

and for the bulk solids phase

$$\rho_{solid}\frac{\partial(\alpha_{solid}v_i)}{\partial t}+\rho_{solid}\frac{\partial(\alpha_{solid}v_iv_j)}{\partial x_j}=\alpha_{solid}\rho_{solid}g_i-\alpha_{solid}\frac{\partial(p+p_{coll})}{\partial x_i} + \alpha_{solid}\mu_{air}\frac{\partial v_i^{\,2}}{\partial x_j\partial x_j}+\alpha_{solid}F_{\mathrm{int},i}/V_{solid}\ +M_{transfer,i} \quad [4.5]$$

Similar to the conservation of mass equations, the conservation of momentum equation for each phase are coupled by the summation of the volume fraction of each phase being equal to unity at each computational cell. In addition, the conservation of momentum equation for each phase are coupled by the momentum source terms, denoted as $M_{transfer,i}$. One of the primary goals of this research is to be able to develop a representation of the momentum exchanges occurring between the phases. The momentum source term represents the sum of the forces, which one phase exerts a force on the other phase.

4.4. Modeling Interphase Momentum Transfer

As discussed in Section 4.2, momentum transfer is based on two primary effects: 1) momentum exchanges between the air and the dispersed particles due to drag effects, and 2) the distributed resistance on the carrier phase due to the concentration and the connectivity of the particles. These two effects can be summed for the total momentum transfer in the following equation. For simplicity, the momentum transfer will be referred to in vector form.

$$\mathbf{M}_{transfer} = \mathbf{F}_{Drag} + \mathbf{F}_{Connectivity} \qquad [4.6]$$

where $\mathbf{M}_{transfer}$ is the momentum exchange occurring between the two phases, and is composed of two components. The first component, $\mathbf{F}_{Drag}$, is the drag force occurring between the phases, and the second component, $\mathbf{F}_{Connectivity}$, accounts for the additional resistances due to the presence of the dispersed fibers, strings, etc., entrained in the flow.

4.4.1. Defining the Drag Effects

The drag force can be based on correlations typically related to the Reynolds number and the shape of the particle. In many cases, the specificity is a common feature for comparison. The relationship between the sphericity and the drag correlation is shown below. The sphericity has a profound effect on the particle drag correlation. The difference in the drag coefficient is generally observed at medium to high Reynolds numbers. Generally, as the particle sphericity decreases, the coefficient of drag due to the particle presence increases. Although spherical particles would be simpler to assume and to model, the drag could be off by a factor of two or greater, thus potentially having a significant impact on the performance and behavior of the flow.

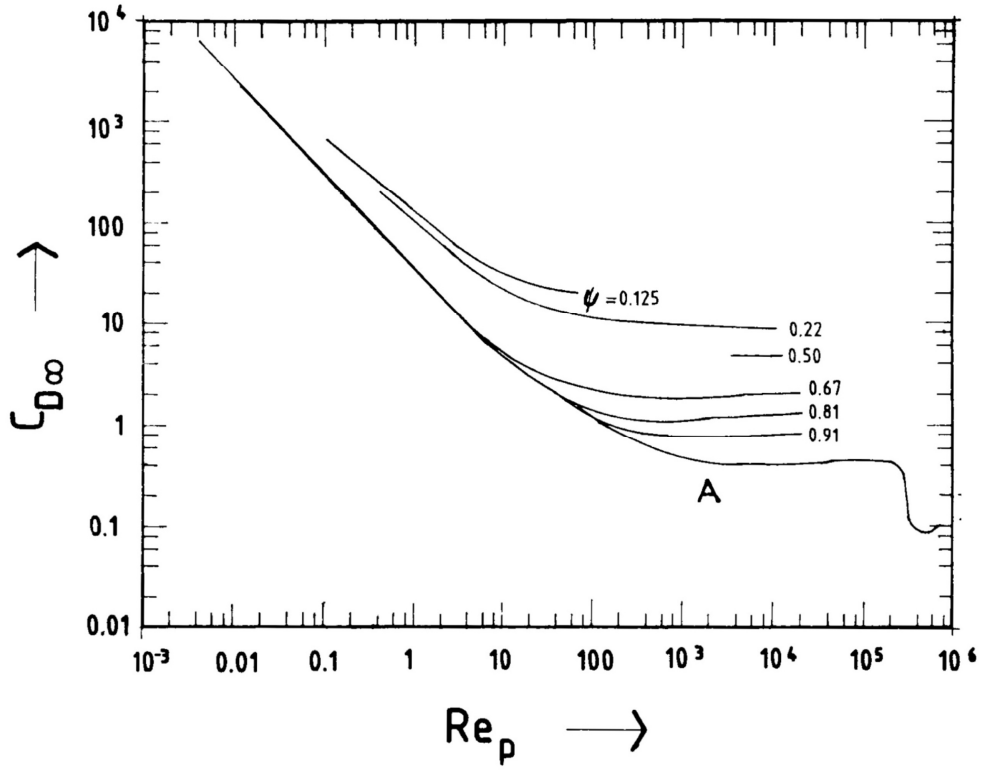

Figure 4.1. Correlations for coefficient of drag versus particle Reynolds number (Klinzing 1997).

Therefore, the drag effects of the bulk solids phase for this study are based upon modified drag correlations developed in Tran-Cong and Michaelides (2004). This function was chosen because it accounts for the relative particle Reynolds number, the relative velocity of the particles entrained in the air, the projected area of the particles, and the shape factor of the particles. For example, if the particle is not spherical (e.g., a relatively flat ellipsoid), this formulation accounts for these effects. The drag coefficient equation is given as follows,

$$C_D = \frac{24}{\mathrm{Re}_d}\frac{d_A}{d_n}\left[1+\frac{0.15}{\sqrt{c}}\left(\frac{d_A}{d_n}\mathrm{Re}_d\right)^{0.687}\right] + \frac{0.42\left(\frac{d_A}{d_n}\right)^2}{\sqrt{c}\left[1+4.25x10^4\left(\frac{d_A}{d_n}\mathrm{Re}_d\right)^{-1.16}\right]} \qquad [4.7]$$

where d_A is the diameter of a sphere with equal projected surface area, and d_n is the diameter of a particle with equal volume, and are equated in the following manner. The relationships for each are given as follows,

$$d_A = \left(4A_p/\pi\right)^{1/3} \qquad [4.8]$$

$$d_n = \sqrt[3]{6V/\pi} \qquad [4.9]$$

In addition, the relative (or particle) Reynolds number for multiphase flows is given as follows (Crowe et al. 1998),

$$\mathrm{Re}_d = \frac{\rho_{air}\left|\mathbf{u}_{relative}\right|d_A}{\mu_{air}}. \qquad [4.10]$$

The relative Reynolds number is one of the fundamental dimensionless relationships in fluid mechanics, and it is used extensively for multiphase flows. It should be noted that the relative

Reynolds number uses relative velocity difference between the air and the particle rather than the velocity of the flowing air, similar to what is done for pipe flows of fluids. The coefficient of drag correlation can then be implemented within the drag force calculation for an Eulerian-Eulerian as follows,

$$\mathbf{F}_{Drag} = C_D\left(\frac{3}{4}\frac{\alpha_{particle}\rho_{air}}{d_{particle}}\left|\mathbf{u}_{relative}\right|\mathbf{u}_{relative}\right) \qquad [4.11]$$

4.4.2. Quantifying the Connectivity Effects

The second effect quantified in the interphase momentum transfer is the connectivity of the dispersed phase. This accounts for momentum exchanges due to the additional resistances of the stringy, fibrous, connected, or rough particles. Since these additional momentum transfer effects are not typically expressed in multiphase flow modeling, the following background is provided for clarity. Often in CFD modeling, a momentum source term is added to account for features through a mesh sub-domain whose effects may be too small to be numerically resolved within the overall calculations. Rather than attempting to resolve these small features numerically, the effects are represented as distributed momentum sinks or resistances. Examples of these situations include flows in porous media, such as packed beds and chemical reactors, honeycomb structures, and flows in fibrous bulk solids.

When one examines fibrous multiphase flows, one can find several similarities between flows such as these and with distributed resistance flows. The fibrous particles are irregularly shaped and have strings that connect several particles together. In addition, the distributed fibers exhibit a resistance that is typically greater than what is experienced with

minute spherical particles. This resistance, in essence, acts in a similar fashion as a moving porous media. These extra resistance effects may be incorporated within the CFD model to aggregate the extra effects not accounted for with the particle drag calculations. These effects may include particle rotation, particle air retention, particle collisions, and particle deformation.

In single-phase flows involving distributed resistances, it is assumed that within a volume containing a distributed resistance, there is a local balance between the pressure and resistance forces, given as follows,

$$-K_i v_i = \frac{\partial p}{\partial \zeta_i} \qquad [4.12]$$

where ζ_i(i=1,2,3) represents the mutually orthogonal orthotropic directions, and

K_i is the porous resistance and

V_i is the superficial velocity in direction

This resistance is assumed to be a quasilinear function of the superficial velocity of the magnitude of the form

$$K_i = \gamma_i |\mathbf{v}| + \beta_i \qquad [4.13]$$

where $\gamma_i$and β_i are user-supplied coefficients with dimensions of [kg/m^4] and [kg/(m^{3}s)], respectively. The coefficients may be uniform or be based on any acceptable correlation. These coefficients can also be set to vary according to additional quantities such as velocity

and temperature. Often these coefficients are derived from empirical data, such as highly porous media (Darcy flow) and moderately porous media. In these instances, the resistance (in other words the pressure drop) is given by an experimental curve as a function of superficial velocity. The superficial velocity is defined as the volumetric flow rate of the air divided by the total cross sectional area.

Using the distributed resistance (porous media analogy), one can apply the principles to quantify the extra effects found in fibrous multiphase gas-solid flows. In single-phase porous media flows, the distributed resistance is stationary and always occupies the same volume. In order to use the same methodology, the model will need to account for the distributed resistance to move in time, while simultaneously changing the volume that it occupies. This can be achieved in the following manner. Beginning with the quasilinear function for the distributed resistance,

$$K_i = \gamma_i |\mathbf{v}| + \beta_i, \qquad [4.14]$$

one can replace the superficial velocity term with a relative velocity term. Therefore, the resistance function will be dependent on the bulk solids velocity in relation to airflow. This relationship is shown as follows,

$$K_i = \gamma_i |\mathbf{u}_{relative}| + \beta_i. \qquad [4.15]$$

This formulation indicates that if the relative velocity is near zero, then the distributed resistance associated with the presence of the particles approaches zero.

The second consideration for the distributed resistance momentum transfer is assuming the magnitude of the resistance to be a function of the dispersed phase concentration. Intuition indicates that as the bulk solids concentration increases, the distributed resistance also increases. One value that it can gather is the volume fraction of the air and bulk solids phases at each cell. However, this cannot be correlated with a linear function associated with the volume fraction. Rather, this is more representative of a particle spacing calculation. Fortunately, the volume fraction information can provide an approximation for calculating the particle spacing. This may be represented as the following,

$$\frac{d}{L} = \left(\frac{6\alpha_d}{\pi} \right)^{1/3} \qquad [4.16]$$

where the d is the representative diameter of the particles, and L is the length between centers of particles.

By accounting for 1) the relative velocities between the air and the solid phases, and 2) the concentration of the particles, the modified correlation of the distributed resistance is as follows,

$$\mathbf{F}_{connectivity} = -\frac{d}{L}\left(\gamma|\mathbf{u}_{relative}| + \beta\right)\mathbf{u}_{relative} \qquad [4.17]$$

where $\frac{d}{L} = \left(\frac{6a_d}{\pi} \right)^{1/3}$ and where γ and β are user supplied coefficients, and are estimated on particle concentration, particle compressibility, and other losses. This formulation is based on the relative velocity of the dispersed phase with the carrier phase and a function of the volume fraction. This function of the volume fraction determines the estimated length between the dispersed particles.

The connectivity resistance is then applied to the momentum transfer terms within the momentum equations for the air phase and the bulk solids phase for each computational cell.

4.5. Implementing Momentum Transfer Functions in STAR-CD™

This section outlines the process for implementing the described momentum transfer functions within STAR-CD™ with user-defined functions or subroutines. STAR-CD™ has built-in correlations based upon previously studied and well-established flows to account for standardized flow and thermal effects. In addition, STAR-CD™ has the ability to allow users to define non-standard effects for their specific flow cases. User-defined functions, also known as subroutines, enable users to define unique features, including transient boundary conditions, rotating meshes, and other complicated models that are not already implemented in the standard CFD solver package. User-defined functions allow a CFD analyst to incorporate additional effects or calculations specific to their particular application. This research utilizes two user-defined functions in STAR-CD™ to incorporate the two resistive effects. Section 4.5.1 will discuss the procedures for implementing the drag correlations in the Eulerian-Eulerian Drag subroutine (uedrag.f), while Section 4.5.2 will discuss how the

additional resistive effects are implemented in the momentum source term subroutine (sormom.f).

4.5.1. The User-Defined Drag Force Subroutine

The first subroutine described is the user drag function for the Eulerian-Eulerian two-fluid model. This subroutine returns a drag force per unit volume for each computational grid point. To implement the drag correlation defined in Equation 4.7 requires that several variables be set. These variables include the carrier phase density, the relative particle velocity, the relative particle Reynolds number, and the representative dimensions of the bulk solids particles. Several of these parameters are defined within the STAR-CD™ model; however additional parameters will need to be defined or calculated. Since the bulk solids particles are assumed to be ellipsoids, three characteristic lengths need to be defined. These are defined as follows within uedrag.f

ELLENGTH='characteristic length of the ellipsoid (m)'
ELWIDTH='characteristic width of the ellipsoid (m)'
ELHEIGHT='characteristic height of the ellipsoid (m)'

Once these characteristic lengths of the ellipsoid are defined, then the ellipsoid volume and three projected areas can be calculated. The ellipsoid volume is determined by the equation of an ellipsoid, which is given as

$$V_{ellipsoid} = \frac{4}{3}\pi\ r_1\ \ r_2\ \ r_3 = \pi\ \ \frac{l_1}{2}\frac{l_2}{2}\frac{l_3}{2} \qquad [4.18]$$

where *r* and *l* are the radius and of the three axes, and is applied to the subroutine as

```
ELLIPVOL=4/3.0*3.141*(ELLENGTH/2.0)*(ELWIDTH/2.0)*(ELHEIGHT/2.0)
```

In addition, the three projected areas are calculated. This study assumes that any one of the three ellipsoid axes is perpendicular to the airflow. The equation for the projected area of an ellipsoid is given by

$$A_{proj\_ellipsoid} = \pi \; r_1 \;\; r_2 = \pi \;\; \frac{l_1}{2}\frac{l_2}{2} \qquad [4.19]$$

and is applied to the subroutine in the following manner for each of the three axes.

```
ELAREAA=3.14159*(ELLENGTH/2.0)*(ELWIDTH/2.0)
ELAREAB=3.14159*(ELLENGTH/2.0)*(ELHEIGHT/2.0)
ELAREAC=3.14159*(ELWIDTH/2.0)*(ELHEIGHT/2.0)
```

Additionally, the d_A values are calculated for each one of the orthogonal projected areas, and is show as

```
DAA= SQRT(4*ELAREAA/3.14159)
DAB= SQRT(4*ELAREAB/3.14159)
DAC= SQRT(4*ELAREAC/3.14159).
```

The d_n value is a single calculation that is based on the ellipsoid volume and is implemented in the subroutine as follows

```
DNVAL=(6.0*ELLIPSVOL/3.14159)**(0.333)
```

Once these values are known, then the variables for the drag function may be constructed. For example, the values of $(d_A/d_n)^2$ may be calculated for each direction, and are given as

```
DADNSQA=(DAA/DNVAL)**2
DADNSQB=(DAB/DNVAL)**2
DADNSQC=(DAC/DNVAL)**2.
```

In the same manner, the (d_A/d_n) value of interest may be calculated, and is implemented as follows

```
DADN=DAA/DNVAL.
```

An additional term that is used is the sphericity of the particle of interest. By definition, the sphericity is a measure of how round an object is, which is determined by the ratio of the surface area of a sphere (with the same volume as the given particle) to the surface area of the particle. In the most general sense, the equation of sphericity ψ is given by

$$\psi = \frac{\pi^{1/3}(6 * V_{particle})^{2/3}}{A_{particle}} = \frac{\pi d_n}{A_{particle}} \qquad [4.20]$$

where $A_{particle}$ is the surface area of the particle. Sphericity is commonly recognized to be an appropriate single dimensionless number for characterizing the shape of non-spherical particles. However, sphericity is often difficult to quantify for highly irregular particles because it requires a measure of the particles surface area, which is not easy to quantify in

many cases. For simplicity, additional shape factors have been used, which are easier to obtain for other particles. One particular factor is known as the particle circularity (also known as surface sphericity *c*), and is defined as follows,

$$c = \frac{\pi d_A}{P_{particle}} \qquad [4.21]$$

where $P_{particle}$ is the projected perimeter of the particle in its direction of motion.

For this study it is implemented into the subroutine as follows:

```
SPHERTOP=3.14159*DAA
SPHERBOT=2.0*3.1415*SQRT(((ELLENGTH/2)**2+(ELWIDTH/2)**2)/2)
SPHER=SPHERTOP/SPHERBOT
```

At this point, the user-defined variables are determined. The rest of the variables necessary for each computational cell may be obtained from knowing the velocities of each phase from STAR-CD™. For example, the air velocity magnitude is obtained from knowing the velocity components. This is done as follows for the air phase as

$$U_{air} = \sqrt{u_{air}^{\ 2} + v_{air}^{\ 2} + w_{air}^{\ 2}}, \qquad [4.22]$$

where *u*, *v*, and *w* are the velocity components. Similarly, the velocity for the particle phase at each location is defined as

$$U_{solid} = \sqrt{u_{solid}{}^2 + v_{solid}{}^2 + w_{solid}{}^2}, \qquad [4.23]$$

while the relative velocity between the air and the particle are determined by

$$U_{relative} = \sqrt{(u_{air} - u_{solid})^2 + (v_{air} - v_{solid})^2 + (w_{air} - w_{solid})^2} \qquad [4.24]$$

The velocity magnitudes for each phase are implemented in the subroutine as follow

```
VAIR=SQRT((U)**2+(V)**2+(W)**2)
VPART=SQRT((UCEL2)**2+(VCEL2)**2+(WCEL2)**2)
VREL=SQRT((U-UCEL2)**2+(V-VCEL2)**2+(W-WCEL2)**2).
```

Please note the terms U, V, and W are defined as the velocity components of the air phase while the terms UCEL2, VCEL2, and WCEL2 are defined as the velocity components of the second phase.

The relative velocity of the bulk solids to the air is used to determine the particle Reynolds number, which is incorporated as follows

```
REYP=DEN*VREL*DNVAL/(VISM),
```

in which the terms DEN and VISM terms are the density and viscosity values assigned to the air phase from STAR-CD™.

With this information, the drag function may be calculated. Since the equation is rather long, it is split into several terms, which are calculated separately and combined at the end.

```
DADNREYP=DADN*REYP
TERMONED=(24.0/REYP)*DADN*(1.0+0.15/SQRTSPH*DADNREYP**0.69)
TERMTWODA=(0.42*DADNSQ)
TERMMTWOB=(SQRTSPH*(1.0+0.000425*(DADN*REYP**(-1.16))))
CD=(TERMONED+TERMTWODA/TERMMTWOB).
```

Once this is complete, the C_D (coefficient of drag) term is used to determine the drag force per unit volume by the following equation

$$F_{drag} = \frac{3}{4}\frac{\alpha_{particle}\rho_{air}C_D}{d_{particle}}\left|\mathbf{u}_{relative}\right| \qquad [4.25]$$

and is implemented in the subroutine as

```
DFAC=0.75*VFCEL2*DEN*VREL*CD/PARTDIA.
```

The DFAC variable for each cell is returned to STAR-CD™, which provides the first primary effect of the fibrous flow to the system. The next section will describe the theory behind adding the second primary effect to the multiphase flow—the connectivity and additional effects that are not directly accounted for in the drag force calculation.

4.5.2. The User-Defined Momentum Source Term Subroutine

The second subroutine utilized in this study is the momentum source subroutine, known as sormom.f in STAR-CD™. The momentum source subroutine for STAR-CD™ has been originally designed to model a distributed resistance, or porous media flow. This modeling framework is utilized for situations in which the flow occurs through a mesh sub-domain containing fine-scale geometric features whose effects may be too small to be numerically resolved within the overall calculations.

The sormom.f subroutine enables the user to specify a momentum source (or sink) term per unit volume on a cell-by-cell basis in linearized form. This linearized form is as follows:

Source in x direction = S1U-S2U*U, (N/m^3)
Source in y direction = S1V-S2V*V, (N/m^3)
Source in z direction = S1W-S2W*W, (N/m^3),

in which the parameters returned to STAR-CD™ are S1U, S1V, and S1W, which are not multiplied by the velocity components, while the terms S2U, S2V, and S2W are multiplied by the U, V, or W velocity components.

Similar to the uedrag.f subroutine, the sormom.f subroutine has access to several variables inherent in the STAR-CD™ model, which can be used as variable for the returned values. Additionally, two coefficients are set within this subroutine, γ and β. The details of the sormom.f subroutine are given as follows.

The relative velocity components are determined by taking the square root of the squared difference in each direction. This is determined as follows in the subroutine

```
URELATIVE = SQRT((U-UCEL2)**2)
VRELATIVE = SQRT((V-VCEL2)**2)
WRELATIVE = SQRT((W-WCEL2)**2).
```

The relative velocity magnitude is determined in a similar manner.

```
VELRELATIVE = SQRT((U-UCEL2)**2+(V-VCEL2)**2+(W-WCEL2)**2).
```

The second item to determine in the subroutine is the factor for the concentration. This is a single line function in which d/L is set as a variable named VFFAC. This line of code is given as follows

```
VFFAC = (6.0*VFCEL2*0.318309866)**0.3333
```

The remaining two variables that are left to calculate the moving distributed resistance are γ and β. These two variables are set based on the bulk solids characteristics observed in experimental tests of the bulk solids of interest. These variables are adjusted in the computational model to match the flow characteristics observed in the experimental tests. These variables may be correlated by one of two methods. The first is by matching the computational velocity profiles with the experimental velocity profiles in the regions of interest. The second is based on matching the pressure profiles in the regions of interest between the computational and experimental data..

GAMMA = ‘parameter set by user based on bulk solids characteristics’
BETA = ‘parameter set by user based on bulk solids characteristics’

Given this information, we can now set the values of the momentum source in each of the three Cartesian directions. In order to return values as a relative velocity rather than an absolute velocity, the S2_ terms ought to be zero. In addition, since the momentum source is assumed to act as a momentum sink for the air phase, the resistance is required to act in the opposite direction as the velocity components of the air. To ensure the momentum source is acting in the opposite direction of the air velocity, conditional statements are utilized to have the momentum source act accordingly. The following demonstrates how this is implemented within the subroutine.

```
IF (U.GT.0.0000) THEN
        S1U = -VFFAC*((GAMMA*VELREL+BETA)*VELREL)
ELSE
        S1U = VFFAC*((GAMMA *VELREL+BETA)*VELREL)
ENDIF

IF (V.GT.0.0000) THEN
        S1V = -VFFAC*((GAMMA *VELREL+BETA)*VELREL)
ELSE
        S1V = VFFAC*((GAMMA *VELREL+BETA)*VELREL)
ENDIF

IF (W.GT.0.0000) THEN
        S1W = -VFFAC*((GAMMA *VELREL+BETA)*VELREL)
ELSE
        S1W = VFFAC*((GAMMA *VELREL+BETA)*VELREL)
ENDIF
```

Since the momentum source terms are accounted for within the S1_ terms, it is not necessary to assign anything other than zero to the S2_ terms, which are provided below.

S2U = 0.0
S2V = 0.0
S2W = 0.0.

The S1_ and S2_ values for each cell are returned to STAR-CD™, which provides the additional resistances of the fibrous flow to the system. This subroutine provides the user with a means to adjust two parameters, γ and β, which are specific to the fibrous bulk solids of interest. If the bulk solids has a high amount of connectivity with other fibers that extend beyond the computational grid, or if the bulk solids has a great deal of porosity or air retention, then γ and β may be increased accordingly to reflect what is occurring in the actual cases. However, if the bulk solids have a low amount of connectivity and do not exhibit a great deal of additional effects, these parameters may be adjusted lower. For this study, the parameters of γ and β are adjusted based on the velocity profiles observed in experimental data. However, they may also be determined by creating a packed bed of the bulk solids and determining the pressure drop associated with varying air velocities flowing through the bulk solids of interest.

4.5.3. Hierarchy of Subroutines in the CFD Solver

Figure 4.2 shows how the two subroutines are implemented in STAR-CD™. Notice the two-way communication between the primary CFD solver and the respective subroutines. However, it should be noted that the subroutines only have the ability to return only the

values allowed, i.e., the subroutine cannot change values such as velocity, temperature, etc., during the solver process.

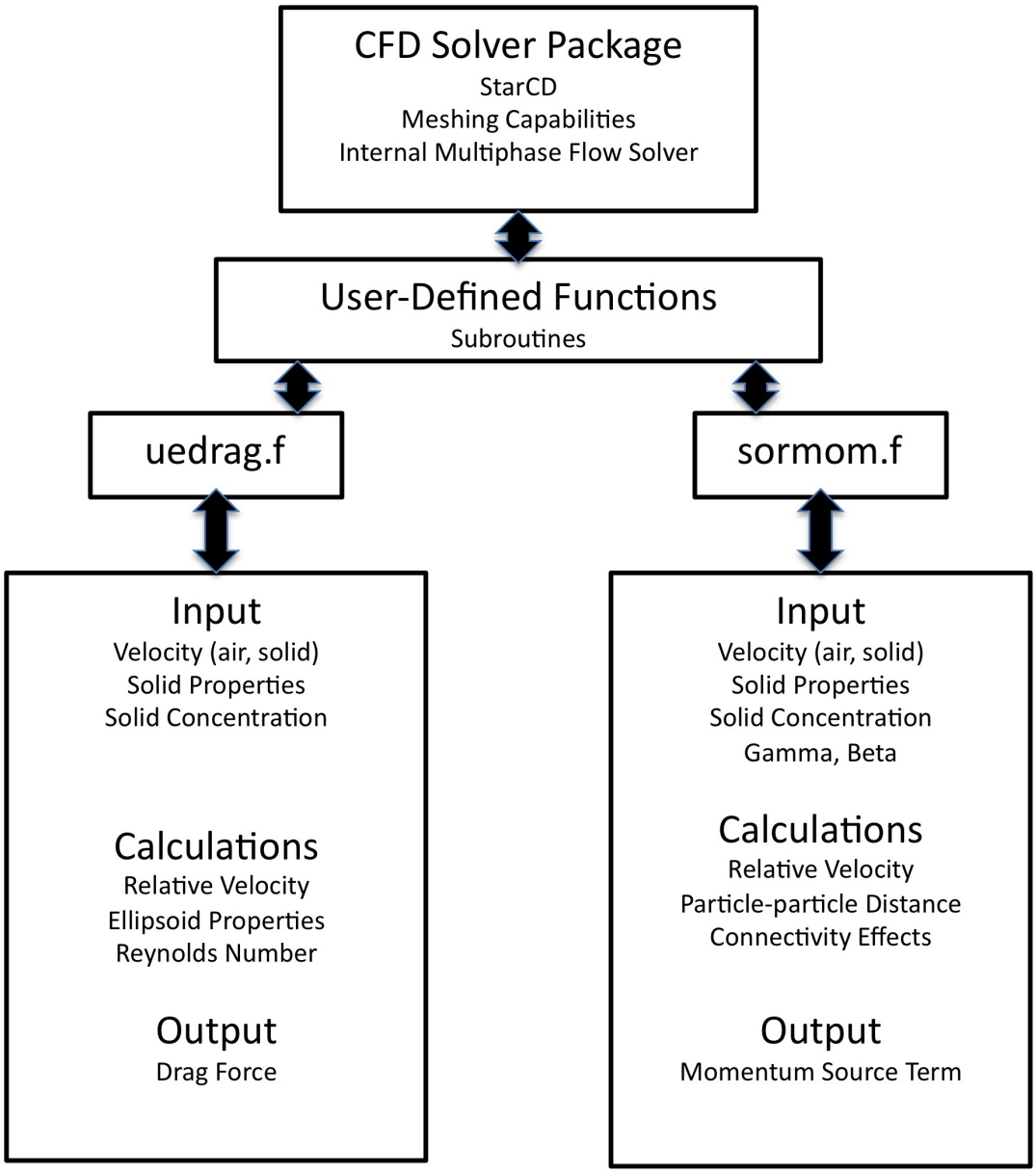

Figure 4.2. Schematic illustrating hierarchy of user-defined functions.

4.5.4.Turbulence Modeling

The turbulence model implemented in this study is the high Reynolds number k-ε model. The following table lists the specified values of the turbulence parameters.

Table 4.1. Coefficients for the k-ε turbulence parameters.

k-ε Turbulence Parameters	Value
C_{μ}	0.09
σ_k	1.0
σ_{ε}	1.22
σ_h	0.9
σ_m	0.9
$C_{\varepsilon 1}$	1.44
$C_{\varepsilon 2}$	1.92
$C_{\varepsilon 3}$	0.00
$C_{\varepsilon 4}$	-0.33
κ	0.419
E	9.0

4.5.5. Convergence and Post-Processing

The process of solving CFD models can be inherently difficult due to issues of computational convergence. This is often the case with single–phase CFD models that have multiple boundary conditions and complicated unstructured grids. When a multiphase system is being solved, the added complexity increases the likelihood of convergence problems. Often, one will be required to solve the CFD model in transient mode and decrease the time steps between iterations. In addition, one may need to set initial conditions within the model by specifying a volume fraction of bulk solids throughout the computational mesh to reduce stability. After each simulation, the velocity profiles for each phase were inspected and

compared with experimentally obtained data. In addition, the pressure drops between the inlet and outlet of the systems were compared with a baseline single-phase air phase.

CHAPTER 5: EXPERIMENTAL STUDY OF COTTON-AIR FLOW

The mathematical description of modeling fibrous flows presented in Chapter 4 provides a generalized representation of incorporating the effects of the fibrous solid phase and its influence of the conveying air phase within a CFD model. The first effect modeled is the drag resistance on the individual particles as they travel with the conveying air. The second effect modeled is the resistance due to additional behaviors of the particles, including particle collisions, rotations, and connections between adjacent particles. Both of these effects are specific to the fibrous bulk solids of interest. The two combined effects are incorporated into the CFD model as source terms in the momentum equation of each phase, which enables interphase momentum transfer between the two phases. The effects are quantified in the model through parameters set within the CFD model in the user-defined functions.

This chapter offers a description of the experimental setup and data analysis of cotton-air flow in a positive pressure pneumatic transport duct. Cotton was chosen for this study because it exhibits similar characteristics as fibrous biomass bulk solids, in which the cotton bolls have a large characteristic size and low particle density. In addition, the information obtained from the experimental models will guide the parameter specifications of the cotton-air CFD model described in Chapter 6.

5.1. Experimental Test Apparatus of Cotton-Air Flow

Figure 5.1 shows the experimental test apparatus used to study the flow behavior of pneumatically transported cotton. The experimental test apparatus is utilized for collecting

and analyzing the flow characteristics of the cotton flow, including velocity profiles and cotton accumulation. The conveying line transports the cotton horizontally through a single 90° elbow, denoted by the diagonally shaded region of interest. The experimental test apparatus is a positive pressure system constructed of square ducting with a cross sectional area of 0.09 m^2 (1 ft^2). The blower is located 6 m (20 ft) upstream from the 90° elbow, and is operated by a variable speed electric motor. The blower supplying air to the test apparatus can provide air volumetric flow rates of up to 125 m^3/min (4500 CFM). This study investigated cotton flows at air volumetric flow rates of 70 and 125 m^3/min (2500 and 4500 CFM). The cotton bolls are fed into the conveyance line by a lock hopper 2 m downstream from the blower. The metering device provided a bulk solids mass flow rate of cotton at 15 to 75 kg/min (1 to 3 T/hr), with an estimated particle density of 250 kg/m^3. The cotton flows 4 m (13 ft) through the conveyance line and enters the 90° elbow. After the cotton leaves the elbow, it travels 4 m (13 ft) where exits to a collection basket at the outlet of the test rig.

Figure 5.2 shows an expanded schematic of the experimental test apparatus at the 90° elbow. The top wall of the elbow is constructed with a Lexan® sight window located on the top wall of the conveyance line. The window enables visual observations of the bulk solids as they travel through the conveyance line. The window extends 0.6 m (2 ft.) upstream from the impact region and extends 0.6 m (2 ft.) downstream to observe the behavior of the cotton as it enters the elbow and reaccelerates after leaving the elbow, respectively.

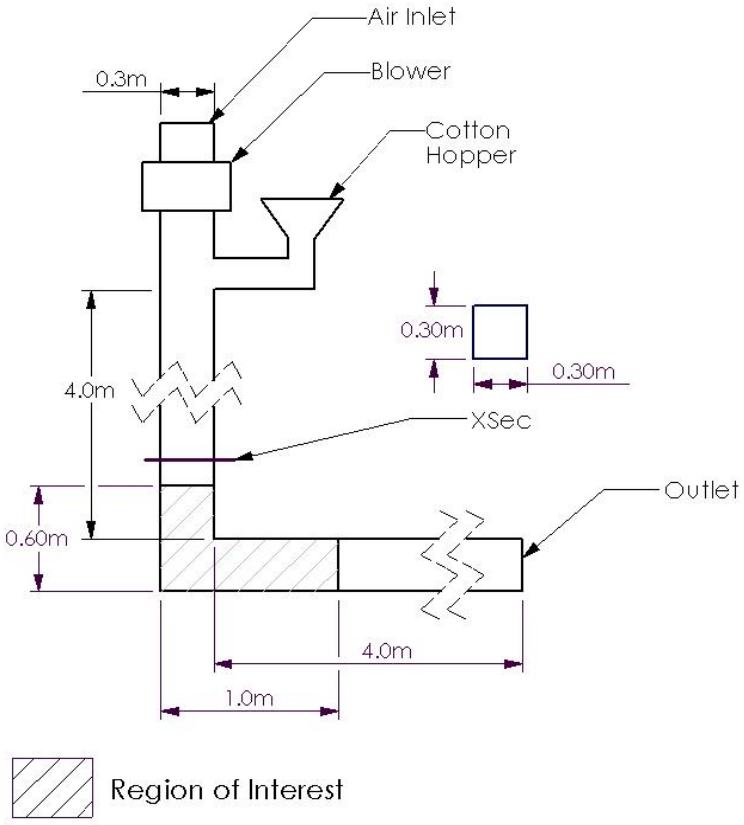

Figure 5.1. Schematic of the experimental test apparatus for cotton-air flow study.

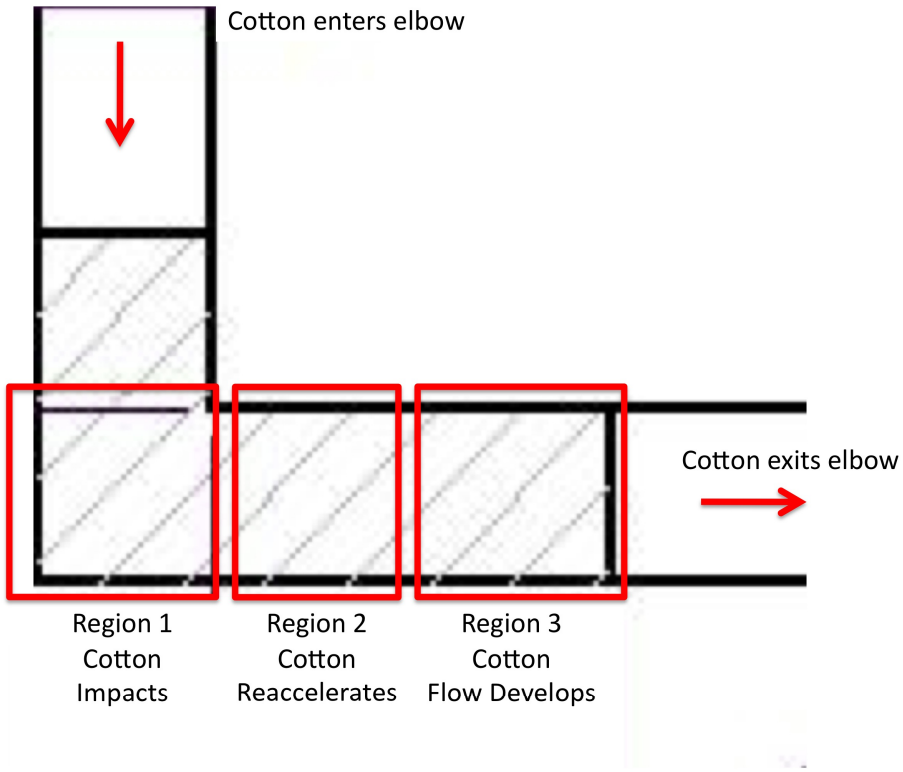

Figure 5.2. Expanded view of test apparatus illustrating three regions of interest.

Figure 5.3 shows a top view of the 90° elbow of the experimental test apparatus. A series of Olympus Encore high-speed digital video cameras capturing at 250 frames per second at a 2 times sampling rate were placed above the conveyance line at the regions of interest. These settings were necessary to capture the flow of the cotton through several consecutive frames for the video analysis while minimizing the blurring of the cotton as it traveled through the video frame. The first camera was placed immediately above the elbow to record the cotton behavior at the impact region. The second camera was placed immediately after the impact region of the bend to record the cotton behavior in the

reacceleration region of the conveyance line. The third camera was placed downstream from the reacceleration region to record the cotton effects after it is reaccelerated and approaching a developed velocity.

Figure 5.3. Photograph of elbow region in experimental test apparatus.

Figure 5.4 shows a still frame from one of the high-speed videos collected directly above the 90° elbow. The cotton bolls travel from the inlet of the conveyance system and impact the outer wall of the 90° elbow. After impact, the cotton particles are re-entrained in the flow stream and exit the bend. In this representation, the cotton is moving to the right. One can observe the large size and rather unique shape of the cotton in addition to the interconnected strings among the cotton bolls. In addition, one may also estimate the size and

orientation of the cotton bolls as they travel through the flow. Although the cotton appears to be quite variable in size and shape, one can make the observation that cotton bolls are ellipsoidal in shape with a long axis diameter of approximately 4 cm, and the secondary axes 2 cm. Furthermore, the cotton bolls generally appear to have their long axis oriented perpendicular to the free stream airflow.

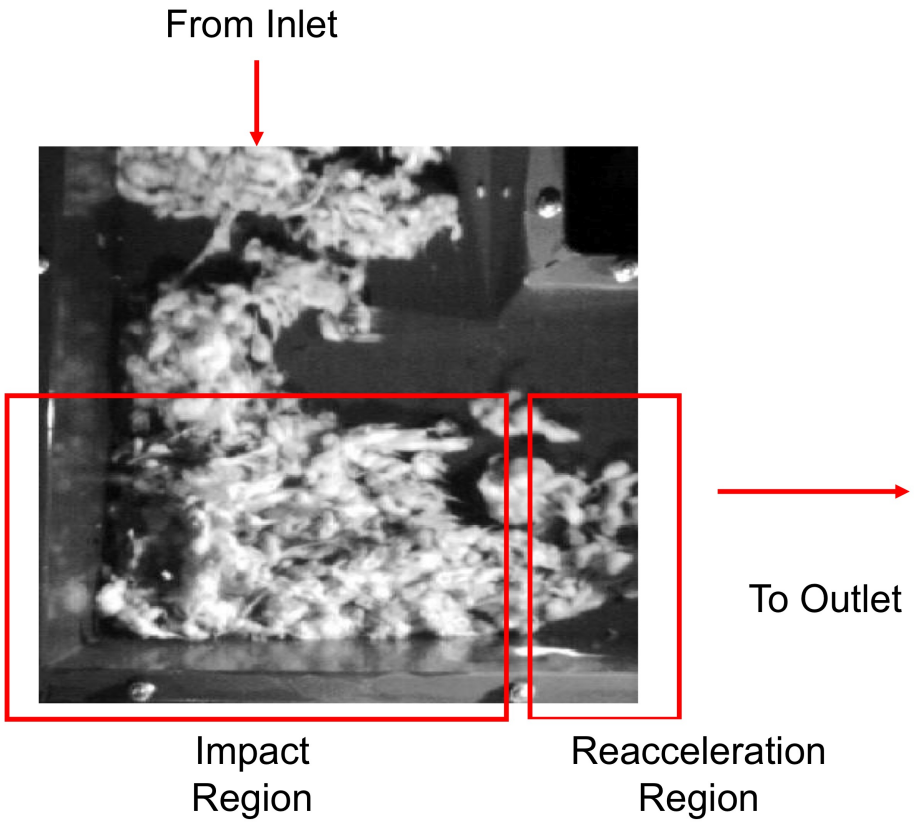

Figure 5.4. Still frame from high-speed video of cotton flow.

Figure 5.5 shows four still frames of the high-speed digital video of the cotton flowing into the 90° elbow. The screenshots show the variability in the flow behavior of

cotton. As the cotton approaches the outer wall of the 90° elbow, it impacts and accumulates along the outer wall. The buildup and cleaning of the cotton occurs regularly in the bend.

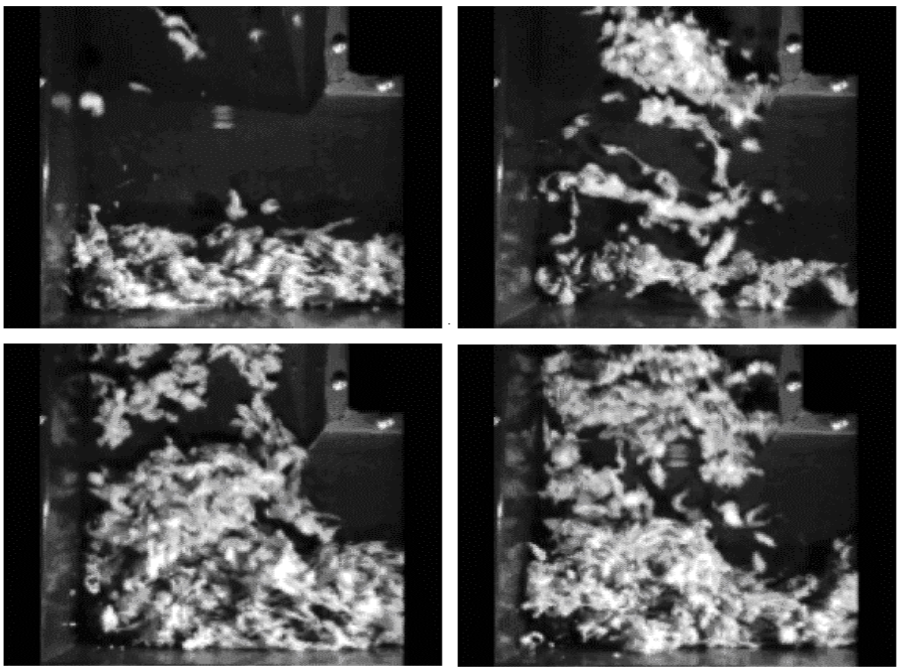

Figure 5.5. Four still frames of high speed video of cotton flow.

5.2. Analysis of the Experimental Cotton Flow Results

After the experimental videos were collected, the videos were processed to determine the trajectory and the velocity of the cotton flowing through the bend. An open-source video processing package, OpenCV (Intel Corporation 2001), with additional user programming was utilized in tracking the cotton features throughout consecutive frames. This program enabled the tracking of the cotton boll features within the videos on a pixel-by-pixel basis. Figure 5.6 shows the particle tracking of several cotton particles as they were flowing through the conveyance line.

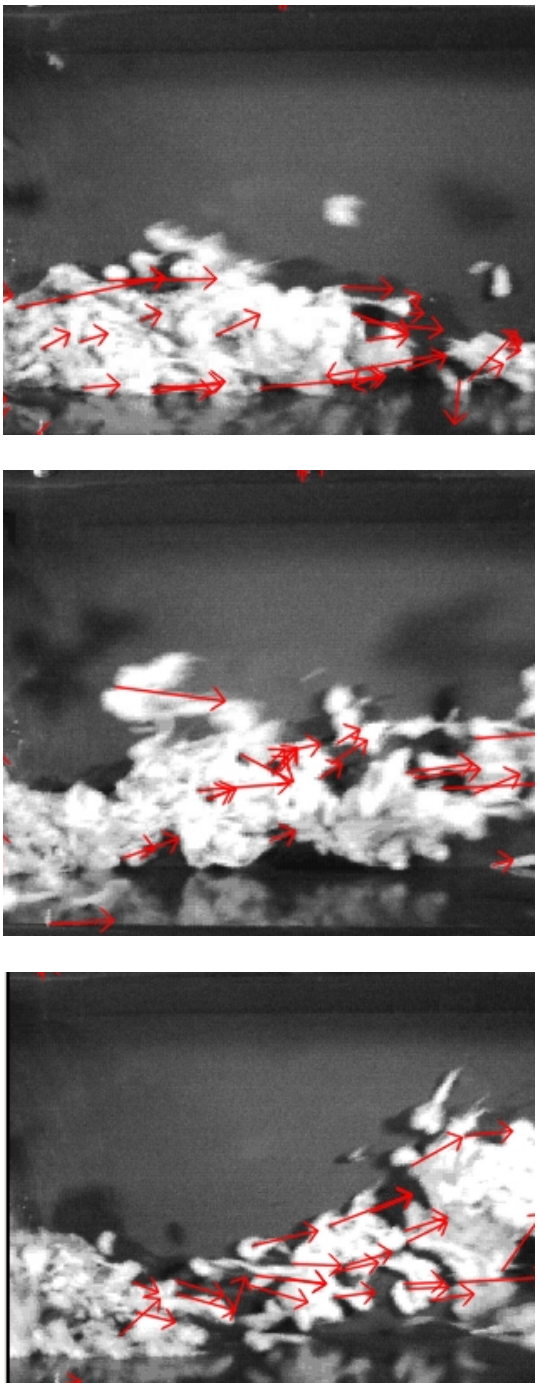

Figure 5.6. Tracking cotton bolls in high-speed video.

The velocity profiles are assembled by tracking a series of particles through several still frames of the high-speed video, which estimates a change in position on a pixel-by-pixel basis. Once the pixel to physical space relationship is determined, one can use the change in pixel measurement per video frame rate to calculate particle velocity profiles. The cotton boll velocities are tabulated and the resulting velocities are mapped in the corresponding region of the test apparatus. Each video picture was subdivided into a 7.5 cm x 7.5 cm (3 in. x 3 in.) sub regions, which resulted in a resolution of velocity profiles of three sub regions wide on the duct. The change of the pixel position of the cotton bolls given the difference in the time step was used to calculate the velocity of the cotton at each location of the recorded regions. The velocity was tabulated and ensemble averaged at each of these sub regions. A composite cotton velocity profile was created for the 70 and 125 m^3/min air volumetric flow rates and are shown in Figures 5.7 and 5.8.

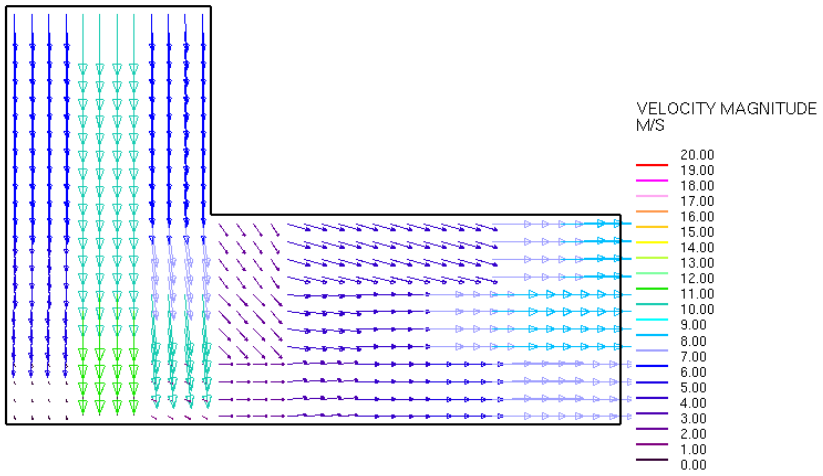

Figure 5.7. Composite of experimental cotton velocity at 70 m^3/min.

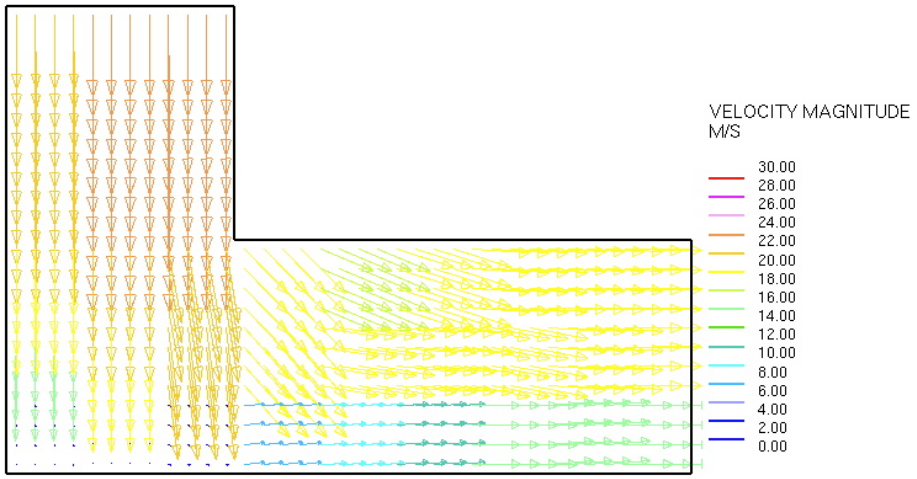

Figure 5.8. Composite of experimental cotton velocity profiles at 125 m^3/min.

The velocity profiles for the two air volumetric flow rate tests are used to adjust the two connectivity parameters for the momentum source terms.

5.3. Experimental Observations of Cotton-Air Flow

Cotton has an irregular shape and is significantly larger in size than most powder type flows. The shape of a cotton particle is primarily a sphere-derived ellipsoid. However, the cotton has strings extending from the boll that deviate it further from being spherically shaped. Even before impact, the cotton is not axisymmetric, so the orientation has an effect on the flow characteristics. In addition, the cotton boll is flexible and deforms significantly upon impact when influenced by air movement. Furthermore, cotton can become entangled with other cotton particles and has these strings that connect various cotton masses together. The distributed fibers contribute to disturbances of the primary flow field and have the ability to deform and absorb momentum from the flow.

The experimental results indicate interesting observations about the behavior of the cotton. In Region 1, the cotton velocity profile is fully developed and maintains its momentum until impacting the outer wall. The cotton is at fully developed flow, as noted by the centerline velocity being at a slightly greater velocity than the outer edges. The cotton then impacts the bend and approaches a momentarily near zero velocity. At this point, the cotton bolls deform to ~50% of the diameter. The corner of the elbow accumulates cotton, which is not able to readily escape the corner and has therefore a low velocity. In addition, the cotton is observed to deform upon impact in the bend.

There are several phenomena that are observed in the cotton flow through the elbow. These include cotton impact with the duct walls, collision with other cotton particles, and re-

entrainment. When cotton bolls are introduced into the airflow, the particles accelerate to a velocity approaching the free stream air velocity. When the cotton approaches an impact region, it has enough momentum that it does not turn with the flow but impacts the wall and any cotton accumulated there and rapidly decelerates. After the cotton is stopped by the outer wall of the impact region, it collides with subsequent cotton particles. It will eventually become re-entrained with the airstream where it re-accelerates; similar to the when cotton was first introduced in the flow field. The cotton is also influenced by the flow characteristics of other cotton particles. The cotton may collide with other cotton particles and combine to form a larger cotton mass. The cotton also has the ability to separate; however, observations have shown that this effect is not very likely to occur. The cotton has strings that will keep the cotton bolls connected as they are conveyed in the system.

Eventually the cotton will leave the bend (Region 1) and enter into the reacceleration region (Region 2). In this region, it will often rebound from the impact wall to approach the centerline of the free stream. Occasionally, the cotton will bounce all the way to the other inner wall. Periodically, the cotton will glide along the outer wall rather than be rebounded into this stream. As the cotton leaves the impact region, it becomes re-accelerated in the airstream, but does not immediately approach free-stream velocity. Occasionally, the cotton rebounds from the bottom wall and approaches the top wall of the conveyance line. Also, if there is a relatively large concentration of cotton impacting the bend, a portion of the cotton does not impact the bend and enters Region 2.

As the cotton enters Region 3, it impacts other cotton bolls and the wall, but the velocity profile tends to approach a developed profile with a higher velocity profile towards the centerline of the duct. Although rebounding does occasionally occur once the cotton

reaches 0.3 m from the exit of the elbow, the velocity profiles tends to become more even with primarily a velocity component parallel to the walls.

In observing the experimental video, it appears there is an oscillation as to when the cotton impacts, accumulates, and then exits the elbow. This oscillation is observed approximately 15-20 times in 8 seconds. This may be attributed to the variability of the cotton loading into the system, which sometimes allows the accumulated cotton to re-entrain with the airflow. It may also be associated with the buildup and clearing of the cotton in the 90° bend. This same type of buildup and clearing were seen in the computational results.

The experimental study of cotton and airflow in a positive pressure pneumatic conveyance system has provided significant insight for setting the parameters of the CFD model described in Chapter 6. The size of cotton can be estimated to be 4 cm x 2 cm x 2 cm ellipsoids with a particle density of 250 kg/m^3. In addition, the flow behavior of cotton is unique due to its irregular shape, varying size, cotton compression upon impact, and stringy fibers connecting the cotton bolls to one another.

CHAPTER 6: COMPUTATIONAL MODEL OF COTTON-AIR FLOW

This chapter applies the methods developed in Chapter 4 for modeling fibrous multiphase flows in pneumatic conveyance systems and incorporates the results and observations obtained from the experimental tests of cotton-air flow through the experimental test apparatus.

6.1. Description of CFD Cotton-Air Model

Once the experimental study was completed, an equivalent CFD model was created. Since the 90° duct is a rather simple geometry, a structured grid was utilized, and the grid was generated within STAR-CD™ using the Pro-STAR™ utility. The dimensions of the CFD model correspond to the dimensions of the test apparatus in all relevant respects. The width of the rectangular channel and the length of the ducting are representative of the test apparatus. However, to further simplify the model, a single cell thick model was created, which represents a two-dimensional slice of the three-dimensional test apparatus. Figure 6.1 demonstrates the grid generated for the cotton-air flow computational study. The air and cotton mixture enters the top left portion of the duct and flows downward and rightward through the elbow. The mixture then exits through the right.

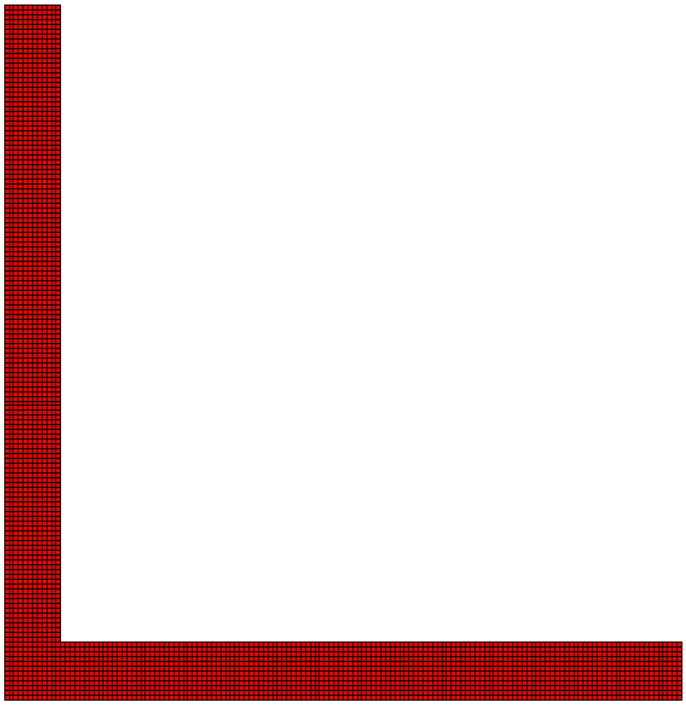

Figure 6.1. Computational grid generated for cotton-airflow study.

Table 6.1 lists the assumed properties of the cotton simulated in this study, while Table 6.2 shows the boundary conditions used in the model. In addition, the connectivity parameters determined for this study are given in Table 6.3. The cotton boll dimensions are estimated from the cotton boll samples from the experimental studies, while the connectivity parameters, γ and β, are adjustable parameters set to account for the connectivity effects. Since cotton bolls tend to be stringy, the cotton flow is more greatly influenced by the connectivity effects compared to other bulk solids that are less stringy. For example, one would expect ground biomass particles to have a lower connectivity effect than cotton. The CFD models are initially set to account for the particle drag effects for representative bulk solids. Once this is complete, the two connectivity parameters are adjusted to match the

velocity profiles observed in the experiment test rig. For the cotton study, appropriate coefficients for γ and β were found to be 50 kg*s/m^5 and 10 kg/m^4, respectively, for the airflow cases of 70-125 m^3/min (2500 to 4500 CFM), which equates to an inlet velocity of 12.7 to 23 m/s. The cotton loading conditions range from 900 to 2700 kg/hr (1-3 T/hr).

The physical properties of the biomass and the connectivity properties are incorporated in the CFD model using the user defined functions as described in Chapter 4. The boundary conditions and the k-ε turbulence model are implemented in the main STAR-CD™ model.

Table 6.1. Cotton properties for cotton-air CFD model.

Cotton Properties	Value	Units
Cotton Density	250	kg/m^3
Diameter 1	4.0	cm
Diameter 2	2.0	cm
Diameter 3	2.0	cm

Table 6.2. Boundary conditions for cotton-air CFD model.

Inlet Boundary Conditions	Value	Units
Air Inlet Velocity	12.7-23	m/s
Cotton Loading Rates	900-2700 (1-5)	kg/hr (T/hr)

Table 6.3. Connectivity parameters for cotton-air CFD model.

Connectivity Parameters	Value	Units
γ	50	kg*s/m^5
β	10	kg/m^4

6.2. Verification and Validation of CFD Cotton-Air Model

During the model development process, it is important to ensure the models are verifiable and valid. Verification is the process of determining that a model implementation accurately represents the developer's conceptual description of the model and the solution to the model, while validation is the process of determining the degree to which a model is an accurate representation of the real world from the perspective of the intended uses of the model.

6.2.1. Model Verification

This research verified the developed CFD models by performing a grid study to ensure grid independence. The grid study consisted of creating models of varying refinement and determining the solved flow conditions of each model. The mesh refinement chosen for this study compared the velocity profiles of models of various refinements. The model with the highest refinement was chosen as the baseline, and the models with a coarser mesh were compared to the baseline. If the coarser converged model provided answers within 5% of the refined model, it is considered grid independent and is considered appropriate to this study.

6.2.2. Model Validation

This research also validated the CFD models developed with the experimental data to ensure they predicted an accurate representation of what was observed in the experiments. The validation process was implemented by comparing the flow characteristics predicted in the model with experimental trends observed in experiments and previous studies.

Figure 6.2 shows the velocity profile obtained computationally for the 70 m^3/min (2500 CFM) airflow model, and Figure 6.3 shows the velocity profile of the cotton for the respective airflow case obtained experimentally. Given the proper parameters for the connectivity and particle drag, the computational model is able to replicate the velocity profiles of the experiments. Prior to the impact at the wall, the cotton has a developed velocity profile in which the centerline cotton velocity is 9 m/s while the cotton flow near the walls is closer to 6 m/s. As the cotton approaches the bend, the high inertial effects of the cotton keep the velocity profile high. This is different than what the airflow experiences through the bend. The model accurately predicts the rapid deceleration of the cotton after impact, and the model also predicts the gradual reacceleration of the cotton as it becomes re-entrained in the airstream.

Figure 6.4 shows the velocity profile obtained computationally for the 70 m^3/min (4500) CFM airflow model, and Figure 6.5 shows the velocity profile of the cotton for the respective airflow case. Again with parameters specified for the connectivity and particle drag the computational model is able to replicate the velocity profiles of the experiments. Prior to the impact at the wall, the cotton has a developed velocity profile in which the centerline cotton velocity is 18 m/s while the cotton flow near the walls is closer to 16 m/s. As the cotton approaches the bend, the high inertial effects of the cotton keep the velocity profile high. The model accurately predicts the rapid deceleration of the cotton after impact, and the model also predicts the reacceleration of the cotton as it becomes re-entrained in the airstream.

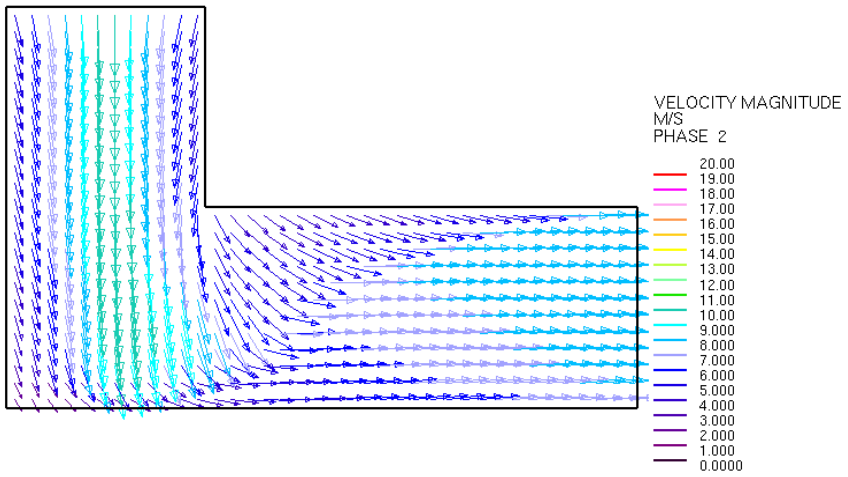

Figure 6.2. Computationally predicted cotton velocity at 70 m^3/min.

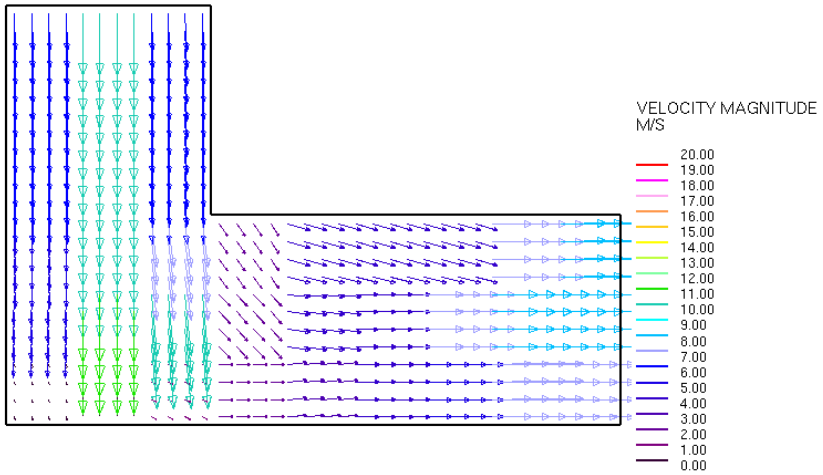

Figure 6.3. Experimental comparison of predicted cotton velocity at 70 m^3/min.

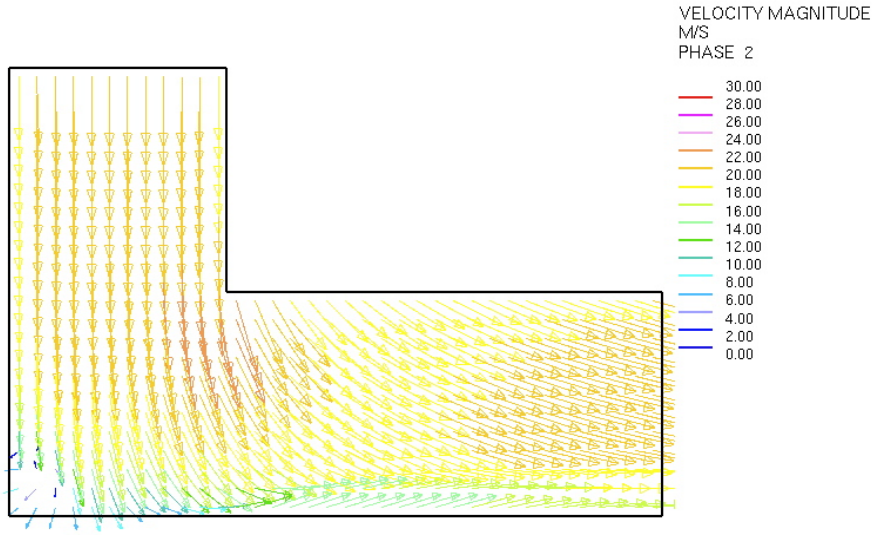

Figure 6.4. Computationally predicted cotton velocity at 125 m^3/min.

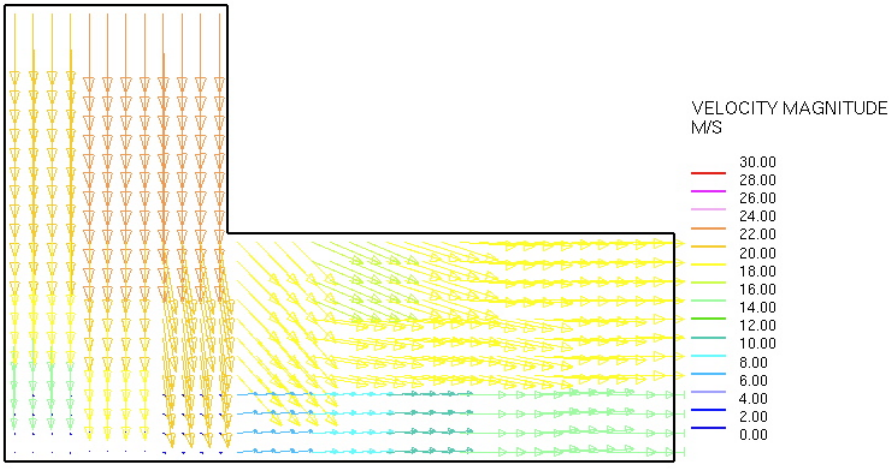

Figure 6.5. Experimental comparison of predicted cotton velocity at 125 m^3/min.

However, it is interesting to note that the cotton is able to reaccelerate at a significantly faster rate than is shown in both the computational and experimental cases for the 70 m^3/min airflow. This is due to the higher air velocity pushing the cotton at a faster rate for the same cotton loading rate. In addition, the reacceleration region of slow moving cotton along the outer wall of the reacceleration region is significantly smaller than was observed for the 70 m^3/min flow cases. Again, this is due to the higher air velocity given the same cotton loading rate.

From this study, there are several observations that can be made when comparing the computational results to the experimental observations and trends.

- The first effect noticed in cotton flow is the inertial effects of the cotton boll in the flow. Due to the high inertia of the cotton, once the cotton is accelerated to near the free-stream air velocity, the cotton boll will continue on its straight-line trajectory path. The inertial effects mean that the cotton boll cannot be redirected in the flow the same way as the air. Therefore, the cotton boll will impact the conveyance system wall. The cotton boll inertial effects should be considered when designing bends in the conveyance systems.

- Second, once the cotton bolls impact a wall or any obstruction, the bolls will rapidly decelerate, and all the momentum that was transferred to the bolls is lost. To reaccelerate the cotton bolls will require more power be added to the system to overcome the cotton boll's inertia so that it can move. The reacceleration of the cotton boll will require the air velocity to be above the pickup velocity threshold for cotton. Unlike traditional pneumatically conveyed bulk solids, the pickup velocity of

cotton can be variable due to the shape and orientation of the cotton bolls. In addition, the pickup velocity can be variable due to the non-smooth surface and strings between the cotton bolls.

- Third, the reacceleration length of cotton is significantly longer than it is for air, again due to the inertial effects. The experimental data shows that the cotton requires a length on the order of a meter to be reaccelerated with the airstream. The reacceleration regions, found immediately after any bend, also need to be considered for being potential bottlenecks in the conveyance system, The reacceleration regions are where the greatest pressure loss will be and are where the airstream will be pushing the cotton forward.

- Fourth, the presence of the cotton at the bends and reacceleration regions increases the flow resistance of the air, and the air will be redirected to travel the path of least resistance. Therefore, the air velocity profile can be significantly different than the velocity profile of single-phase airflow.

During the model validation process, we were able to correlate the CFD models of cotton and airflow with the experimental models. The models are able to agree well with the velocity profiles determined from the experimental studies.

6.3. Discussion of the CFD Cotton-Air Model

After the CFD models are validated, they can be utilized to predict the flow characteristics that cannot be predicted with traditional single-phase flow models. The additional information that can be predicted by the CFD models can provide further insight for the flow characteristics of cotton-air flow, thus providing a designer with new ways to investigate the design of pneumatic conveyance systems. This section will discuss additional answers that these multiphase CFD models can provide and add value to the design process compared to single-phase airflow models.

6.3.1. Comparing Airflow in Single-phase and Multiphase Models

To demonstrate how the cotton influences the airflow characteristics, Figures 6.6 and 6.7 show the predicted airflow behavior in the elbow when there is no cotton present, and how the airflow behaves when cotton is present. Figure 6.6 shows how the single-phase air behaves as it enters and exits the bend at 70 m^3/min. When no cotton is present, the air flows along the path of least resistance, and the air rapidly accelerates immediately at the exit of the bend. The inside wall at the exit of the bend has a small recirculation region and has little airflow. By comparison, the air phase of the multiphase flow model indicates that the air velocity profile is changed significantly. The presence of the cotton, particularly at the impact and reacceleration regions, increases the resistance of the air. This resistance causes the air velocity profile to be altered. Figure 6.7 shows the redistribution of the air velocity profile at 70 m^3/min. The recirculation region is no longer present because the buildup of cotton at the outer wall redirects the airflow to the inner wall.

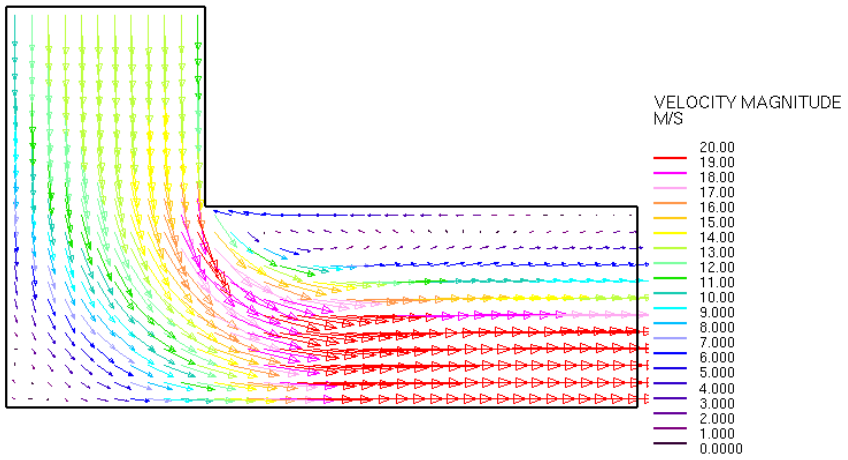

Figure 6.6. Computationally predicted single-phase air velocity at 70 m^3/min.

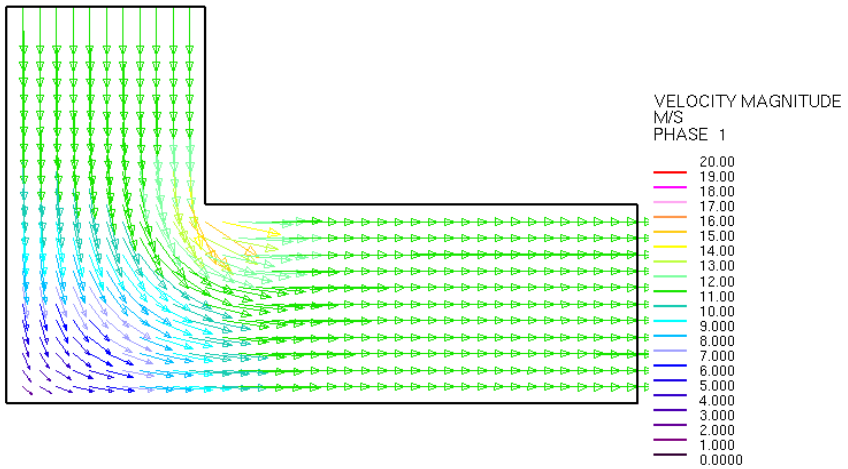

Figure 6.7. Computationally predicted multiphase air velocity at 70 m^3/min.

6.3.2. Predicting Cotton Accumulation

The next feature the multiphase CFD models can predict is cotton buildup and cleanout. The response of multiphase flows in an elbow or bend is critical in the design of multiphase systems. In practically all cases, this interaction is a transient effect. Figures 6.8 through 6.11 show the changes in predicted cotton concentration in the elbow model over a 5 second timeframe. Notice how the cotton is high concentrated (indicated by the red contour plot) at the impact region in all cases, and the size of the highest concentration changes in size as the cotton accumulates in the outside corner of the elbow.

Once the cotton accumulates, it eventually becomes re-entrained in the airflow and then exits the elbow. The cotton tends to stay along the outside wall of the flow since it is being pushed by the flowing airstream exiting the bend. However, there are instances in which the cotton will make its way to the inside wall of the duct then will oscillate back so that the primary concentration is along the outer wall. These flow conditions are interesting to predict computationally, and these computational predictions provide the designer with insight for how cotton accumulates and disburses in the flow as the cotton moves in time. This information is also useful because it can help the designer determine if the cotton accumulation will cause plugging within the bend computationally, before any conveyance system configuration is constructed. In addition, the computational model can be reconfigured to see if another bend design would reduce or eliminate cotton accumulation.

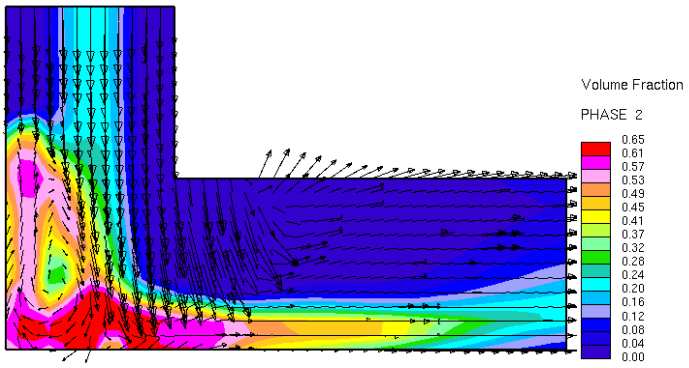

Figure 6.8. Volume fraction contour plot of cotton concentration at t = 2.0 s.

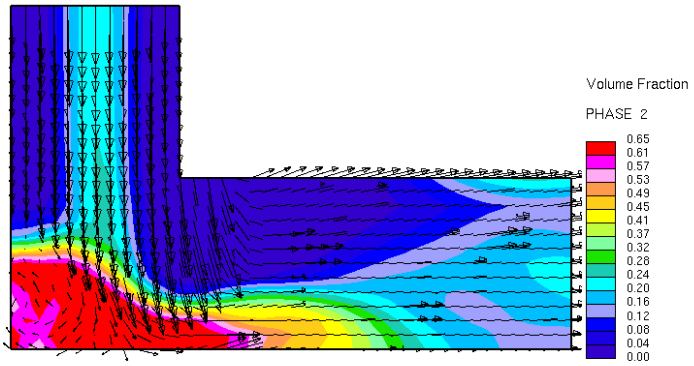

Figure 6.9. Volume fraction contour plot of cotton concentration at t = 3.0 s.

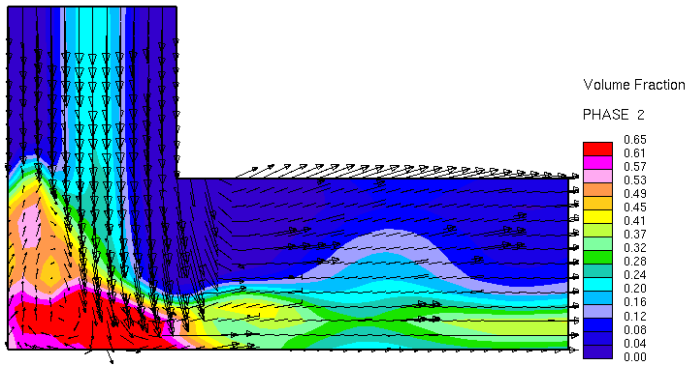

Figure 6.10. Volume fraction contour plot of cotton concentration at t = 4.0 s.

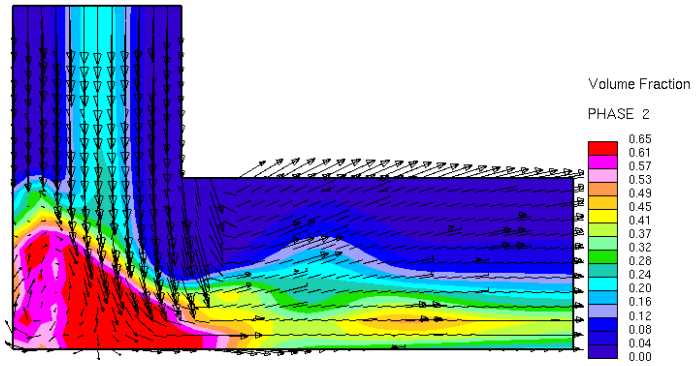

Figure 6.11. Volume fraction contour plot of cotton concentration at t = 7.0 s.

Another interesting feature is the ability to predict the limitation of a particular pneumatic conveyance system configuration. In a pneumatic conveyance system, conditions may arise in which the air velocity profile falls below the bulk solids pickup velocity, or the accumulation of the bulk solids becomes so great that it restricts the airflow, thereby creating a plug. Experimental models and correlations in tables may indicate the limits of a system, but are restricted to existing conveyance systems. Being able to accurately predict the bulk solids concentration in a pneumatic conveyance system computationally is beneficial because it can be based on the configuration of interest and can be mitigated before building the actual conveyance line.

6.3.3. Predicting Pressure Drop for Conveying Cotton

The third feature that can be predicted by the developed CFD models is pressure drop due to the presence of the material. Being able to predict these performance characteristics is especially useful since they are all related to system reliability, power consumption, and product development costs.

An important use of the developed computational models is to be able to estimate pressure drop for conveying bulk solids through a specific configuration, which is related to power requirements. Single-phase airflow models are helpful in predicting pressure drop through a transport duct, pipe, etc. The pressure drop is influenced by major losses in the piping (friction factor, pipe diameter, Reynolds number), and by minor losses (pipe bends, obstructions, valves, etc). However, once the bulk solids are introduced to the flow, it increases the resistance of the flow, thereby increasing the pressure drop experienced in the

system. To overcome the extra resistance of the bulk solids, an increase in pressure is required, thereby increasing the power requirements.

An example of the pressure drop experienced in a bend due to the presence of a bulk solids are generalized in Figure 6.12. Prior to the bend (the approach region), the pressure drop is minimal. As the multiphase mixture passes through the bend, the bulk solids impact the outer wall and lose momentum. As the bulk solids travel further down the pipe, it is reaccelerated with the flowing air. Although the bulk solids impact the wall at the bend, the majority of the pressure drop occurs in the straight region following the bend. This is due to the reacceleration of the bulk solids due to the momentum exchange from the air as it approaches the free stream air velocity.

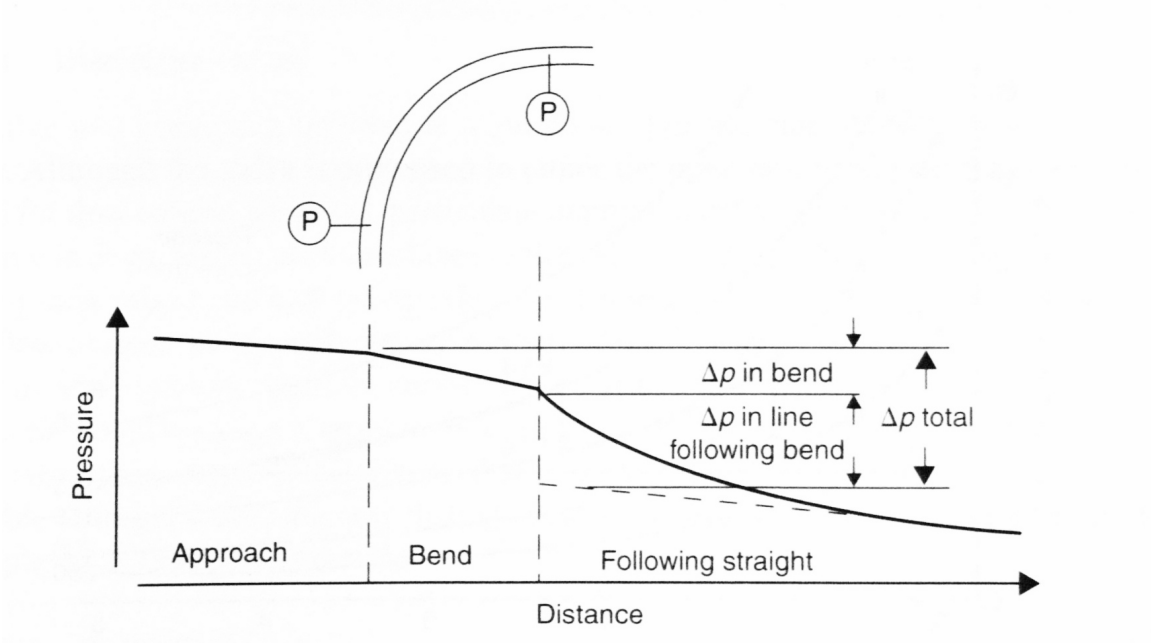

Figure 6.12. Pressure drop relative to position of the bend in conveyance line (Mills 2004).

In a similar manner, CFD can be used to predict the pressure drop through a pneumatic system. Figure 6.13 shows the pressure profile of single-phase airflow through the elbow. One notes the pressure drop is insignificant prior to the bend. Once the air approaches the bend, the pressure increases significantly in the corner of the bend, and the pressure drop is significant upon exiting the bend. However, the pressure profile actually increases slightly as the air moves further away from the bend before the pressure tapers and slightly decreases upon exiting the duct.

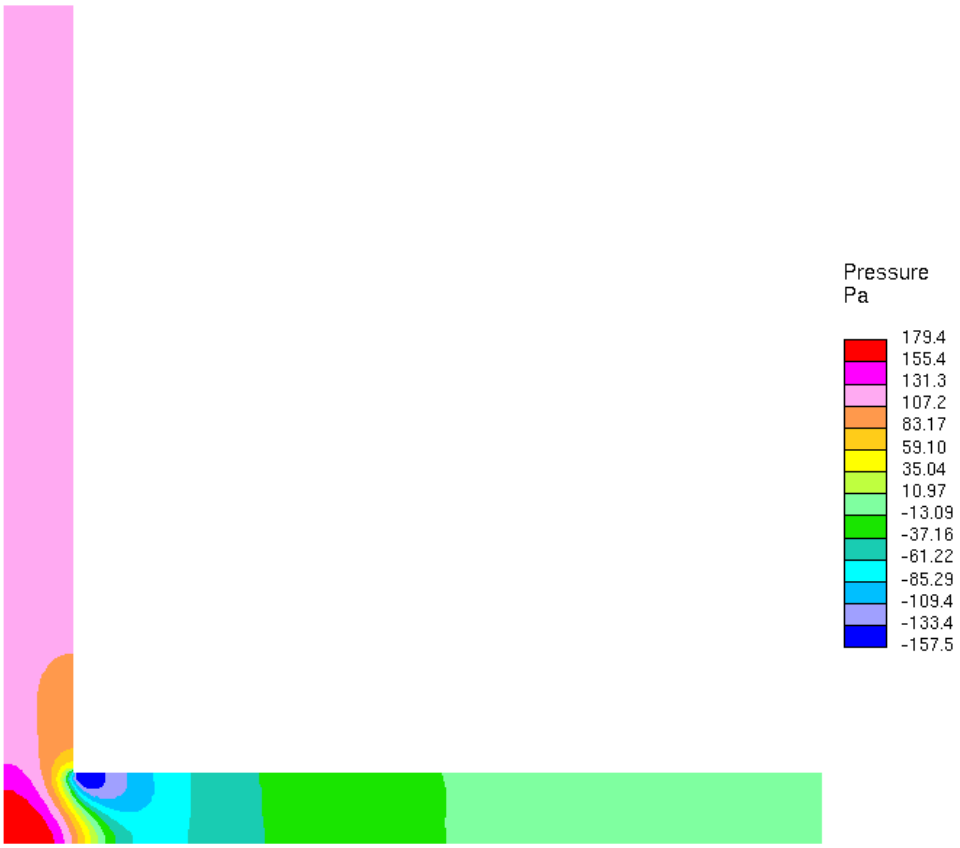

Figure 6.13. Computationally predicted pressure for single-phase airflow.

In contrast, Figure 6.14 shows the pressure profile of the air phase with cotton loading rate of 3 T/hr. At first glance, the pressure gradient is significantly higher than the single-phase airflow. As the multiphase air-cotton mixture approaches the bend, the air exhibits a more significant pressure drop than what is observed in the single-phase air model. More importantly, the pressure of the air in the multiphase flow model decreases more rapidly upon exiting the bend due to the presence of the reaccelerating cotton particles. The pressure drop behavior follows the same trend as shown in Figure 6.12.

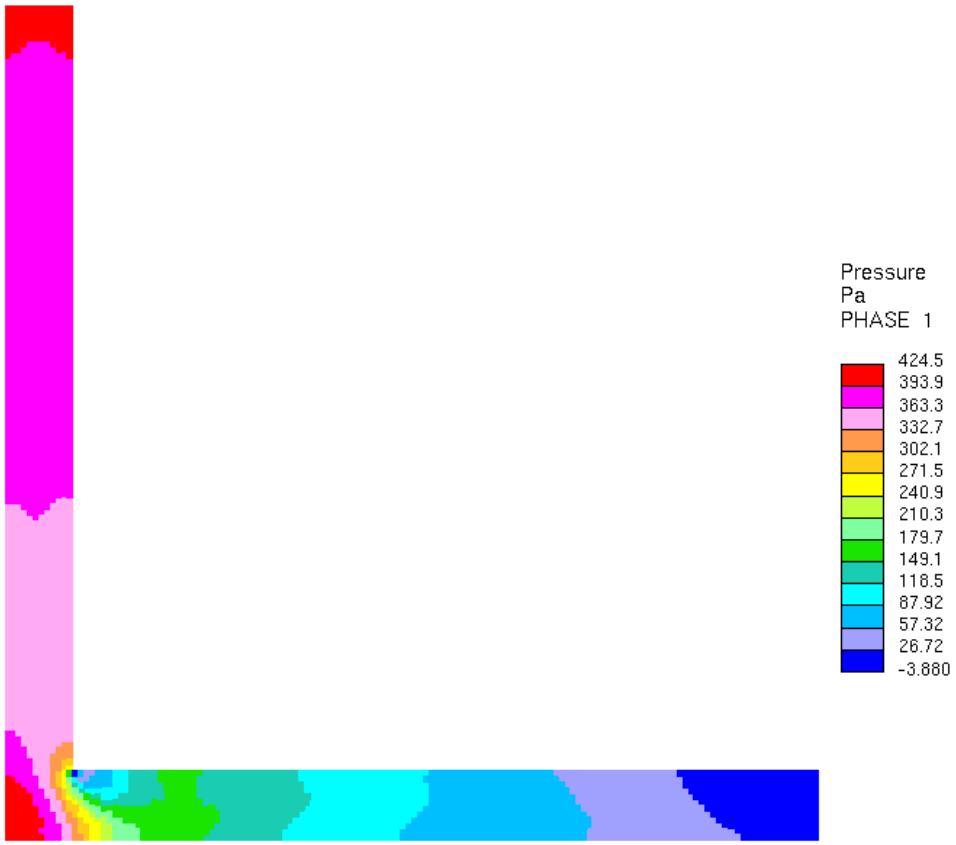

Figure 6.14. Computational predicted air pressure for multiphase airflow.

Pressure drop is important for determining the power consumption of a pneumatic conveyance system due to pressure drop being directly correlated with power. The power input to a pneumatic conveyance system is limited by how much material the blower may be able to maintain. Generally, the increase in bulk loading will increase the pressure drop for a particular system, and if the pressure drop and volumetric flow rate exceed what the air mover is capable of producing, then the system has met its limitations of bulk transport. Currently, pressure drop curves are created from empirical data for a particular configuration and bulk solids. However, this method is time consuming and is only applicable for the configuration and bulk solids of interest.

The following figures demonstrate the capability of computationally predicting the pressure drop for the 90° bend of cotton and airflow for various cotton loading conditions and air volumetric flow rates. Figure 6.15 shows the trends of the pressure drop seen in the system for 15-75 kg/min of cotton loading at air volumetric flow rates ranging from 70-125 m^3/min. These plots are compared with the pressure drop of air only being moved within the system. The pressure drop trends are compared with Figure 6.16, which is the same figure shown in Chapter 2 for conveying cement. Notice that the pressure drop curves for cotton conveyance exhibit similar trends as the cement. Rather than developing these curves using an experimental apparatus and a series of test runs (as was done for the cement pressure drop curves), the cotton pressure drop curves were generated computationally, making it faster and easier to develop relationships.

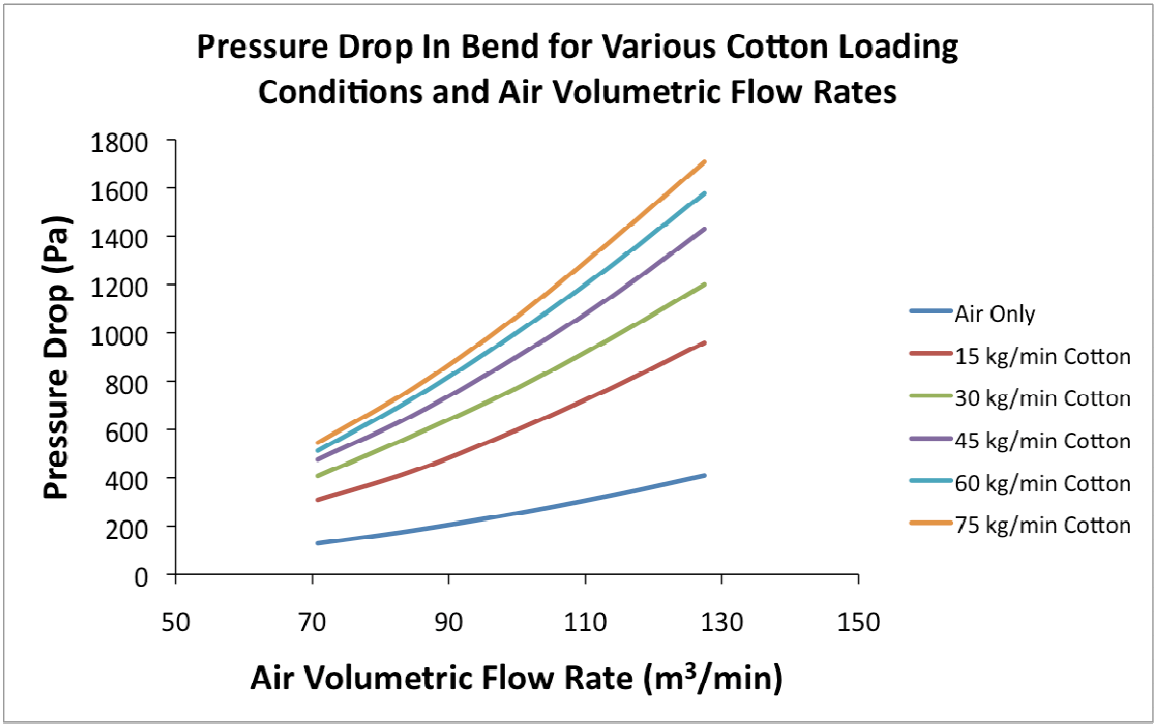

Figure 6.15. Predicted pressure drops of cotton flow through a 90° elbow.

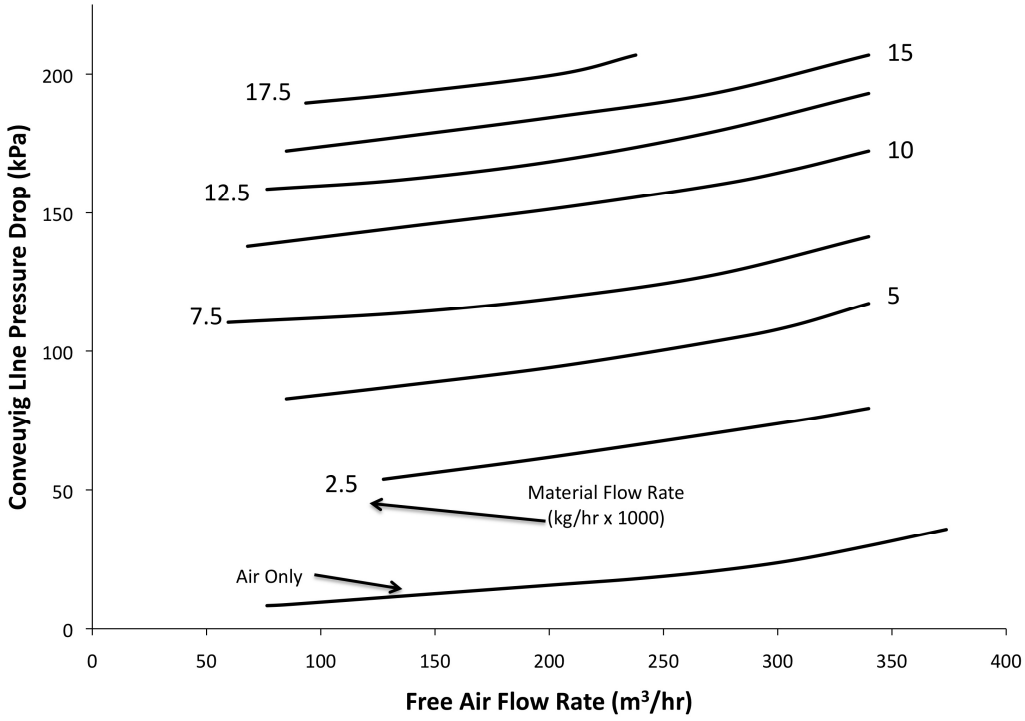

Figure 6.16. Comparison of pressure drops for cement in conveyance line.

The computational models developed for this study provide further insight into the effects of cotton flow through a pneumatic conveyance system because it has the ability to predict the pressure drop due to the presence of cotton being conveyed with the airflow. In addition, the models have the ability to predict how and where the cotton will accumulate in the conveyance system. Predicting cotton behavior and the pressure drop associated with conveying cotton with computational models can streamline the design process of cotton conveyance systems by reducing, or eliminating, the need for physical experiments of full-scale systems. In addition, the designers will not be required to over-design systems to help ensure that the conveyance system will transport cotton efficiently and reliably. Pneumatic conveyance systems that are designed to match the application will not only be more reliable but also more efficient by reducing pressure losses.

CHAPTER 7: EXTENSION OF METHODOLOGY TO BIOMASS CONVEYANCE SYSTEMS

Once the computational models have been developed and validated, the methods developed in creating the models can be extended to additional modeling applications. This chapter demonstrates the ability to model and predict the behavior of biomass and air flowing through a negative-pressure conveyance system.

7.1. Biomass Conveyance Systems Background

The second application of fibrous-based multiphase flows in pneumatic conveyances systems is in biomass conveyance systems for biorefinery applications. In recent years, government mandates and fossil fuel energy costs have significantly increased interest in producing energy from renewable energy sources. One method is to convert biomass feedstock (wood chips, wood pellets, switchgrass, etc) into biofuels. Extensive research has been done in modeling the thermochemical and biochemical processes within a biorefinery. However, little has been modeled in terms of the feedstock conveyance systems that precede the chemical processes for converting the solid biomass to a gaseous or liquid fuel.

Petroleum is currently the largest energy source in the United States, supplying approximately 40 percent of its energy (Wyman 2007). Developing a sustainable alternative is important to overcoming dependence on petroleum, and biomass is the only known, large-scale renewable resource that can be converted into the liquid fuels that are currently well suited for transportation (Wyman 2007). The U.S. Department of Energy (DOE) Office of the Biomass Program envisions biorefineries will utilize two conversion processes, the

biochemical platform and the thermochemical platform. The biochemical program utilizes biological conversion to ferment biomass sugars into fuel ethanol. In the thermochemical conversion platform, the solid biomass is converted to a gaseous or liquid fuel by introducing heat with limited oxygen. Gasification and pyrolysis processes are utilized to produce synthetic gases (syngas), pyrolysis oil, hydrothermal oils, and hydrogen and methane based gases. The OBP Program views gasification to be "important in providing a source of fuel for electricity and heat generation in an integrated biorefinery" (National Renewable Energy Laboratory 2006).

Introducing fibrous biomass feedstocks into thermochemical reactors remains one of the key challenges in gasification technology development (Ingram 2004). The challenge with feed handling systems is that they are required to provide a continuous and consistent supply of biomass, generally a non-flowing solid, while accommodating additional conditions such as pressure changes and oxygen filtration. Several mechanisms have been explored as options to handle the biomass, including a high-pressure screw feeder (Evans et al. 1998), dual distribution systems (Ergudenler 1993), and lock hoppers. These mechanisms have had varying levels of success but not have been viable options for commercial scale biorefineries. Another issue with biomass feed mechanisms is that they must not only satisfy the constraints of the gasifier, but they are also subject to the constraints of the feedstock assembly system, which includes all the processes required to prepare and transport the biomass, including harvest and collection, storage, preprocessing, and transportation. Due to the non-flowing behavior of bulk cellulosic feedstocks, problems such as agglomeration, segregation, plugging, and throughput must be addressed in feed system design through the

incorporation of active transport mechanisms, including augers, conveyors, and pneumatic conveyance systems.

Reliable feed systems that manage these strict performance parameters are viewed as "key to any successful project system," (Wyman 2007). For example, the gasification process relies on specific feedstock properties, including particle size, particle size distribution, and moisture content. Feedstock assembly processes establish these feedstock characteristics, and they significantly affect feedstock flow properties, resulting in significant impacts on mechanical feed system design. Consequently, feedstock specifications are important not only for gasifier operation, but also for feed system designs that must achieve consistent flow rates.

Figure 7.1 shows a schematic of the pilot scale Thermochemical Process Development Unit developed at the National Renewable Energy Laboratory in Golden, CO. Currently, the biomass feedstock is conveyed thorough a series of hoppers, pneumatic conveyors, and augers before the feedstock is introduced into the gasifier. However, an investigation of alternative conveyance systems for biomass is underway which includes pneumatic conveyance systems. In either process, once the feedstock undergoes the gasification process, it undergoes a series of thermal crackers and separators before producing the final products, syngas and char.

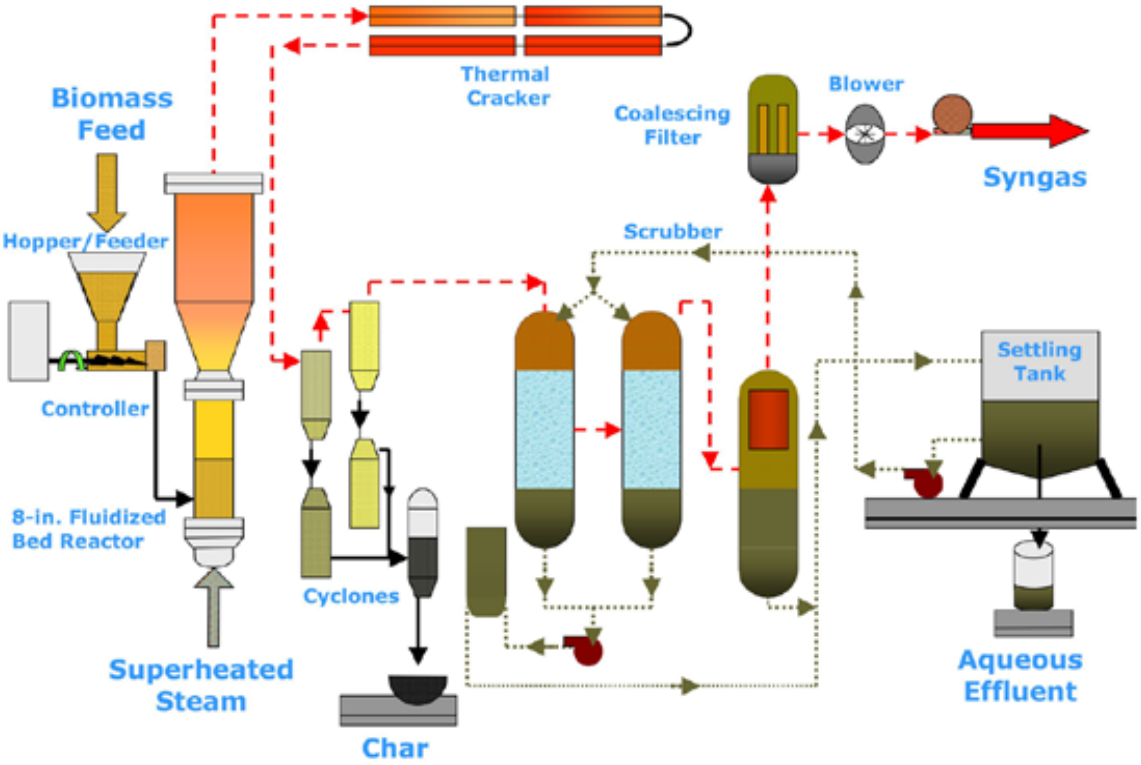

Figure 7.1. Thermochemical Process Development Unit Schematic (National Renewable Energy Laboratory 2003).

7.2. Experimental Test Apparatus of Biomass Conveyance System

The focus of this research is to predict the flow behavior of pneumatic systems that transport the biomass feedstock prior to the refining process. Figure 7.2 shows a computer-generated representation of the test loop used, and Figure 7.3 shows the schematic of the experimental apparatus. A negative pressure pneumatic test apparatus was constructed to study the flow behavior of representative biorefinery feedstocks in a controlled environment. The biomass is drawn through the conveyance line with a blower configured to provide a maximum vacuum of 25 inches of water (6200 Pa) at 3250 RPM. The blower is driven by a three-phase variable speed electric motor.

The inlet of the experimental test apparatus consists of a vibrating hopper with an auguring screw, which introduces a pre-measured amount of biomass feedstock into the conveyance line. The biomass flow rate is set constant at 20 kg/min (0.322 kg/s) for this study. The biomass leaves the vibrating hopper and enters a radius bend and travels horizontally through a 6.35 by 6.35 cm (2.5 x 2.5 in.) square conveyance line for 5.5 m (20 feet). The biomass then enters a second radius bend, which redirects the flow upward. A third radius bend redirects the flow horizontally again before entering the cyclone separator. Once the biomass enters the MAC 54AVR4 cyclone filter, it is deposited into a 208 liter (55 gallon) drum attached to the separator for collection. The drum is weighed and compared to the pre-measured amount of bulk solids in the hopper at the beginning of the conveyance line.

The conveyance line is equipped with a series of pressure taps and sensors to measure the pressure drop, air volumetric flow rate, ambient temperature, and blower power input to

the electric motor. Note the locations of the ten pressure taps spaced evenly along the horizontal portion of the pipe and more frequent pressure taps located at the radius bends.

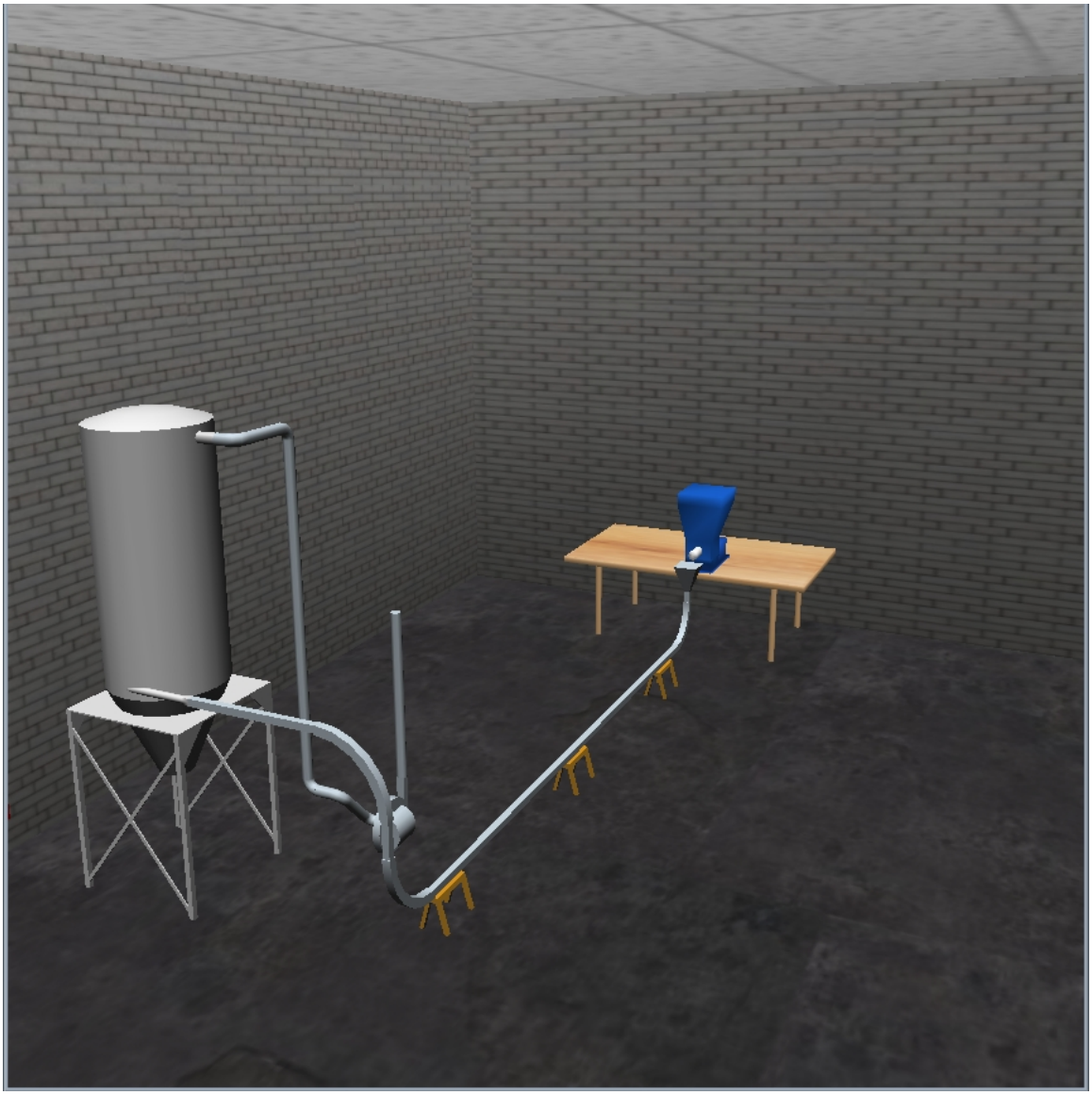

Figure 7.2. Computational representation of biomass test apparatus.

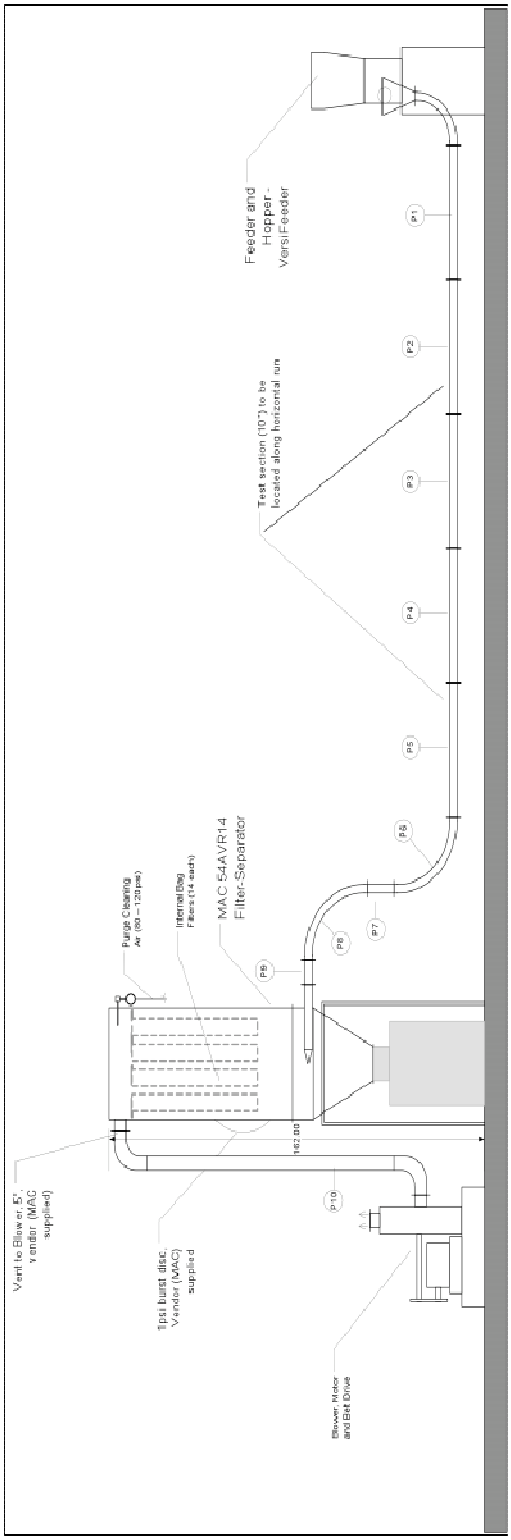

Figure 7.3. Schematic of negative-pressure biomass test apparatus.

7.3. Experimental Biomass Flow Results

Figure 7.4 shows the experimental data of the pressure drop at each of the nine pressure taps in the conveyance for three fan speeds. Location 1 is the pressure at the upstream point of the conveyance line, while Location 9 is the pressure at the exit of the conveyance line, just before the filter separator.

The air-only flow cases show that the pressure drop increases as the flow travels thought he conveyance line. The pressure drop is highly correlated with the motor speed of the blower. However, it is not a linear function. The pressure drops for the high fan speed case are almost five times that of the pressure drops for the lowest fan speed case, which is approximately 50 percent of the fan speed of the high air flow case.

When biomass is introduced to the airflow at 20 kg/min, we notice two interesting effects. First, the pressure drops of biomass entrained in the flow are relatively close to that of the pressure drops of the single-phase airflow. This is due to the pressure drop limit of the vacuum for a particular fan speed. Second, at pressure tap locations 6, 8 and 9, we observe the pressure loss is greater for the multiphase flows. This makes sense since there is significant separation of the biomass from the flowing air, and the behavior of the air is influenced more by the presence of the biomass. The fact that different flow cases are limited by pressure means that the boundary conditions should be defined as pressure boundaries rather than inlet boundary conditions that correspond with the pressure the blower requires. This indicates the air volumetric flowrate is reduced with the presence of biomass.

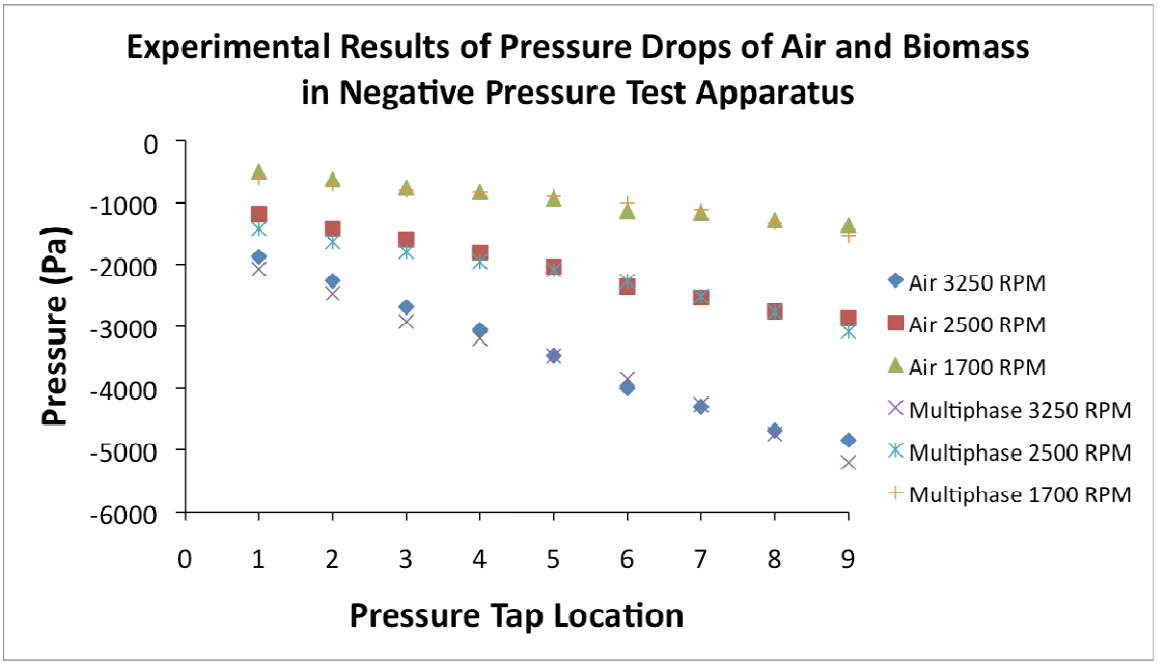

Figure 7.4. Experimental graph of pressure drops in biomass test apparatus.

7.4. Description of CFD Biomass-Air Flow

The CFD model of the biomass conveyance system is constructed to incorporate the same conveyance line geometry as the experimental test apparatus. Figures 7.5 through 7.7 show the computational mesh created for the biomass flow study. The biomass hopper at the inlet is not included in the CFD model, but is represented as a pressure boundary condition. The filter separator is not modeled in CFD but is assigned a representative negative pressure boundary condition to simulate the vacuum.

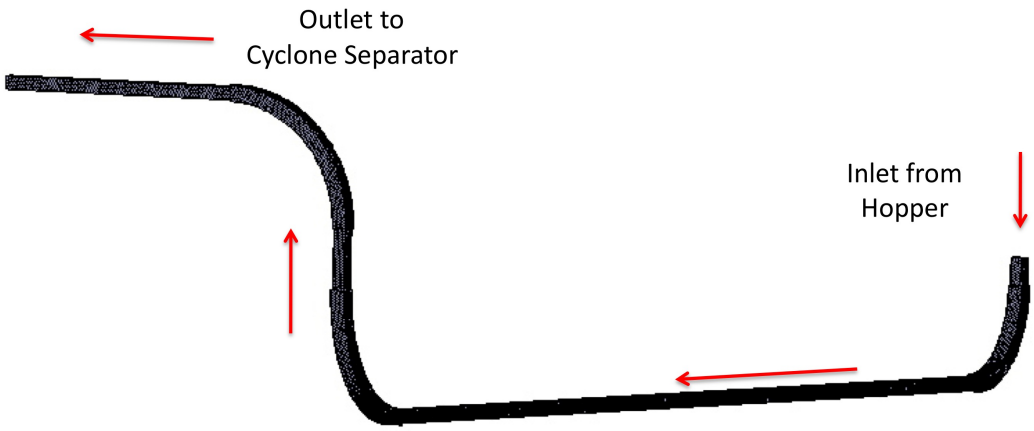

Figure 7.5. Isometric view of computational grid for biomass study.

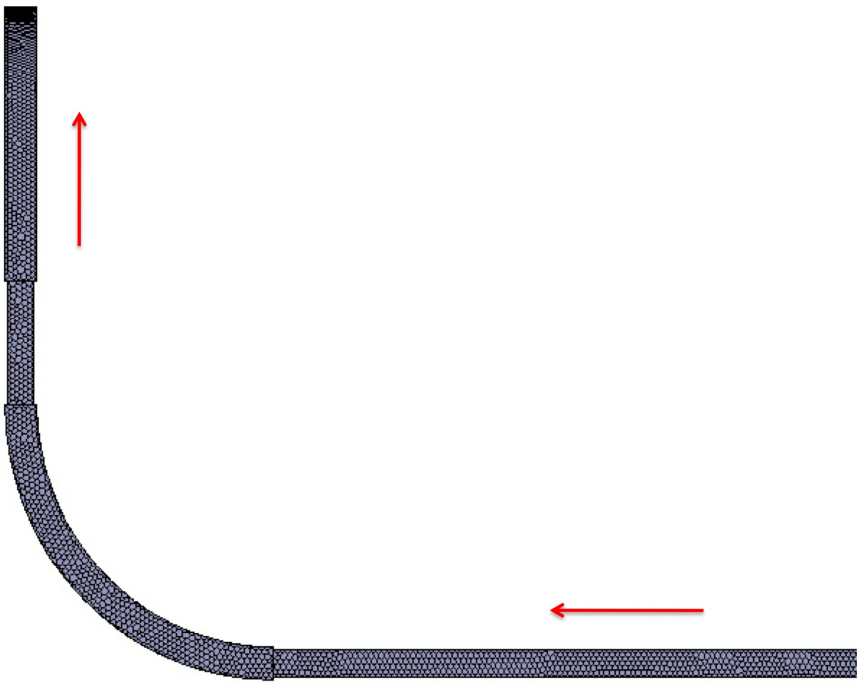

Figure 7.6. Side view of computational grid at horizontal-to-vertical bend.

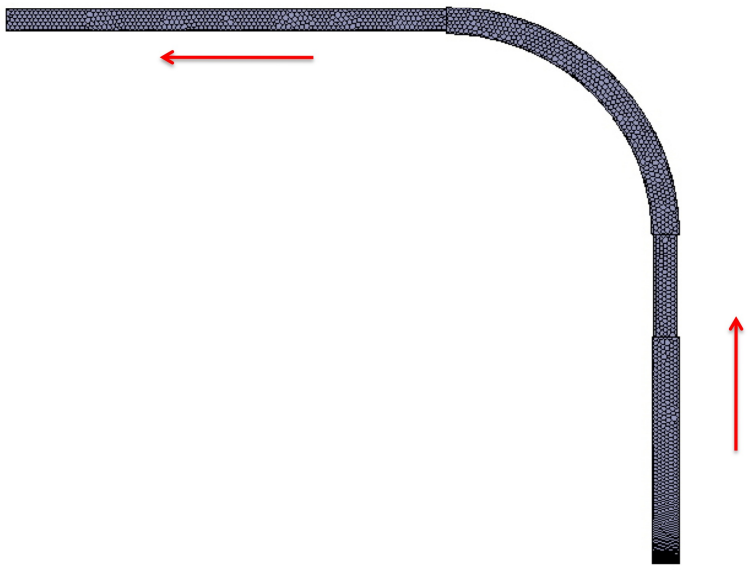

Figure 7.7. End view of computational grid at vertical-to-horizontal bend.

Table 7.1 shows the assumed properties of the biomass simulated in this study, while Table 7.2 shows the boundary conditions used in the model. In addition, the connectivity parameters determined for this study are given in Table 7.3. The connectivity parameters are based on the results of the experimental pressures obtained in the experimental test apparatus. Biomass exhibits properties that are significantly different than what is observed in cotton. The most significant difference is the smaller size of biomass particles. In addition, the biomass in this study does not have the interconnected strings associated with cotton bolls. This means the resistance due to the presence of biomass will be more dominated by the particle drag effects rather than the connectivity effects. Therefore, the expected values of γ and β are less than they are for cotton flow. In this study, it was determined that the appropriate values of γ and $\beta$are 10 kg*s/m^5 and 1 kg/m^4, respectively, for the flow conditions of interest in this study. The values of the connectivity parameters are correlated against the experimentally obtained pressure drops observed in the test apparatus, in which the two connectivity parameters are adjusted in the computational model to correlate with the flows of interests observed in the experimental test apparatus. The physical properties of the biomass and the connectivity properties are incorporated in the CFD model using the user defined functions as described in Chapter 4. The boundary conditions and the k-ε turbulence model are implemented in the main STAR-CD™ model in a similar manner as was done in the CFD cotton-air model.

Table 7.1. Biomass properties for biomass-air CFD model.

Biomass Properties	Value	Units
Biomass Density	450	kg/m^3
Diameter 1	6.0	mm
Diameter 2	3.0	mm
Diameter 3	3.0	mm

Table 7.2. Boundary conditions for biomass-air CFD model.

Boundary Conditions	Value	Units
Air Inlet Pressure	-300 to -800	Pa
Air Outlet Pressure	-1600 to -5000	Pa
Biomass Loading Rates	20 (1.26)	kg/min (T/hr)

Table 7.3. Connectivity parameters for biomass-air CFD model.

Connectivity Parameters	Value	Units
γ	10	$kg*s/m^5$
β	1	kg/m^4

7.5. CFD Results of Biomass-Air Flow

The computational results in this study include the ability to predict the air pressure at each location in the conveyance line due to the presence of the biomass. In addition, it is also interesting to determine the velocity profiles of the air and the biomass as they travel through the bends of the conveyance line. Section 7.5.1 will discuss the results of the pressures predicted in the conveyance line, while Section 7.5.2 will discuss the predicted air and biomass velocity profiles in two of conveyance line bends.

7.5.1. Pressure Results

Figure 7.13 shows the computationally predicted pressure drops through the conveyance line of the pneumatic system. For the three fans speeds, the computationally predicted pressure drops for the single-phase air cases are within 5% of the experimental air test cases. The single-phase CFD model is able to capture the non-linearity of the pressure drops for the single phase flows.

In addition, the three biomass-air flow cases shown indicate that the pressure drop due to the biomass presence is similar to the single-phase air cases. The pressure drops for the biomass flows show slightly more variation from the single-phase counterparts, particularly for the low fan speeds. Since the bulk solids mass flow rate is constant in all three biomass cases, the bulk solids loading ratio is higher for the lower fan speed. The increased bulk solids loading ratio would have an effect on the increased pressure drop.

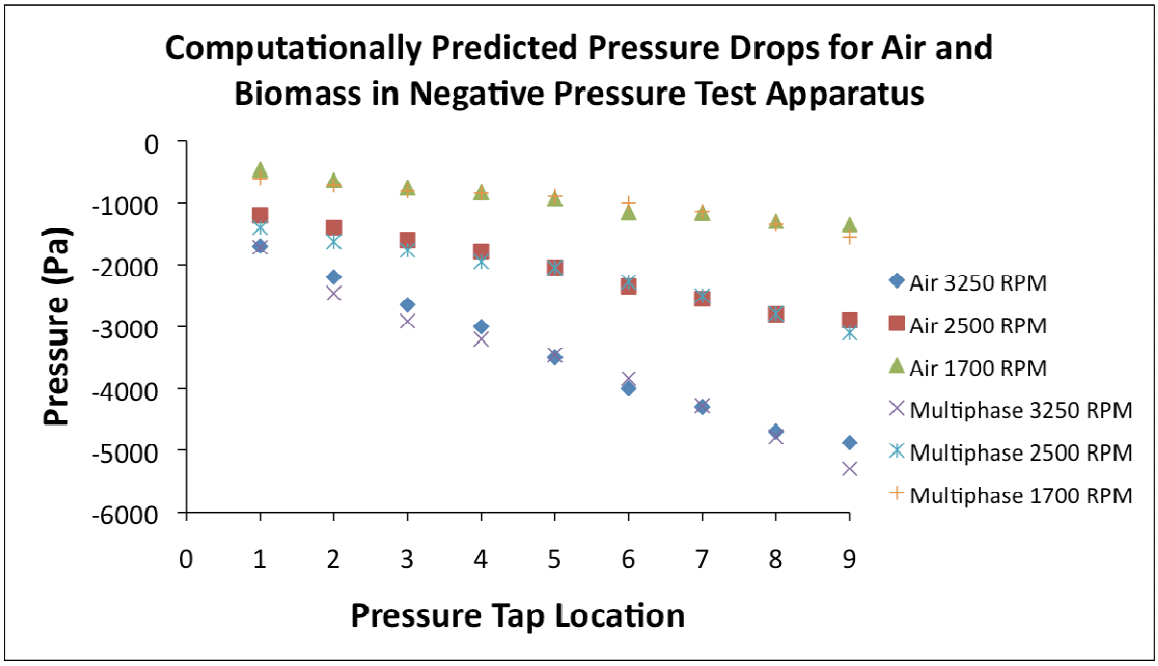

Figure 7.8. Computationally predicted pressure drops for biomass test apparatus.

7.5.2. CFD Velocity Results of Biomass-Air Flow

The CFD models for biomass-air flow can also be used to determine the velocity profiles in particular regions of interest. Two locations of interest in this study are the radius bends nearest to the cyclone separator. The first bend guides the air and biomass mixture from a horizontal fully developed flow to a vertical flow. The second bend guides the bulk solids from a vertical, non-developed flow to a horizontal flow before entering the cyclone separator.

Figure 7.9 shows the air phase velocity profile, while Figure 7.10 shows the biomass phase velocity profile at the horizontal to upward vertical radius bend in the multiphase flow model. The air phase enters the bend at a uniform 30 m/s, but suddenly decelerates to 24 m/s. The reason this deceleration occurs is due to the slightly larger cross sectional area

constructed in the radius bend. However, as the air approaches the halfway point of the radius bend, the velocity profile stratifies and the air velocity reaches 30 m/s along the inner wall. This is due to the presence of the biomass accumulation along the outer edge of the wall.

The velocity profile of the biomass phase has a significantly different behavior than the air phase. Prior to entering the leading edge of the radius bend, the biomass is traveling at a lower velocity than the carrier phase, on the order of 20 m/s rather than 30 m/s. Although the air phase rapidly decelerates as it enters the leading edge of the bend, the biomass phase maintains its inertia before it impacts the outer wall of the radius bend. In fact, the biomass phase maintains a high velocity flow, almost half the distance of the bend. However, the biomass decelerates rapidly as it travels upward. The deceleration is due to the inertial effects of the biomass as it reaccelerates, and it is also being influenced by gravity. As the biomass exits the radius bend, it reaccelerates to approximately 12 m/s due to the influence of the high speed air traveling through the reduced cross section of the vertical duct.

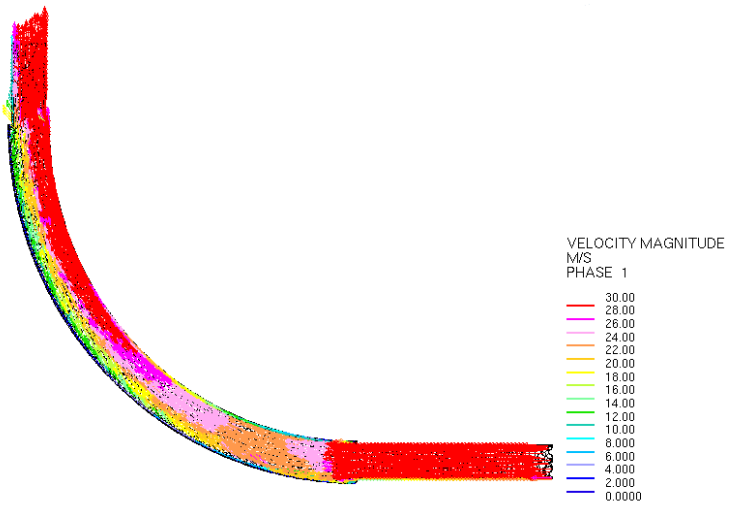

Figure 7.9. Air phase velocity profile in horizontal-to-vertical bend.

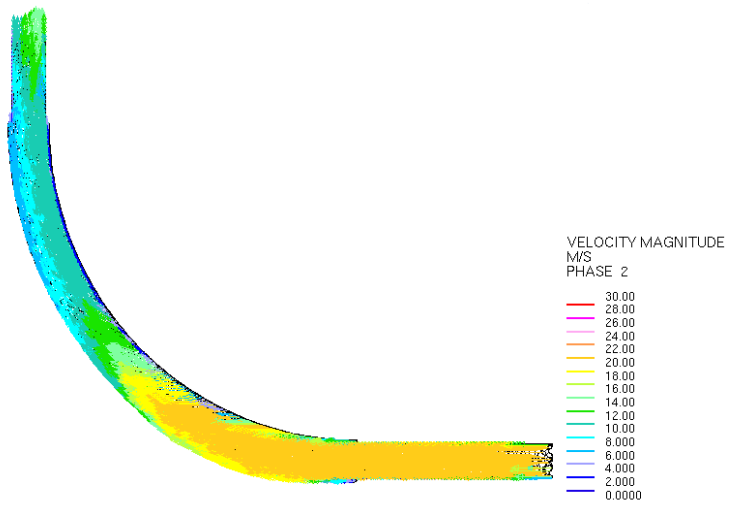

Figure 7.10. Biomass phase velocity profile in horizontal-to-vertical bend.

Figure 7.11 shows the air phase velocity profile, while Figure 7.12 shows the biomass velocity profile at the upward vertical to horizontal radius bend in the multiphase flow model. The air phase enters the bend at a uniform 30 m/s, but decelerates to 25 m/s, again due to the slightly larger cross sectional area constructed in the radius bend. As the air travels a third of the way thorough the radius bend, the velocity profile stratifies and the air velocity reaches 30 m/s along the inner wall and is closer to 18 m/s along the outer edge of the wall. This is due to the presence of the biomass accumulation along the outer edge of the wall. As the air exits the bend and travels horizontally, it again reaches 30 m/s.

Again, the velocity profile of the biomass phase shows a significantly different behavioral pattern than the air phase. The biomass enters the radius bend at 12 m/s, or about one third of the velocity of the air velocity. The inertial effects of the biomass allow it to maintain its velocity through the bend, and it travels one third of the distance of the radius before decelerating to 6-8 m/s. As the biomass exits the radius bend and travels horizontally it gradually reaccelerates to approximately 12 m/s due to the influence of the high speed air.

Figure 7.11. Air phase velocity profile in vertical-to-horizontal bend.

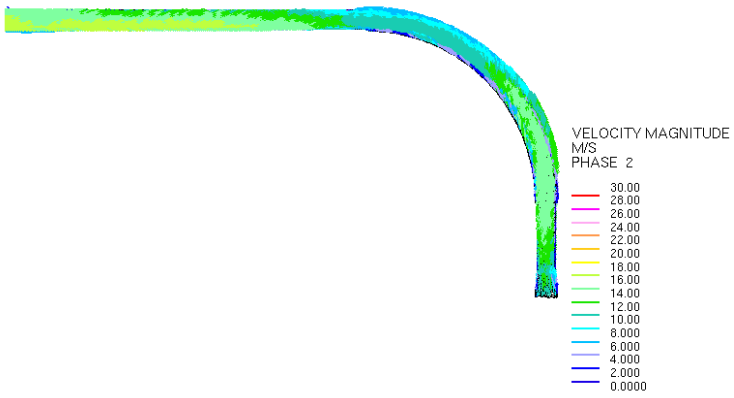

Figure 7.12. Biomass phase velocity profile in vertical-to-horizontal bend.

CHAPTER 8: CONCLUSIONS AND FUTURE RESEARCH

8.1. Conclusions

A modeling framework for predicting multiphase fibrous flows has been developed. The main features of the developed framework is that it (1) accounts for the large, low density of fibrous bulk solids, (2) predicts the flow conditions of each of the two phases, and (3) may be implemented for a variety of fibrous bulk solids. The modeling framework was applied to two distinct fibrous bulk solids. The first application was cotton-air flow within a positive pressure pneumatic conveyance system, and the second was biomass-air flow within a negative pressure pneumatic conveyance system.

The computational model presented in this research begins with the Eulerian-Eulerian multiphase modeling approach, which represents the conveying air phase and the fibrous bulk solids phase with the conservation equations of mass and momentum. The conservation of mass equations are coupled by the volume fraction concentration of the bulk solids and conveying air at each computational grid point. The conservation of momentum equations are also coupled by the interphase momentum transfer that occurs between the bulk solids and air phases.

This research developed a representation for quantifying the interphase momentum transfer between the two phases, which is based on two effects. The first effect is the particle drag force between the flowing air and the moving bulk solids. The drag force is calculated based on the size and shape of the bulk solids and the relative velocity between the particles and the air. The second effect incorporates the additional flow resistance due to the unique characteristics of the fibrous bulk solids. These additional flow resistances can include the

rough surface, rotation effects of the fibrous bulk solids, and interconnected strings between fibers of the bulk solids that extend beyond the computational grid. The additional resistance is based on the concept of the Ergun equations, in which air flows through a porous media. In this case, the porous media is moving relative to the flowing air. The drag effect and the additional resistance effects are based on the properties of the fibrous bulk solids as they are transported through the conveyance system.

To understand the behavior of the two bulk solids of interests, two experimental test apparatuses were constructed to measure the flow conditions of the respective bulk solids as they are being transported. These measurements include the velocity profiles of the fibrous bulk solids and the pressure profiles of the air flowing through the experimental test apparatus. Once the flow characteristics of the fibrous bulk solids are understood, they are applied to the computational model. Comparable CFD models were developed to replicate the flow conditions observed in the respective lab test apparatus by comparing the experimental results with the computational results. The flow characteristics of the fibrous bulk solids are incorporated in a commercially available CFD solver through external user-defined functions. The converged CFD models are compared to the experimental flow characteristics of the fibrous bulk solids, and the parameters available in the user-defined functions are adjusted to correlate with the experimental tests.

This research has shown that flow characteristics of fibrous bulk solids flows can be predicted using the developed framework with computational models. The computational modeling of the interphase momentum transfer terms discussed in this research had the ability to match the flow characteristics observed in the experimental test apparatus for each of the two bulk solids studied. In addition, the models have the ability to answer engineering

design questions that were previously based on extensive experimental data, iterative flowcharts, and previous experience.

Additionally, this research shows the potential and utility of using computational models to predict fibrous bulk solid flows for engineering design and to be able to answer additional engineering design questions. Examples of this include having the ability to predict accumulation of fibrous bulk solids and the pressure drops due to the presence of the bulk solids.

8.2. Future Research

The techniques for modeling multiphase fibrous flows are in place to allow modeling of various pneumatic conveyance systems. However, additional research is necessary to further expand the utility and capability of the framework for engineering design. For instance, additional bulk solids can be studied and correlated to the connectivity parameters described in this research. Additionally, many of the assumptions made for this research were done to simplify the modeling approach, which allow shorter solution times. Possible opportunities for expanding this research include developing more intricate correlations for the connectivity resistance and for the particle drag resistance.

Furthermore, this research can be applied directly to engineering design problems Practical technologies for modeling heterogeneous products are needed, particularly in segregation processes currently found in combine harvesters. For example, having the capability to model segregation of bulk solids could have significant potential in developing single-pass harvesters, which harvest the nodes, stems and seeds of the plant in a single pass.

REFERENCES

Atchison, J., & Hettenhaus, J. (2004). Innovative methods for corn stover collecting, handling, storing and transporting. National Renewable Energy Laboratory. April 2004. NREL/SR-510-33893.

Badger, P. (2002). Processing cost analysis for biomass feedstocks. *USDOE Office of Energy Efficiency and Renewable Energy: Biomass Program.* Budget Activity Number EB 24 04 00 0.

Bilirgen, H., Levy, E., & Yilmaz, A. (1998). Prediction of pneumatic conveying flow phenomena using commercial CFD software. *Powder Technology, 95*, 37-41.

Biomass Research and Development Board. (2008). *National Biofuels Action Plan: October 2008. Retrieved May 1, 2009, from* www1.eere.energy.gov/biomass/pdfs/nbap.pdf.

Bradley, M., Burnett, A., & Woodhead, S. (1995). Measurement of pressure profiles in pneumatic conveying pipelines. *Instrumentation and Measurement Technology Conference, 1995. IMTC/95. Proceedings. 'Integrating Intelligent Instrumentation and Control', IEEE.* Waltham, MA, USA. 766-780.

Carruthers, A., & Filippone, A. (2005). Aerodynamic Drag of Streamers and Flags. *Journal of Aircraft, 42, 4,* 976-982.

Chen, S., Phan-Thein, N., Khoo, B., & Fan, X. (2006). Flow around spheres by dissipative particle dynamics. *Physics of Fluid, 18*(1), 1-14.

Crowe, C., editor. (2006). Multiphase Flow Handbook. Boca Raton, FL: CRC Press, Taylor and Francis Group, LLC.

Crowe, C. (2000). On models for turbulence modulation in fluid-particle flows. *International Journal of Multiphase Flow, 26,* 719-727.

Crowe, C., Sommerfeld, M., & Tsuji, Y. (1998). *Multiphase Flows with Droplets and Particles.* Boca Raton, FL: CRC Press, LLC.

Crowe, C., Troutt, T., & Chung, J. (1996). Numerical models for two-phase turbulent flows. *Annual Review of Fluid Mechanics, 28,* 11-43.

Crummer, K., & Brown, R. (2002). Ancillary equipment for biomass gasification. *Biomass and Bioenergy, 23,* 113-128.

Cui, H. & Grace, J. (2007a). Flow of pipe fibre suspension and slurries: A review. *International Journal of Multiphase Flow, 33,* 921-934.

Cui, H. & Grace, J. (2007b). Fluidization of biomass particles: A review of experimental multiphase flow aspects. *Chemical Engineering Science, 62,* 45-55.

Cui, H. & Grace, J. (2006). Pneumatic conveying of biomass particles: A review. *China Particulology, 4*(3-4), 183-388.

Das, P. & Meloy, J. (2002). Effect of close-coupled bends in pneumatic conveying. *Particulate Science and Technology, 20,* 253-266.

Datta, B. & Ratnayaka, C. (2005). A possible scaling-up technique for dense phase pneumatic conveying. *Particulate Science and Technology, 23,* 201-204.

Deloughry, R., Pickup, E., & Ponnapalli, P. (2001). Closed loop control of a pneumatic conveying system using tomographic imaging. *Journal of Electronic Imaging, 10*(3), 653-660.

Du, W., Bao, X., Xu, J., & Wei, W. (2006). Computational fluid dynamics (CFD) modeling of sprouted bed: Influence of frictional stress, maximum packing limit and coefficient of restitution of particles. *Chemical Engineering Science, 61,* 4558-4570.

Elperin, T. & Vikhansky, A. (2002). Variational model of granular flow in a three-dimensional rotating cylinder. *Physica A.* 33 48-56.

Energy Information Administration (2009). EIA Renewable Energy: Biomass Data and Information. *Retrieved April 4, 2009, from* http://www.eia.doe.gov/cneaf/solar.renewables/page/biomass/biomass.html.

Ergundenler, A & Ghaly, A. (1993). Agglomeration of silica sand in a fluidized bed gasifier operating on wheat straw. *Biomass and Bioenergy, 4*(2), 135-147.

Fan, L. & Zhu, C. (1998). *Principles of Gas-Solid Flows.* Cambridge, UK: Cambridge University Press.

Ferreira, M., Freire, J., & Massarani, G. (2000). Homogeneous hydraulic and pneumatic conveying of solid particles, *Powder Technology, 108,* 46-54.

Fokeer, S., Kingman, S., Lowndes, I., & Reynolds, A. (2003). Characterisation of the Cross Sectional Particle Concentration Distribution in Horizontal Dilute Flow Conveying: A Review. *Chemical Engineering and Processing, 43,* 677-691.

Guiney, P., Pan, R., & Chambers, J. A., (2002). Scale-up technology in low-velocity slug-flow pneumatic conveying. *Powder Technology, 122,* 34-45.

Gyenis, J., Ulbert, Z., Szepvolgyi, J., & Tsuji, Y. (1999). Discrete particle simulation of flow regimes in bulk solids mixing and conveying. *Powder Technology 104,* 248-257.

Hayden, K., Park, K., & Curtis, J. (2003). Effect of particle characteristics on particle pickup velocity. *Powder Technology, 131* 7-14.

Henderson, M. S. & Perry, R. L. (1976). *Agricultural Processing Engineering, Third Edition.* Westport, CT : The AVI Publishing Company.

Henthorn, K., Park, K., & Curtis, J. (2005). Measurement and prediction of pressure drop in pneumatic conveying: effect on particle characteristics, mass loading and Reynolds number. *Ind. Eng. Chem. Res.* 44 5090-5098.

Hlungwani, O., Rikhotso, J., Dong, H., & Moys, M. (2003). Further validation of DEM modeling of milling: effects of linear profile and mill speed. *Minerals Engineering, 16,* 993-998.

Holst, J., Ooi, J., Rotter, M., & Rong, G. (1999). Numerical modeling of silo filling 1: Continuum analyses. *Journal of Engineering Mechanics, 125*(1), 94-103.

Holzer, A. & Sommerfeld, M. (2009). Lattice Boltzmann simulations to determine drag, life and torque acting on son-spherical particles. *Computers and Fluids.* 38 572-589.

Hong, J. & Tomita, Y. (1995). Analysis of high density gas-solids stratified pipe flow. *International Journal of Multiphase Flow,* 21(4), 649-665.

Hoskinson, R., Karlen, D., Birrell, S., Radthke, C., & Wilhelm, W. (2007). Engineering, nutrient removal, and feedstock conversion evaluations of four corn stover harvest scenarios. *Biomass and Bioenergy, 31,* 126-136.

Huber, N. & Sommerfeld, M. (1998). Modelling and numerical calculation of dilute phase pneumatic conveying in pipe systems. *Powder Technology, 98,* 90-101.

Hyder, L. M., Bradley, M.S.A., Reed, A R., & Hettiaratchi, K. (2000). An investigation into the effect of particle size on straight-pipe pressure gradients in lean-phase conveying. *Powder Technology, 112,* 235-243.

Intel Corp. (2001). Open Source Computer Vision Library Reference Manual. *Retrieved May 11, 2008, from* www.itee.uq.edu.au/~iris/CVsource/OpenCVreferencemanual.pdf

Jaworski, A. & Dyakowski, T. (2002). Investigations of flow instabilities within the dense pneumatic conveying system. *Powder Technology, 125,* 279-291.

Joppich, A., & Salman, H. (1999). Wood powder feeding, difficulties and solutions. *Biomass and Bioenergy, 16,* 191-198.

Kalman, H., Satran, A., Meir, D., & Rabinovich, E. (2005). Pickup (critical) velocity of particles. *Powder Technology, 160,* 103-113.

Kalman, H. & Klinzing, G. E. (2005). Freight Pipelines-2005 Review.

Kartushinsky, A., & Michaelides, E. (2007). Gas-solid particle flow in horizontal channels: Decomposition of the particle-phase flow and the interparticle collision effects. *Journal of Fluids Engineering, 129,* 702-712.

Kilfoil, M. (2003). Numerical simulation of simultaneous drying and pneumatic conveying: small metallic filter cake particles. *Applications of Computers and Operations Research in the Minerals Industries,* 283-288.

Kiliçkan, A., & Guner, M. (2006). Pneumatic conveying characteristics of cotton seeds. *Biosystems Engineering, 95*(4), 537-546.

Klinzing, G (1987). Particle velocity measurements through electrostatic field fluctuations using external probes. *Particulate Science and Technology, 5*(1), 95-104.

Klinzing, G. & Leung, F. (1997). *Pneumatic Conveying of Solids: A Theoretical and Practical Approach.* Chapman and Hall.

Kraus, M. (1980). *Pneumatic Conveying of Bulk Materials, Second Edition.* McGraw-Hill Publications.

Landry, H., Thirion, F., Lague, C., & Roberge, M. (2006). Numerical modeling of the flow of organic fertilizers in land application equipment. *Computers and Electronics in Agriculture, 51,* 35-53

Landry, H., Lague, C., & Roberge, M. (2006). Discrete element modeling of machine-manure interactions. *Computers and Electronics in Agriculture, 52,* 90-106.

Laouar, S. & Molodtsof, Y. (1998). Experimental characterization of the pressure drop in dense phase pneumatic transport at very low velocity. *Powder Technology, 95,* 165-173.

Larsen, J., Petersen, M., Thirup, L., Li, H., & Iversen, F. (2008). The IBUS process-lignocellulosic bioethanol close to a commercial reality. *Chemical Engineering Technology, 31*(5), 765-772.

Li, J., Webb, C., Pandiella, S., Campbell, G., Dyakowski, T., Cowell, A., & McGlinchey, D. (2005). Solids deposition in low-velocity slug flow pneumatic conveying. *Chemical Engineering and Processing, 44,* 167-173.

Li, Y., Xu, Y., & Thorton, C. (2005). A comparison of discrete element simulations and experiments for 'sandpiles' composed of spherical particles. *Powder Technology, 160,* 219-228.

Li, J., Pandiella, S., Webb, C., Dyakowski, T., & Jones, M. (2003). Analysis of gas-solids feeding and slug formation in low-velocity pneumatic conveying. *Particulate Science and Technology, 21,* 57-73.

Lim, E., Zhang, Y, & Wang, C.-H. (2006). Effects of an electrostatic field in pneumatic conveying of granular materials through inclined and vertical pipes. *Chemical Engineering Science, 61,* 7889-7908.

Limtrakul, S., Boonsrirat, A., & Vatantham, T. (2004). DEM modeling and simulation of a catalytic gas-solid fluidized bed reactor: a sprouted bed as a case study. *Chemical Engineering Science, 59,* 5225-5231.

Littman, H., Morgan, M., Jovanovic, S., Paccione, J., Grbavcic, Z., & Vukovic, D. (1995). Effect of particle diameter, particle density, and loading ratio on the effective drag coefficient in steady turbulent gas-solids transport. *Powder Technology, 84,* 49-56.

Manninen, M., & Taivassalo, V. (1996). *On the Mixture Model for Multiphase Flow*. Julkaisija-Utgivare,VTT Finland: VTT Publications.

Mckendry, P. (2002). Energy production from biomass (part 1): Overview of biomass. *Bioresoruce Technology, 83,* 195-204.

Melander, O. & Rasmuson, A. (2004). PIV measurements of velocities and concentrations of wood fibres in pneumatic transport. *Exp. Fluids,* 37, 293-300.

Mills, D., Jones, M., & Agarwal, V. (2004). *Handbook of Pneumatic Conveying Engineering.* Marcel Dekker, Inc.

Mills. D. (2004). *Pneumatic Conveying Design Guide: Second Edition*. Elsevier Butterworth Heinemann.

Mortensen, P., Andersson, H., Gillissen, J., & Boersma, B. (2008) On the orientation of ellipsoidal particles in turbulent flow. *International Journal of Multiphase Flow, 34,* 678-683.

Munson, B., Young, D., & Okiishi, T. (2006). *Fundamentals of Fluid Mechanics, Fifth Edition.* Anderson, Wayne, acquisitions editor. New York, NY: John Wiley & Sons, Inc.

Nadaoka, K., Nihei, Y., & Yagi, H. (1999). Grid-averaged Lagrangian LES model for multiphase turbulent flow. *International Journal of Multiphase Flow, 25,* 1619-1643.

National Renewable Energy Laboratory (2007). Research advances cellulosic ethanol. NREL/BR-510-40742

National Renewable Energy Laboratory (2006). From biomass to biofuels. NREL/BR-510-39436.

National Renewable Energy Laboratory (2003). DOE Thermochemical users facility: a proving ground for biomass technology. DOE/GO-102003-1783.

Ocone, R. & Delebarre, A. (2006). Predicting the similar profile regime of upflowing gas-solid suspensions. *Transactions of IChemE, 80*(A), 631-636.

Oden, J., Belytcshko, T., Fish, J., Hughes, T., Johnson, C., Keyes, D., Laub, A., Petzold, L., Srolovitz, D., & Yip, S. (2006). Simulation-based engineering science: revolutionizing engineering science through simulation. *Report of the National Science Foundation Blue Ribbon Panel on Simulation-Based Engineering Science*. *Retrieved April 14, 2008, from* http://www.nsf.gov/publications/pub_summ.jsp?ods_key=sbes0506.

Office of the Biomass Program. (2007). Biomass multi-year program plan. *Energy Efficiency and Renewable Energy.* U.S. Department of Energy.

Papatheofanous, M., Koullas, D., Fuglsang, H., & Schade, J. (1995). Biorefining of agricultural crops and residues: effect of pilot plant fractionation on properties of fibrous fractions. *Biomass and Bioenergy, 8*(6), 419-426.

Raheman, H. & Jindal, V. (2002). Drag coefficients of agricultural grains in vertical pneumatic conveying. *Applied Engineering in Agriculture, 19*(2), 197-202.

Raji, A. & Favier, J. (2003). Model for the deformation in agricultural and food particulate materials under bulk compressive loading using discrete element method. I: Theory, model development and validation. *Journal of Food Engineering, 64,* 359-371.

Ratnayake, C. (2005). A comprehensive scaling up technique for pneumatic transport systems (Doctoral dissertation, Telemark University College, 2005). Dep. Of Technology, Kjoles Rnin, N-391 Porsgrunn, Norway.

Reinfried, R. (date unknown). Pocket glossary of pneumatic conveying terms, Conveyor Equipment Manufacturers Association (CEMA) Standard 805: Understanding pneumatic conveying lingo. *Powder and Bulk Engineering* CSC Publishing.

Schallert, R. & Levy, E. (2000). Effect of a combination of two elbows on particle roping in pneumatic conveying. *Powder Technology, 107,* 226-233.

Segler, G. (1952). *Pneumatic Grain Conveying: with Special Reference to Agricultural Applications.* Published by G. Segler.

Shrivastava, K. (2002). Pneumotransport of grains through a pipeline. *ASME-PUBLICATIONS-Fluids Engineering Division. Symposium: 252*1305-1310.

Sokhansanj, S., Turhollow, A., Tagore, S. & Mani, S. (2006). Integrating biomass feedstock with an existing grain handling system for biofuels. In the *2006 ASABE Annual International Meeting, Portland, OR.* 9-12 July. 1-16.

Sokhansanj, S., Cushman, J. & Wright, L. (2003). Collection and delivery of biomass for fuel and power production. *Agricultural Engineering International: the CIGR Journal of Scientific Research and Development.* Invited Overview Paper, 5 1-22.

Sokhansanj, S., Turhollow, A., Cushman, J., & Cundiff, J. (2002). Engineering aspects of collecting corn stover for bioenergy. *Biomass and Bioenergy, 23,* 347-355.

Sommerfeld, M. (2003). Analysis of collision effects for turbulent gas-particle flow in a horizontal channel: part 1. particle transport. *International Journal of Multiphase Flow, 29,* 675-699.

Sommerfeld, M. (2001). Validation of a stochastic Lagrangian modelling approach for inter-particle collisions in homogeneous isotropic turbulence. *International Journal of Multiphase Flow, 27,* 1829-1858.

Sommerfeld, M. & Huber, N. (1999). Experimental analysis and modelling of particle-wall collisions. *International Journal of Multiphase Flow, 25,* 1457-1489.

Srinivasan, K., Wang, Z., Yuan, W. & Sun, R. (2004). Vehicle thermal management simulation using a rapid omni-tree based adaptive Cartesian mesh generation methodology. *ASME Heat Transfer/Fluids Engineering Summer Conference. 2*(B) 1229-1236.

Stavens, D. (2005). Introduction to OpenCV. *Presentation for Stanford Artificial Intelligence Lab.* Computer Science 223B. Stanford, CA. *Retrieved May 11, 2008, from* ai.stanford.edu/~dstavens/cs223b/stavens_opencv_optical_flow.pdf.

Stoess, H. (1983). *Pneumatic Conveying: Second Edition.* John Wiley and Sons.

Takayama, S. & Aoki, K. (2004). Flow characteristics around a rotating circular cylinder. *Transactions of the Japan Society of Mechanical Engineers, 71*(3), 833-839.

Tan, S., Williams, K., Jones, M., & Krull, T. (2008). Determination of slug permeability factor for pressure drop prediction of slug flow pneumatic conveying. *Particuology, 6,* 307-315.

Tannehill, J., Anderson, D., & Pletcher, R. (1st ed.). (1980). *Computational Fluid Mechanics and Heat Transfer.* Taylor and Francis, Inc.

Thorn, R., Beck, M., & Green, R. (1982). Non-intrusive methods of velocity measurement in pneumatic conveying. *Journal of Physics E: Scientific Instruments, 15,* 1131-1139.

Tomita, Y., Agarwal, V., Asou, H., & Funatsu, K. (2008). Low-velocity slug conveying in horizontal pipe for coarse particles and fine particles. *Particuology, 6,* 316-321.

Tran-Cong, S., Gay, M., & Michaelides, E. (2004). Drag coefficients of irregularly shaped particles. *Powder Technology, 139,* 21-32.

Triesch, O., & Bohnet, M. (2001), Measurement and CFD prediction of velocity and concentration profiles in a decelerated gas-solids flow. *Powder Technology, 115,* 101-113.

Vessia, O. (2005). Biofuels from lignocellulosic material: In the Norwegian context 2010—Technology, Potential and Costs. Project report. Norwegian University of Science and Technology.

Wang, W., Lu, B., & Li, J. (2007). Choking and flow regime transitions: Simulation by a multi-scale CFD approach. *Chemical Engineering Science, 62,* 814-819.

Williams, K., Jones, M., & Cenna, A. (2008). Characterization of the gas pulse frequency, amplitude, and velocity in non-steady dense phase pneumatic conveying of powders. *Particuology, 6,* 301-306.

Wu, M., Wu, Y., & Wang, M. (2006). Energy and emission benefits of alternative transportation liquid fuels derived from switchgrass: a fuel life cycle assessment. *Biotechnol. Prog, 22*(4), 1012-1024.

Wyman, C. (2007). What is (and is not) vital to advancing cellulosic ethanol. *Trends in Biotechnology, 25*(4), 153-157.

Wyman, C. (2003). Potential synergies and challenges in refining cellulosic biomass to fuels, chemicals, and power. *Biotechnol. Prog, 19,* 254-262.

Wypych, P., Yi, J., & Hastle, D. (2003). Minimum transport for dense-phase conveying of granules. *Particulate Science and Technology, 21,* 75-82.

Xiang, J., & McGlinchey, D. (2004). Numerical simulation of particle motion in dense phase pneumatic conveying. *Granular Matter, 6,* 167-172.

Yilmaz, A., & Levy, E. (2001). Formation and dispersion of ropes in pneumatic conveying. *Powder Technology, 114,* 168-185.

Zhu, K., Rao, M., Wang, C., & Sundaresan, S. (2003). Electrical capacitance tomography measuements on vertical and inclined pneumatic conveying of granular solids. *Chemical Engineering Science, 58,* 4225-4245.

APPENDIX A: PROPERTIES OF BULK SOLIDS

The tables in Appendix A show the properties and characteristics for several commodities that are successfully conveyed pneumatically. This information is provided to indicate the variability of pneumatically conveyed products.

Table A.1. Minimum safe air velocities for various bulk solids (Klinzing 1997).

Bulk Solids	Average Bulk Density (kg/m^3)	Approximate Size Grading (mm)	Minimum Safe Air Velocity: Vertical (m/s)	Minimum Safe Air Velocity: Horizontal (m/s)
Coal	720	13	12.00	15.00
Coal	720	6	9.00	12.00
Wheat	753	5	9.00	12.00
Polythene Cubes	480	3	9.00	12.00
Cement	1400	90	1.5	7.6
Flour	560	150	1.5	4.6
Pulverized coal	720	75	1.5	4.6
Pulverized ash	720	150	1.5	4.6
Fullers earth	640	106	1.5	6.1
Bentonite	900	75	1.5	7.6
Barite	1750	63	4.6	7.6
Silica flour	880	106	1.5	6.1
Fluorspar	1760	75	3.0	9.1
Phosphate rock	1280	150	3.0	9.1
Tripolyphosphate	1040	180	1.5	7.6
Common salt	1360	150	3.0	9.1
Soda ash	560	106	3.0	9.1
Soda ash	1040	180	3.0	12.2
Sodium sulphate	1360	106	3.0	12.2
Sodium perborate	865	180	3.0	9.1
Ground bauxite	1440	106	1.5	7.6
Alumina	930	106	1.5	7.6
Kieselguhr	240	75	1.5	7.6
Magnesite	1600	75	3.0	3.0
Uranium dioxide	3520	75	6.1	18.3

Table A.2. Comparison of velocities in pressure and vacuum systems (Klinzing 1997).

Bulk Solids	Bulk Density (kg/m^3)	Velocity: Pressure System (m/s)	Velocity: Vacuum System (m/s)
Alum	800	19.8	33.5
Calcium carbonate	440	19.8	33.5
Coffee beans	672	13.7	22.9
Hydrated lime	480	12.2	27.4
Malt	449	16.8	30.5
Oats	400	16.8	30.5
Salt	1440	25.3	36.6
Starch	640	16.8	27.4
Sugar	800	18.3	33.5
Wheat	769	16.8	32.0

Table A.3. Recommended air velocities for fibrous bulk solids (Henderson and Perry 1976).

Bulk Solids	Air Velocity (ft/min)	Air Velocity (m/s)
Barley	5000-6000	25.4-30.5
Coffee Beans	3000-3500	15.3-17.8
Corn	5000-7000	25.4-35.5
Cotton	4000-6000	20.3-30.5
Cotton Seed	4000-6000	20.3-30.5
Oats	4500-6000	22.9-30.5
Rags	4500-6500	22.9-33.0
Salt	5500-7500	27.9-38.0
Sand	6000-9000	30.5-45.7
Sawdust	4000-6000	20.3-30.5
Wheat	5000-7000	25.4-35.5
Wool	4500-6000	22.9-30.5

APPENDIX B: USER DEFINED SUBROUTINES

The following information contains the particle drag (uedrag.f) and the momentum source term (sormom.f) subroutine required for STAR-CD™ V4 to account for the momentum exchanges between the continuous air phase and the dispersed fibrous phase.

```
C*******BEGINNING OF SUBROUTINE UEDRAG.F*************C

C***********************************************************************
      SUBROUTINE UEDRAG(DFAC)
C     Specify linearised drag force coefficient in Eulerian multi-phase.
C***********************************************************************
C----------------------------------------------------------------------*
C     STAR-CD VERSION 4.08.000
C----------------------------------------------------------------------*
      INCLUDE 'comdb.inc'
      COMMON/USR001/INTFLG(100)
      INCLUDE 'usrdat.inc'
      DIMENSION SCALAR(50)
      EQUIVALENCE( UDAT12(001), ICTID )
      EQUIVALENCE( UDAT03(019), VOLP )
      EQUIVALENCE( UDAT04(002), DEN )
      EQUIVALENCE( UDAT04(003), ED )
      EQUIVALENCE( UDAT04(005), PR )
      EQUIVALENCE( UDAT04(008), TE )
      EQUIVALENCE( UDAT04(009), SCALAR(01) )
      EQUIVALENCE( UDAT04(059), U )
      EQUIVALENCE( UDAT04(060), V )
      EQUIVALENCE( UDAT04(061), W )
      EQUIVALENCE( UDAT04(062), VISM )
      EQUIVALENCE( UDAT04(063), VIST )
      EQUIVALENCE( UDAT04(007), T )
      EQUIVALENCE( UDAT04(067), X )
      EQUIVALENCE( UDAT04(068), Y )
      EQUIVALENCE( UDAT04(069), Z )
C-----------------------------------------------------------------
C
C     This subroutine enables the user to define the linearized drag
C     coefficient force per unit volume (defined as Ad in the methodology
```

```
C    manual) on a cell-by-cell basis for Eulerian multi-phase
C    simulations.
C
C    For multi-phase applications ...
C    - this is a cell-based routine
C    - this routine is called for each fluid-pair
C    - the index of the active fluid-pair is IPHAPR
C    - multiphase properties and fields need to be accessed
C      directly using MODULE emp_variables
C    - density, viscosity and conductivity properties accessed
C      through MODULE emp_variables, will include a volume fraction
C      factor, if flag vf2_weighted in MODULE emp_user is .TRUE.
C
C    ** Parameter to be returned to STAR-CD: DFAC
C
C-----------------------------------------------------------------------
C
C     Note:
C
C        When this subroutine is used, STAR-CD cannot work out the
C        drag coefficient from drag force (DFAC) specified by the user.
C        Therefore, values of drag coefficient in ccmp/ccmt file
C        will be zero. Users must write the drag coefficients
C        into a separate user post file (.usr) for post-processing.
C
C-----------------------------------------------------------------------

C
C Coding for having a modified drag force for the closure terms
C MomTransfer = DragForce + VirtualMassForce + LiftForce
C These are done on a mass per unit volume basis
C
C Look at chapter 13 of the 4.0 user guide for how to use subroutines
C Also look at supplemental StarCD material
C
C To use this, the user coding needs to be activated for the
C drag force under the Eulerian two-phase flow GUI.
C
C-----------------------------------------------------------------------
C         This is put into check the beginning of the subroutine.
C         ITER is the iteration number
C         IP is the cell number

C-----------------------------------------------------------------------
```

```
C This is when we transition from a low single particle drag to a high
C particle loading
      ALPHATRANSITION=0.5

C This alpha factor is determined on observations of the particle flow
      GALPHA = 5.0

C This beta factor is determined on observations of the particle flow
      GBETA = 1.0

C Define the Level of Print Output
      PRINTOUTPUT=2

C Assuming the dispersed phase is a 3-dimensional ellipsoid (need to set)
C These are listed in meters
      ELLENGTH=0.04
      ELWIDTH=0.02
      ELHEIGHT=0.02

C---------------------------------------------------------------------

      IF (PRINTOUTPUT.GT.1) THEN
        IF (ITER.EQ.1) THEN
          IF (IP.EQ.1000) THEN
            print *, 'This Lists the lengths of the particle'
                  print *, 'ELLENGTH=', ELLENGTH, ' m'
                  print *, 'ELWIDTH=', ELWIDTH, ' m'
                  print *, 'ELHEIGHT=', ELHEIGHT, ' m'
          ENDIF
        ENDIF
      ENDIF

C     IF (PRINTOUTPUT.GT.1) THEN
C       IF (ITER.EQ.1) THEN
C         IF (IP.EQ.1000) THEN
C           print *, 'This is at the beginning of the subroutine'
C            print *, 'IP=', IP
C            print *, 'ITER=', ITER
C       print *, VELRELATIVE, VELREL, VFCEL2, VFFACTOR, IPHA, IP
C         ENDIF
C       ENDIF
C     ENDIF

C---------------------------------------------------------------------
```

```
C This line defines the multiplication factor of the
C volume fraction of the particles. Based on the concentration of the
C particles
C This is based on the D/L of spheres
      VFFACTOR = (6.0*VFCEL2*0.318309866)**0.3333

      if(VFFACTOR.gt.1.0)then
        VFFAC = 1.0
      else
        VFFAC = VFFACTOR
      endif

C Calculate Volume of Ellipsoid
C The equation for volume of ellipsoid is 4/3 * pi * r1 * r2 * r3
      ELLIPSVOL=1.33*3.141*(ELLENGTH/2.0)*(ELWIDTH/2.0)*(ELHEIGHT/2.0)

      IF (PRINTOUTPUT.GT.2) THEN
        IF (ITER.EQ.1) THEN
          IF (IP.EQ.1000) THEN
            print *, 'This Lists the Volume of the Ellipsoid'
                  print *, 'ELLIPSVOL=', ELLIPSVOL, ' m^3'
          ENDIF
        ENDIF
      ENDIF

C Calculate the 3 projected areas
C This is done by taking the area of an oval
C The equation for the area of an oval is pi*r1*r2
      ELAREAA=3.14159*(ELLENGTH/2.0)*(ELWIDTH/2.0)
      ELAREAB=3.14159*(ELLENGTH/2.0)*(ELHEIGHT/2.0)
      ELAREAC=3.14159*(ELWIDTH/2.0)*(ELHEIGHT/2.0)

      IF (PRINTOUTPUT.GT.2) THEN
        IF (ITER.EQ.1) THEN
          IF (IP.EQ.1000) THEN
            print *, 'These are the three projected areas'
                  print *, 'ELAREAA=', ELAREAA
                  print *, 'ELAREAB=', ELAREAB
                  print *, 'ELAREAC=', ELAREAC
          ENDIF
        ENDIF
      ENDIF

C Calculate the d_a values
      DAA=sqrt(4*ELAREAA/3.14159)
```

```
      DAB=sqrt(4*ELAREAB/3.14159)
      DAC=sqrt(4*ELAREAC/3.14159)

      IF (PRINTOUTPUT.GT.2) THEN
        IF (ITER.EQ.1) THEN
          IF (IP.EQ.1000) THEN
            print *, 'These are the three d_a values'
                  print *, 'DAA=', DAA
                  print *, 'DAB=', DAB
                  print *, 'DAC=', DAC
          ENDIF
        ENDIF
      ENDIF

C Calculate the d_n value
      DNVAL=(6.0*ELLIPSVOL/3.14159)**(0.333)

      IF (PRINTOUTPUT.GT.2) THEN
        IF (ITER.EQ.1) THEN
          IF (IP.EQ.1000) THEN
            print *, 'This is the d_n value'
                  print *, 'DNVAL=', DNVAL
          ENDIF
        ENDIF
      ENDIF

C Calculate the (d_a/d_n)**2 in each dir
      DADNSQA=(DAA/DNVAL)**2
      DADNSQB=(DAB/DNVAL)**2
      DADNSQC=(DAC/DNVAL)**2

      IF (PRINTOUTPUT.GT.2) THEN
        IF (ITER.EQ.1) THEN
          IF (IP.EQ.1000) THEN
            print *, 'These are the three (d_a/d_n)**2 values'
                  print *, 'DADNSQA=', DADNSQA
                  print *, 'DADNSQB=', DADNSQB
                  print *, 'DADNSQC=', DADNSQC
          ENDIF
        ENDIF
      ENDIF

C Drag coefficient multiplier for the elliptical shape
      CDMULTA=1.0/DADNSQA
      CDMULTB=1.0/DADNSQB
```

```
      CDMULTC=1.0/DADNSQC

      IF (PRINTOUTPUT.GT.2) THEN
        IF (ITER.EQ.1) THEN
          IF (IP.EQ.1000) THEN
            print *, 'These are the three drag coef. Multiplier vals'
                  print *, 'CDMULTA=', CDMULTA
                  print *, 'CDMULTB=', CDMULTB
                  print *, 'CDMULTC=', CDMULTC
          ENDIF
        ENDIF
      ENDIF

C  Sphericity calculation for the three dimensions
      SPHERTOP=3.14159*DAA
      SPHERBOT=2.0*3.1415*sqrt(((ELLENGTH/2)**2+(ELWIDTH/2)**2)/2)

C  Assuming the sphericity of an ellipsoid
      SPHER=SPHERTOP/SPHERBOT


C  This is the value we care about for the drag function
      SQRTSPH=SQRT(SPHER)

      IF (PRINTOUTPUT.GT.2) THEN
        IF (ITER.EQ.1) THEN
          IF (IP.EQ.1000) THEN
            print *, 'These are the sphericity values'
                  print *, 'SPHERA=', SPHERA
                  print *, 'SPHERB=', SPHERB
                  print *, 'SPHERC=', SPHERC
                  print *, 'SPHER=', SPHER
                  print *, 'SQRTSPHER=', SQRTSPH
          ENDIF
        ENDIF
      ENDIF


C  Calculate the d_a/d_n of interest
C  Assuming that the Projected Area is the ellipse flowing
C  perpendicular to the free stream
      DADN=DAA/DNVAL

      IF (PRINTOUTPUT.GT.2) THEN
        IF (ITER.EQ.1) THEN
```

```
          IF (IP.EQ.1000) THEN
            print *, 'This is the d_a/d_n values'
                  print *, 'DADN=', DADN
          ENDIF
        ENDIF
      ENDIF


C---------------------------------------------------------------------
C Calculate the Relative velocity at each cell
      VAIR=SQRT((U)**2+(V)**2+(W)**2)
      VPART=SQRT((UCEL2)**2+(VCEL2)**2+(WCEL2)**2)
      VREL=SQRT((U-UCEL2)**2+(V-VCEL2)**2+(W-WCEL2)**2)

C Calculate the Equivalent Diameter for a nonspherical particle
C This is for the Reynolds Number calculations
C This will need to be reconsidered
C      PARTDIA=(ELLENGTH+ELWIDTH+ELHEIGHT)/3.0

C UPDATED: Have the PARTDIA be equal to the DNVAL
      PARTDIA=DNVAL

      IF (PRINTOUTPUT.GT.2) THEN
        IF (ITER.EQ.1) THEN
          IF (IP.EQ.1000) THEN
            print *, 'This compares d_n to particle diameter.'
                  print *, 'DNVAL=', DNVAL
                  print *, 'PARTDIA=', PARTDIA
          ENDIF
        ENDIF
      ENDIF

C Particle Reynolds number
      REYP=DEN*VREL*PARTDIA/(VISM+SMALL)


C  This number is used frequently in the Cd calculation
C  We will calculate it here for clarity
C  This is (d_a/d_n)*Reynolds number
      DADNREYP=DADN*REYP

C  This number is also used frequently in the C_d calculation
C  This is (d_a/d_n)^2
      DADNSQ=DADN**2
```

```
C-----------------------------------------------------------------
C Coefficient of Drag based on Reynolds number
C Please refer to pp. 70 of Crowe, Sommerfeld and Tsuji
C The following line is needed to not make the solution diverge
     IF(REYP.LT.SMALL) THEN
       DFAC=18.*VFCEL2*VISM/(PARTDIA*PARTDIA)
     ELSE
C The following drag correlation is based on the work of Tran-Cong
C        TERMONED=(24.0/REYP)*DADN*(1.0+0.15/SQRTSPH*DADNREYP**0.687)
C        TERMTWODA=(0.42*DADNSQ)
C        TERMMTWOB=(SQRTSPH*(1.0+0.000425*(DADN*REYP**(-1.16))))
C        CD=0.75*(TERMONED+TERMTWODA/TERMMTWOB)

        TERMONED=(24.0/REYP)*DADN*(1.0+0.15/SQRTSPH*DADNREYP**0.687)
        TERMTWODA=(0.42*DADNSQ)
        TERMMTWOB=(SQRTSPH*(1.0+0.000425*(DADN*REYP**(-1.16))))
        CD=(TERMONED+TERMTWODA/TERMMTWOB)

        IF (PRINTOUTPUT.GT.3) THEN
          IF (IP.EQ.1000) THEN
            print *, 'This outputs the C_d drag coefficient.'
            print *, 'REYP=', REYP
            print *, 'CD=', CD
            print *, 'TERMONED=', TERMONED
                  print *, 'TERMTWODA=', TERMTWODA
                  print *, 'TERMMTWOB=', TERMMTWOB
          ENDIF
        ENDIF

C  The DFAC is based on the A_d equation found on pp. 13-4
C  in the StarCD 4.0 methodology manual
C  If I understand correctly, this will be multiplied by the
C  relative particle velocity
C-----------------------------------------------------------------
        IF(VFCEL2.LT.ALPHATRANSITION) THEN
C  Drag due to the irregular shape (SHAPEDRAG)
               SHAPEDRAG=0.75*VFCEL2*DEN*VREL*CD/PARTDIA
C  Resistance due to the String Effects shape (SHAPEDRAG)
C            FIBERRESIST=VFFAC*(GALPHA*VREL+GBETA)*VREL

          FIBERRESIST=0.0

C  Sum these RESISTANCES
             DFAC=SHAPEDRAG+FIBERRESIST
```

```
          IF (PRINTOUTPUT.GT.3) THEN
            IF (IP.EQ.1000) THEN
              print *, 'This compares drag due to shape and fiber.'
                    print *, 'SHAPEDRAG=', SHAPEDRAG
                    print *, 'FIBERRESIST=', FIBERRESIST
            ENDIF
          ENDIF

        ELSE
C  Resistance is due to High Particle Loading (Ergun-based)
          ERGUNTERMA=150*VFCEL2**2*VISM/((1-VFCEL2)*PARTDIA**2)
                ERGUNTERMB=1.75*VFCEL2*DEN*VREL/PARTDIA
                DFAC=ERGUNTERMA+ERGUNTERMB

          IF (PRINTOUTPUT.GT.3) THEN
            IF (IP.EQ.1000) THEN
              print *, 'This compares term A and B of Ergun.'
                    print *, 'ERGUNTERMA=', ERGUNTERMA
                    print *, 'ERGUNTERMB=', ERGUNTERMB
            ENDIF
          ENDIF

        ENDIF

      ENDIF

C-----------------------------------------------------------------------
      RETURN
      END
C

C*******END OF SUBROUTINE UEDRAG.F*************C
```

```
C*******BEGINNING OF SUBROUTINE SORMOM.F*************C

C**********************************************************************
      SUBROUTINE SORMOM(S1U,S2U,S1V,S2V,S1W,S2W,POROS)
C     Source-term for momentum
C**********************************************************************
C----------------------------------------------------------------------*
C     STAR VERSION 4.08.000
C----------------------------------------------------------------------*
      INCLUDE 'comdb.inc'
      COMMON/USR001/INTFLG(100)
      INCLUDE 'usrdat.inc'
      DIMENSION SCALAR(50)
      EQUIVALENCE( UDAT12(001), ICTID )
      EQUIVALENCE( UDAT03(001), CON )
      EQUIVALENCE( UDAT03(006), G1 )
      EQUIVALENCE( UDAT03(007), G2 )
      EQUIVALENCE( UDAT03(008), G3 )
      EQUIVALENCE( UDAT03(019), VOLP )
      EQUIVALENCE( UDAT04(001), CP )
      EQUIVALENCE( UDAT04(002), DEN )
      EQUIVALENCE( UDAT04(003), ED )
      EQUIVALENCE( UDAT04(005), PR )
      EQUIVALENCE( UDAT04(008), TE )
      EQUIVALENCE( UDAT04(009), SCALAR(01) )
      EQUIVALENCE( UDAT04(059), U )
      EQUIVALENCE( UDAT04(060), V )
      EQUIVALENCE( UDAT04(061), W )
      EQUIVALENCE( UDAT04(062), VISM )
      EQUIVALENCE( UDAT04(063), VIST )
      EQUIVALENCE( UDAT04(007), T )
      EQUIVALENCE( UDAT04(067), X )
      EQUIVALENCE( UDAT04(068), Y )
      EQUIVALENCE( UDAT04(069), Z )
C----------------------------------------------------------------------
C
C     This subroutine enables the user to specify the momentum source
C     term (per unit volume) in linearized form:
C
C        Source in x direction = S1U-S2U*U, (N/m3)
C        Source in y direction = S1V-S2V*V, (N/m3)
C        Source in z direction = S1W-S2W*W, (N/m3)
C
C
C     ** Parameters to be returned to STAR:  S1U,S2U,S1V,S2V,S1W,S2W,
```

```
C                              POROS
C
C---------------------------------------------------------------------
C
C     Sample coding: Body forces due to rotation around the z-axis
C
C      OMEGA=100.
C      S1U=DEN*X*OMEGA**2
C      S1V=DEN*Y*OMEGA**2
C---------------------------------------------------------------------C
C
C This subroutine is used to introduce the stringy effects among the
C fibrous particles.
C---------------------------------------------------------------

C This is based upon the porous media model and the
C Ergun equation sets.

C This also assumes that the cotton strings are not moving in relation
C to the airflow.

C The study shows that this is close to being the case.

C The galpha and gbeta values are based
C on the properties of the cotton (in theory).

C To use this subroutine, the momentum source term needs to be
C activated in StarCD.

C        This line defines the multiplication factor of the
C        volume fraction of the particles.
C        This is based on the D/L of spheres (for the moment)
      VFFACTOR = (6.0*VFCEL2*0.318309866)**0.3333

      if(VFFACTOR.gt.1.0)then
        VFFAC = 1.0
      else
        VFFAC = VFFACTOR
      endif

C        This is the velocity magnitude of each node
      gvmag = sqrt(u**2+v**2+w**2)

C        This alpha factor is determined on observations of the particle flow
      galpha = 5.0
```

```
C       This beta factor is determined on observations of the particle flow
      gbeta = 1.0

C       Here we define the relative velocities of the particles to the carrier
      URELATIVE = SQRT((U-UCEL2)**2)
      VRELATIVE = SQRT((V-VCEL2)**2)
      WRELATIVE = SQRT((W-WCEL2)**2)

C       Here we define the relative velocity
        VELRELATIVE = SQRT((U-UCEL2)**2+(V-VCEL2)**2+(W-WCEL2)**2)

      if(VELRELATIVE.lt.100) then
        VELREL = VELRELATIVE
      else
        VELREL = 100.0
      endif

      if(U.gt.0.0000) then
       s1u = -VFFAC*((GALPHA*VELREL+GBETA)*VELREL)
      else
       s1u = VFFAC*((GALPHA*VELREL+GBETA)*VELREL)
      endif

      if(V.gt.0.0000) then
       s1v = -VFFAC*((GALPHA*VELREL+GBETA)*VELREL)
      else
       s1v = VFFAC*((GALPHA*VELREL+GBETA)*VELREL)
      endif

      if(W.gt.0.0000) then
       s1w = -VFFAC*((GALPHA*VELREL+GBETA)*VELREL)
      else
       s1w = VFFAC*((GALPHA*VELREL+GBETA)*VELREL)
      endif

      s2u = 0.00
      s2v = 0.00
      s2w = 0.00

      RETURN
      END

C*******END OF SUBROUTINE SORMOM.F*************C
```